PHYSICS
ფიზიკა

34

PHYSICS

ფიზიკა

34

PHYSICS
ფიზიკა

34

that we consider the fast spectral diffusion in TLS so that the unit temperature is considered for TLS. Here

$$\alpha = \frac{\pi B^2}{16} P \frac{N_D}{N_J}$$

$$\delta = \frac{\pi B^2}{16} P \frac{N_D}{N_S}$$

$$\gamma = \frac{\pi B^2}{16} P \frac{\omega_J}{\omega_S}$$

P is the density of states of TLS, T_{JL}, T_{SL}, T_{DL} nuclear, electron and TLS lattice relaxation time, β_L the inverse temperature of lattice.

Due to the high rate of electron relaxation we consider $\beta_S = \beta_L$. If the saturation sound is applied at stationary case the following expression for nuclear inverse temperature is achieved (with the following initial conditions): $\beta_J(0) = \beta_L$, $\beta_D(0) = 0$:

$$\beta_J = 2 \frac{\omega_S}{\omega_J} \frac{\alpha T_{JL}}{1 + \frac{\omega_S}{\omega_J} \gamma T_{DL} + \alpha T_{JL}} \tag{5}$$

In order to estimate the quantity of gained inverse nuclear spin temperature let us consider the following parameters for the sample: $\hbar \sim 10^{-34}$ J.sec, $\omega_S \sim 10^{11}$ Hr, $\omega_J \sim 10^{-3} \omega_S$, $N_D \sim 10^{-5} N_J$, $P \sim 10^{20} J^{-1}$, $B \sim 10^8$ Hr, $\frac{1}{T_{JL}} \sim 10^{-2}$ sec^{-1} [4].

In this case α, γ and $\frac{1}{T_{DL}}$ parameters are

$$\alpha \sim 2 10^{-4} \text{ sec}^{-1}, \quad \gamma \sim 2 10^{-2} \text{ sec}^{-1}, \quad \frac{1}{T_{DL}} \sim 3 10^{-2} \text{ sec}^{-1}$$

and the inverse nuclear spin temperature is:

$$\beta_J \sim 40 \beta_L$$

So the nuclear inverse spin temperature became 40 times higher.

Tbilisi I. Javakhisvili State University

3.

INVESTIGATION OF MAGNETIC AND PERCOLATION PROPERTIES OF THE SUPERCONDUCTING COMPOSITE CERAMICS $(YBa_2Cu_3O_{7-\delta})_{1-x}(Y_2BaCuO_5)_x$

J.Sanikidze, S.Odenov, R.Kokhreidze, G.Mumladze, I.Mjavanadze, N.Sabashvily

Abstract: In this article physical properties of the Y-containing two component HTSC composite are investigated. The magnetic properties of the composite are studied. This composite consists of the superconducting phase $YBa_2Cu_3O_{7-\delta}$ and the dielectric green phase Y_2BaCuO_5. We investigated percolation processes in this composite and defined percolation limit in this mixture. The percolation limit is equal to $(17\pm2)\%$ of superconducting phase, which is in a good agreement with the theoretical prediction.

Physical properties of the two-component superconducting ceramics have been investigated in a number of works. These materials were the composites based on yttrium superconducting systems to which different non-superconducting substances were added. Here were studied the samples of ceramics with addition of silver [1], polystyrene [2], the ceramics phase $BaPb_{0.75}Bi_{0.25}O_3$ [3], etc. These substances consist of a system of superconducting grains connected with metallic or dielectric layers and forming complex superconducting networks. In such systems the conductivity is of a percolation type.

In the classic percolation theory a number of quantum effects, which exist in superconductors, is not concerned, namely the proximity effect, flux quantization effect, tunneling, Josephson effect [4]. All of them can add some contributions to the percolation processes. So, because of the proximity effect the superconducting current can go through a normal conductor or through a superconductor in a normal state.Because of the Josephson effect the superconducting current can go even through the isolator layer between two superconducting grains. The flux quantization makes the percolation

processes strongly dependent on magnetic field, so does the Josephson effect in weak links formed between the grains.

It is necessary to say that percolation processes in superconductors based on high temperature superconducting ceramics (HTSC) play a role not only in the composite samples. These processes musthave taken place in a weakly annealed samples as well, and in the samples with the superconducting phase deficit, and with oxigeñ deficite too, as well as in common samples near the field H_{C2J} (where the index shows that in this field the Josephson weak links are brought into the normal state). When the weak links are partly normal, the critical current of the links decrease, because the superconducting current goes only through the remaining superconducting links. If this quantity is less than some critical value, the continuous superconducting chain of the links will not appear even for an infinitely weak current and on the sample a voltage will appear.

The real situation is even more complex. At any finite temperature in superconductors there are normal electrons which take part in thermal motion.As a result of this motion there arises thermal noise i,e chaotic currents through superconducting links. If HTSC is near the percolation limit, its critical current may exceed the critical value, and the normal resistance will appear.

Clearly, the percolation processes, their regularities and influence must be taken into account in many cases of some theoretical and practical interest. In the present work some physical properties of the composite $(YBa_2Cu_3O_{7-\delta})_{1-x}(Y_2BaCuO_5)_x$ have been investigated, using Y_2BaCuO_5 ceramics (the green phase) as dielectric phase.We have studied the behavior of composite superconductors in ac and dc magnetic fields, changing the value of dc field from 0 up to 300 Oe, which was sufficient for our purpose.

As it is known, on the magnetic moment curve $M_{ZFC}(H)$ (the cooling in zero magnetic field) there is a place, where to the magnetic moment of grains the weak links moment $M_J(H)$ is added. The latter moment increases with field, reaches the maximum value and then gradually decreases to zero.The field, where $M_J=0$, was defined as the critical field H_{C2J}. A little higher there is a non-hysteresis region, where it is possible to measure a differential susceptibility $\chi_{d}=\chi_{d}'$ (the imaginary part χ_{d}'' here is equal to zero). As it is known [7], by the use of this value it is possible to measure with a

sufficient accuracy the volume part of superconducting phase by the following relation

$$x_{sv} = -4\pi\chi_d' = -4\pi\chi_d.$$

In the used method the value of χ_d' in the field $> H_{C2J}$ was measured, where the H_{C2J} value was determined by the curve decreasing to the constant, corresponding to the grain diamagnetic moment. The following condition must be fulfilled

$$H << H_{C1g} \qquad (2)$$

where H_{C1g} is the first critical field of the grains. The other condition must be on the skin layer depth in a normal sample $\varepsilon >> D,t$, where D,t are sample dimensions[8]

$$\varepsilon = 5 \cdot 10^3 \sqrt{\rho_n / f} \qquad (3)$$

Here ρ_n is a sample normal resistivity, ohm.cm, f is the AC field frequency.

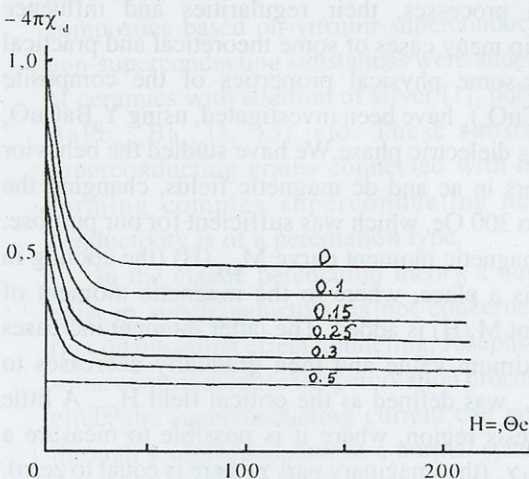The results obtained are given in Fig.1. The dependence of the real part of susceptibility on DC magnetic field shows, that for 1kHz AC field with an amplitude $<<1$ Oe there is a sharp decrease at the beginning with a gradual transition to a plateau. This can be explained by diamagnetism supression of the weak links and by the constant diamagne-tism of grains. From here it is easy to calculate the volume and the mass part of superconducting phase (the calibration was made by the super-conducting sample in a
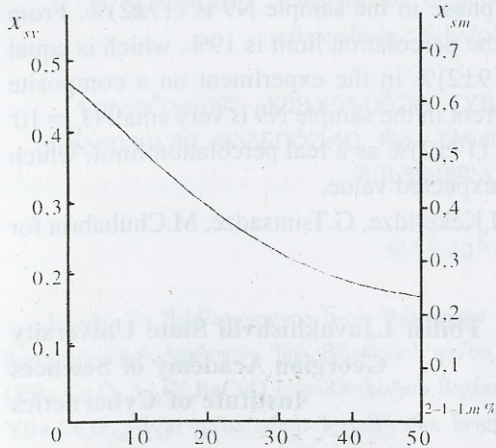

Fig.1.

Fig. 2.

zero DC field). The mass part of superconducting phase can be determined by the relation

$$x_{sm} = x_{sv} \, \rho_t / \rho_e, \qquad (4)$$

where ρ_t, ρ_e are the theoretical and experimental values of the ceramics density (the theoretical values for the both ceramics are almost the same). In Fig.2 there is shown the dependence of x_{sv}, x_{sm} on the content of the phase Y_2BaCuO_5. Figs.1,3. show, that for H=0 there is a sharp decrease of $\chi'(0)$ with the increase of dielectric phase. The possible explanation is the following: the probability of percolation chain forming is sharply decreasing with the increase of this phase. Therefore the sample N9 (50% of dielectric) has such a behaviour, as if there were almost no weak links in it and χ=const. The sample resistivity also increases strongly (Fig.4), which qualitatively agree with a theoretical percolation dependence [1]. It is necessary to note, that in reality there exists an additional phase in the initial sample, nearly ~ 33 mass % (Fig.2). So, as it can be seen,
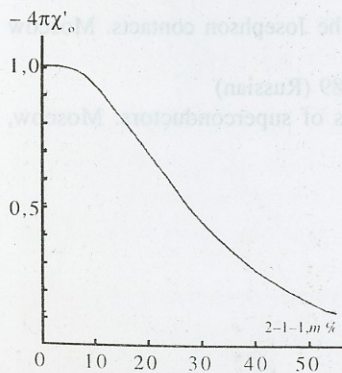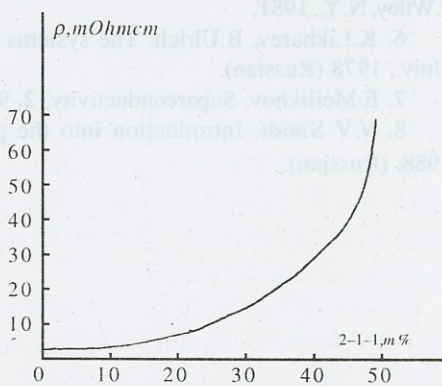

Fig. 3.

Fig. 4.

7

the content of superconducting phase in the sample N9 is $(17\pm2)\%$. From the classical percolation theory the percolation limit is 19%, which is equal to the experimental value of $(19\pm2)\%$ in the experiment on a composite HTSC-Ag [1]. As the critical current in the sample N9 is very small ($J_C \cong 10^{-6}J_{C0}$), one can consider the value $(17\pm2)\%$ as a real percolation limit, which is in a good agreement with the expected value.

Tbilisi I.Javakhishvili State University
Georgian Academy of Sciences
Institute of Cybernetics

REFERENCES:

1. J.Sanikidze, S.Odenov, R.Kokhreidze et. al. Superconductivity **4**,7, 1218, 1991.
2. Yu.A.Vidadi, E.Yanmaz, M.Altunbas, H.Karl. Physica C, 225, 124, 1994
3. N.I.Petrov, D.A.Balayev, etal. Solid State Physics. **39**, 3, 418, 1997 (Russian).
4. T.Van Duser, C.W.Turner. Principles of superconducting devices and circuits. Elsevier, 1981.
5. A.Barone, G. Paterno. Physics and Applications of the Josephson Effect, J.Wiley, N.Y., 1981.
6. K.Likharev, B.Ulrich. The systems with the Josephson contacts. Moscow Univ., 1978 (Russian).
7. E.Meilikhov. Superconductivity, **2**, 9,5, 1989 (Russian)
8. V.V Smidt, Introduction into the physics of superconductors. Moscow, 1988. (Russian).

ჯ. სანიკიძე, ს. ოდენოვი, რ. კოხრეიძე, გ. მუმლაძე,
ი. მჭავანაძე, ნ. საბაშვილი

ზებამბარულ კომპოზიტურ $(YBa_2Cu_3O_{7-\delta})_{1-x}(Y_2BaCuO_5)_x$ კერამიკებში მაგნიტური და პერკოლაციური თვისებების შესწავლა

დასკვნა

სტატიაში შესწავლილია 6-ის შემცველი ორკომპონენტიანი კომპოზიტური მადალტემპერატურული ზეგამტარების ფიზიკური თვისებები. გამოკვლეულია $(YBa_2Cu_3O_{7-\delta})_{1-x}(Y_2BaCuO_5)_x$ კომპოზიტის მაგნიტური თვისებები. ამ კომპოზიტში $YBa_2Cu_3O_{7-\delta}$-ში ფაზა არის ზეგამტარი, ხოლო Y_2BaCuO_5 — მეორანი ფაზა არის დიელექტრიკი. ჩვენ შევისწავლეთ პერკოლაციური პროცესები კომპოზიტში და დავადგინეთ გამტარებლობის პერკოლაციური ზღვარი. პერკოლაციური ზღვარი აღმოჩნდა (17±2)% ტოლი ზეგამტარი ფაზის მიხედვით, რაც ეთანხმება თეორიულ გამოთვლებს.

9

THE INVESTIGATION OF FUNDAMENTAL EMISSION OF ZnO CRYSTAL GROWN BY RADICAL BEAM EPITAXY METHOD

T. Butkhuzi, M. Sharvashidze, G. Natsvlishvili,
E. Kekelidze, D. Peikrishvili, E. Chikoidze, L. Trapaidze

ABSTRACT. The *PL* spectra of *ZnO* obtained by original method of Radical Beam Epitaxy are investigated. In the samples of $10^{13}\Omega$ cm resistivity the exiton luminescence of free *A*, *B* and *C* exitons is observed. In the samples of 10^9-$10^{11}\Omega$ cm resistivity the new T line, *B* exiton and M line – known from the literature – are observed. The nature of T line is explained and the new interpretation of M line is given. The observation of free exitons and polariton emission justify, that emission recombination of free exiton is prevalence them nonrecombination processes. This means that the layers obtained by us are of light purity and monocrystallinity.

To obtain the monocrystalline semiconductive layers of high purity and to regulate its optical properties is a very important problem of optical electronics. These semiconductors should have the absorption and emission ability in visible and UV range of spectrum. That's why it is very important to investigate the fundamental emission of wide band gap compounds, in particular, *ZnO* samples.

In spite of that this compound has clearly marked semiconductive properties at wide band zone, vertical optical transitions, high efficiency of emission and absorption, photo, cathode and electroluminescence, high photoconductivity and etc, the use of *ZnO* crystals in practice is very limited, due to the following demerits:

1) The high temperatures (1800-2000°C) of synthesis lead to the existence of great amount of uncontrollable impurities into this compound.

2) They have good compensation ability, therefore they are of monopolarity n-type conductivity.

It was impossible to obtain hole conductivity in ZnO crystal by traditional methods. [1].

The method of Radical Beam Epitaxy [2] (RBE) makes possible to obtain ZnO crystals of both n- and p-type conductivity. During the above-mentioned method the growth of crystal layers occurs on the surface of the base crystal. The growth process proceeds by metal component, extracted from base crystal and by oxygen radicals absorbed from the activated oxygen atmosphere.

The interpretation of photoluminescence (PL) spectrum of ZnO, in spite of theoretical and experimental data is still under the discussion. It is due to the existence of great amount of defects (impurities) in the crystals, which are obtained by traditional methods. For example, the photoluminescence spectrum of ZnO obtained by traditional methods (from gas phase, epitaxial layer, hydrothermal method) consists of fundamental bands in ultraviolet area and of yellow-orange wide non-structural band in visible area. These bands are caused by intrinsic defects and uncontrollable impurities. Some authors connect the latter with alkali atoms (Li and Na) [3-5]. Ga, Al, Cd [6], Se [7] and etc. Also there was not the interpretation of M band in fundamental area of emission.

The investigation of optical properties of ZnO crystals, grown by RBE method, makes possible to interpret the emission bands.

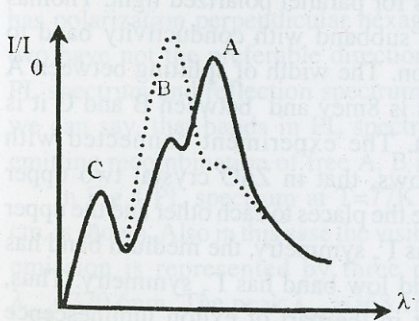In Fig.1 the PL spectrum at T=77K of the ZnO crystal grown by this method with resistivity $\rho \sim 10^{13}\Omega$ cm is shown. The registration of PL was carried out by the device, block diagram of which is shown in Fig.2. The spectrum contains three peaks of fundamental emission: $\lambda_{max} = 367.7$nm, $\lambda_{max} = 366.8$nm, $\lambda_{max} = 362.7$nm (the continuous line, Fig1). For $\lambda_{max} = 367.7$nm and $\lambda_{max} = 366.8$nm bands the half width is $\Delta l = 10$-12meV, and $\Delta l = 6$meV for $\lambda_{max} = 362.7$nm.

According to Thomas exiton model [8], the s-type conductivity band of ZnO crystal has Γ_7 sym-

Fig. 1 The PL spectrum of t~0 layers of $\rho \approx 10^{13}\Omega$cm resistivity, at T=77K, $\lambda_{exit.} = 337,1$ nm.
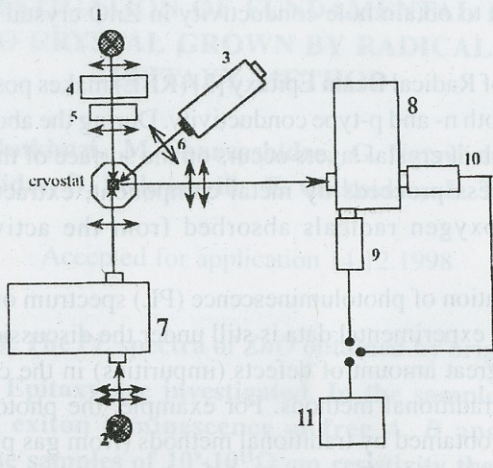
11

Fig. 2 Device for registration of PL spectra: (1) Mercury tub ДРШ-100, (2) Xenon tub ДКСШ-100, (3) Nitrogen LASER ЛГИ-21, (4) (5) by light filter was separated $\lambda_{excit.}$ =313nm, (6) Quartz lens, (7) Monocromator МДР-12, (8) monocromator МДР-23, (9) ФЕУ-100, (10) ФЕУ-62, (11) Recorder ЛКС-003, (12) ↕ collecting lenses.

metry. The p-type wave functions are transformed by Γ_9, Γ_7 and Γ_7 representation. The Γ_9 symmetry has upper valence band. Due to the selection rule $\Gamma_7 \to \Gamma_9$ transition is allowed for light, polarized perpendicular to c
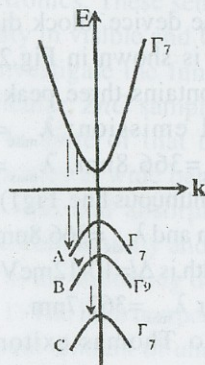
Fig. 3 The energetical bands of t~0.

hexagonal axe. But $\Gamma_7 \to \Gamma_7$ transition is allowed for perpendicular as for parallel polarized light. Thomas connected each subband with conductivity band to A,B and C exiton. The width of splitting between A and B subbands is 8mev and between B and C it is 40meV (Fig.3). The experiment connected with polarization shows, that in ZnO crystal two upper subbands change the places to each other and the upper valence band has Γ_7 symmetry, the medium band has Γ_9 symmetry and low band has Γ_7 symmetry. Thus, we can say that in the part of exiton luminescence spectrum, A and B exiton emission should not have preferably expressed polarization. B exiton should have the polarization perpendicular of hexagonal axe.

12

It is known from the literature, that it is impossible to registrate B and C exitons with short wave length in PL spectrum due to strong self-absorption and thermalization processes [9].

The transition of high-energy exiton into low energy state by thermalization processes is impossible, because close to k~0 area the interaction takes place only with longitudinal optical phonons. The energy of these phonons is E_{LO}=70meV which is more than the splitting energy between valence bands. This process should be accompanied by emission of infrared quantum of λ=25.8mkm and λ=31.0mkm wavelength. These bands are not observed in PL spectrum.

The non-emission degradation of free exiton by impurities and structural defects can be realized by two mechanisms:

1) The degradation of free exiton in electron-hole is possible pair during the interaction with electrical field, which is created by charged defects and impurities.

2) The realized energy after exiton annihilation is transmited to electrons bound with defects. Then electrons transmit to conductivity band and by consequent thermalization give a part of their energy to the crystal lattice.

The bond energy of B and C exiton is less than A exiton. Therefore the probability of decay on structural defects for short wavelength exitons is higher than for A exitons.

The hexagonal axe is perpendicular of the surface of the crystal. The investigation of luminescence direction shows that λ_{max}=366.8nm emission has polarization perpendicular hexagonal axe (dash line, Fig.1). The other two have not the preferable direction of polarization. After comparison of PL spectrum and reflection spectrum and after using Thomas exiton model we can say, that bands in PL spectra registered by us are connected with emitting recombination of free A, B and C exitons.

In Fig.4 PL spectrum at T=77K of layers with resistivity ρ~10^9-$10^{11}\Omega$ cm. is shown. Also in this case the visible part is not observed. The fundamental emission is represented by three peaks: λ_{max}=363.1nm, λ_{max}=366.8nm, λ_{max}=370.6nm. The peak λ_{max}=363.1nm in PL spectrum is registered for the first time. It is denoted as T. After the comparison with reflection spectra it is clear that λ_{max}=366.8nm band corresponds to recombination emission of free B exiton. As to λ_{max}=370.6nm peak, in literature it is known as M line.

Fig. 4 The PL spectrum of ZnO
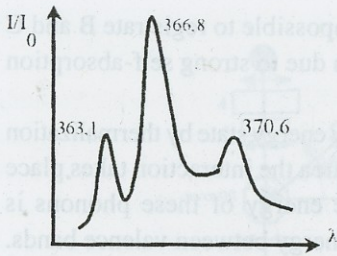layers of $\rho \approx 10^9$-$10^{11}\Omega$.cm. resistivity,
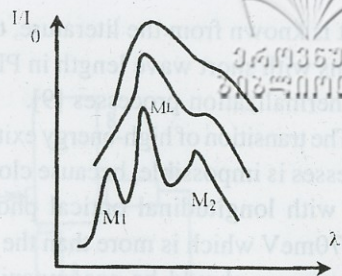at T=77K, λ_{excit}=337.1nm

Fig. 5 The structure of M line at
different excitation.

The interpretation of it, is not unambiguous. Some authors think that it is the
emission of electron-hole plasma [10,11]. This band was observed at law
temperature under high excitation conditions. At excitation I=10^4vt/cm^2 of
M_1=368.5nm, M_L=370.0nm and M_2=373.0nm Fig.5.

For identification of T line and for interpretation of M line it is necessary
to take into account new types of excitations in crystal.

In particular during the consideration of exiton dynamics, it is necessary
to consider the interaction between exitons and fields of other particles. This
leads to the creation of stationary state of exiton-photon field. The
transformation of exiton and photon spectrum into polariton takes place.

The dispersion curve of polariton is created by dispersion law of photon
and by parabolic dispersion law of exiton after interaction:

$$E_\Phi = \hbar c k$$

$$E_{EX} = E_A - \frac{G}{n^2} + \frac{\hbar^2 k^2}{2M}$$

Close to the cross point of dispersion curves of photons and exitons the
strong exiton-photon mixing is observed. The new type of excitation is created,
which is not neither photon nor exiton Fig. 6.

In the area of big $\vec{k}$, the state of polariton is similar to the structure of
the state of Coulomb exiton. In $\vec{k} \sim 0$ area polariton has nature of light. The
polariton states corresponding to this area, are called light like states. Just
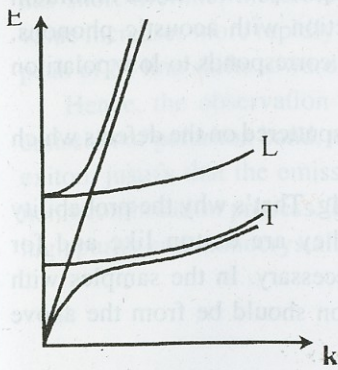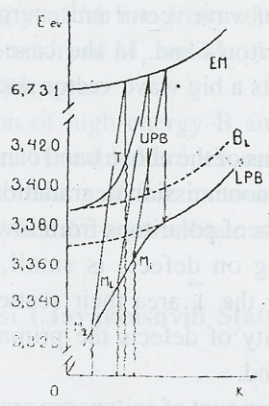within this area polariton can leave crystal and appear in the exiton

14

Fig. 5

Fig. 6

luminescence spectra. Within the middle area where the exiton-photon mixing is very important, the dispersion law of polariton is different of both exiton and photon dispersion law. Just this area of polariton spectrum corresponds to the fundamental absorption in crystal. The registration of polaritons from this area in PL spectrum is possible if the free path of polariton is less than the thickness of the crystal. Within the area of big $\vec{k}$, multiple collision between polariton and phonons takes place. So, the intensity of luminescence is determined by big wave vector of polariton from $\vec{k} \sim 0$ area and by the probability of transition within middle area.

During the interaction between exiton and phonon besides the mentioned polariton band one more band is appeared. This band posses in the more high-energy state and approaches asymptotically to dispersion law of phonons. The states, which correspond to high polariton bands, are called light like. Because those states are similar to dispersion law of light the law polariton band is called exiton like. This means the existence of two type exitons: small mass exiton of above polariton band and heavy mass exiton of low polariton band. The light can be realized from crystal in case of quasiparticles which create light have parameters corresponding to dispersion law of light. Quasiparticiles from the above polariton band can be easily transferred into light and leave crystal.

During the radiation by energy more than band gap energy, at first the exiton of above polariton band is created. Then this exiton transmits phonons

15

to the parts of wave vector and energy and occupies position in the minimum of the polariton band. In the case of interaction with acoustic phonons, polariton gets a big wave vector and this state corresponds to low polariton band.

Polaritons of the above band can be easily sputtered on the defects which leads to the nonemission degradation of it.

The mass of polaritons from low band is big. That's why the probability of scattering on defects is small, though they are exiton like and for approaching the $\vec{k}$ area their scattering is necessary. In the samples with small quantity of defects the primary emission should be from the above polariton band.

A great amount of exitons are created at strong band-band laser excitation. The overlap of wave functions of exitons produce the creation of exiton molecules. In principal state it has Γ_1 symmetry and J=0 orbital moment corresponds to it. The selection laws allow $\Delta J = \pm 1$ transitions. The canals of exiton molecules decay are shown in Fig 7. There are three canals of degradation of exiton molecules:

$$E.M. \rightarrow L.P.B. + h\nu_1$$
$$E.M. \rightarrow B_L + h\nu_L$$
$$E.M. \rightarrow U.P.B. + h\nu_2.$$

The energy of exiton molecule in ZnO is 6.73~6.740eV. The energy of low polariton band is $E_{L.P.B.}$=3.369eV. From this we can obtain values for $h\nu_1$, $h\nu_L$ and $h\nu_2$ – 3.362eV, 3.348eV, 3.320eV. These values correspond to maxima of M_1, M_L, M_2 bands. The emission energy from above polariton band is $E_{E.M.}$-($h\nu_2$); it gives quantities $362,92nm \leq \lambda_{U.P.B.} \leq 363,89nm$. The obtained values are in good agreement with the position of T line. So, λ=363. 1nm line is connected with the emission of the above polariton band. There is little information in references about emission of the above polariton band due to the strong absorption of photon like polariton on the surface.

The shift of peak of M line towards long wavelength can be explained by the following. During the increasing of excitation energy the states with comparatively long lifetime, which correspond to low polariton band and B_L exiton, approach a saturated regime. Polariton from the above polariton band

has short lifetime, therefore the intensity of M line from some excitation value increases more rapidly than the intensity of M_I and M_L. As a result, the peak of M line shifts towards long wavelength.

Hence, the observation of emission of high energy B and C exitons, emission of polariton band, nonexistence of visible luminescence and bound exiton, justify that the emission recombination of free exitons prevail over nonrecombination process. This means that the layers obtained by us are of high purity and monocrystallinity.

Tbilisi I.Javakhishvili State University

REFERENCES

1. F. Kreger. Khimia nesovershenykh kristalov. M.; Mir, 1979. - 657.
2. T. V. Butkhuzi, A. N. Georgobiani, M. B. Êîtliarevski. Avtorskoe svidetelstvo ¹31175182, 1985.
3. O.F. Schirmer, D. Zwingle. Sol. State Commun. **8**, 1970, 1559-1563.
4. E. Mollwo D. Zwingle J. Luminescence, **12/13**, 1976, 441-445.
5. V. D. Cherni Candidate thests. - МИЭТ, 1977.
6. F.A. Kröger, H.J. Vink, J. Chem. Phys. **22**, 1954, N2, 250-252.
7. W. J. Lehman Electrochem. Soc. **115**, 1979, 538-540.
8. D. G. Thomas, J. Phys. and Chem. Solids, **15**, 1960, 86-89.
9. I. P. Kuzmina,   V. A. Nikitenko "Okis tsinka, poluchenie i opticheskie svoistva. - Ì. Nauka, 1984. – 165.
10. J. Segawa S. Namba. J. Luminescence, **12/13,** 1976, 569.
11. T. Sketrup. Ibid, **23, 1977, 741.

2.
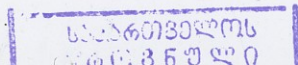
თ. ბუთხუზი, მ. შარვაშიძე, გ. ნაცვლიშვილი, ე. კეკელიძე,
დ. ფეიქრიშვილი, ე. ჩიკოიძე, ლ. ტრაპაიძე
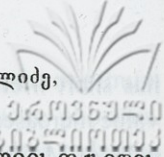
რადიკალურ-სხივური ექიტაქსიის მეთოდით მიღებული თუთიის ოქსიდის ფუნდამენტური გამოსხივების შესწავლა

დასკვნა

გამოკვლეულია ორიგინალური მეთოდით რადიკალურ-სხივური ეპიტაქ-
სია, მიღებული თუთიის ოქსიდის ფენების ფოტოლუმინესცენცია. 10 სმ
Ωcm კუთრი წინაღობის ნიმუშებში დამზერილია თავისუფალი A B და C
ექსიტონების გამოსხივება. 10^9-10^{11} Ωcm კუთრი წინაღობის ფენებში დამზერი-
ლია ახალი T ზოლი, B ექსიტონი და ლიტერატურაში ცნობილია M ზოლი.
ახსნილია T ზოლის წარმოშობის ბუნება და მოწოდებულია M ზოლის
ახალი ინტერპრეტაცია. თავისუფალი ექსიტონებისა და პოლარიტონული
გამოსხივების დამზერა ადასტურებს, რომ თავისუფალი ექსიტონების გა-
მოსხივებად რეკომბინაცია დომინირებს არაგამოსხივებად პროცესებზე,
რაც იმის მანიშნებელია, რომ რადიკალურ-სხივური ეპიტაქსიით მიღებული
კრისტალური ფენები არიან ზედმიწევნით სუფთა და ამაღლებული
მონოკრისტალურობის ხარისხით.
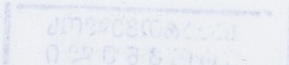
OPTIMIZATION OF WEIGHTS FOR THESHOLD REDUNDANCY OF BINARY CHANNELS BY THE METHOD OF GENERALIZED DISTANCE (MAHALANOBIS')

Zh. Gogiashvili, O. Namicheishvili, G. Shonia

Abstract. Method of optimization of generalized distance (Mahalanobis) has been used to define the weights at the inputs of the threshold element and the new result is obtained for the abovesaid values. Determination of threshold element error probability according to the pattern recognition theory derives an algorithm with the weights estimated by Mahalanobis, distance optimization.

Introduction. Let a binary signal with the code +1 or −1 be received on the n-homogeneous information channels $B_1, B_2, ..., B_n$. Due to the probable failure of the channels the quantity of variable x at the output is formulated as a set of $x_1, x_2, ..., x_n$ or there is n probability of realization of variable x. Clearly, each x_i ($i = \overline{1, n}$), in its turn, is a binary variable getting the meanings +1 or −1. This redundant information (n version of the variable x) will be given to the decision receiving or restoring element (organ).

Decision receiving element is a device defining the decision, or the value of the outputting signal y on the basis of the signals $x_1, x_2, ..., x_n$ given to the input. In other words, decision receiving element is a switching circuit realizing the binary function $y = f(x_1, x_2, ..., x_n)$ of the n binary argument $x_1, x_2, ..., x_n$.

If probabilities $q_1, q_2, ..., q_n$ of binary channels $B_1, B_2, ..., B_n$ are different, then to each information input will be ascribed its weight a_i, ($i = \overline{1, n}$), where a_i is a real number ($-\infty < a_i < \infty$). In that case, on the basis of the weighed input signals the decision y is received using the relation $y = \mathrm{sgn}\left(\sum_{i=1}^{n} a_i x_i - \Theta \right)$,

19

where Θ is the so-called threshold of the element (quorum). Therefore, the elements working on this principle are called the threshold elements. The latter relation can also be written as $y = \mathrm{sgn}\left(\sum_{i=1}^{n+1} a_i x_i\right)$ if we formally assume that $\Theta = a_{n+1}$, and $x_{n+1} \equiv -1$, what means that the information channel B_{n+1} always generate the signal $x_{n+1} \equiv -1$ for an arbitrary meaning of the input signal x. Accordingly

$$\mathrm{sgn}\, z = \begin{cases} -1, & for \quad z < o \\ 0, & for \quad z = 0 \\ +1, & for \quad z > 0 \end{cases}$$

The present work aims to define the up to now unknown optimal weights a_i, ($i = \overline{1, n+1}$) at the inputs of the threshold organ [1] with the help of generalized distance (Mahalanobis') (Fig.1).

Determination of optimal weights. Let us agree to consider the given problem as that of classification when the input signal x is to be ascribed to the class Ω_1 or Ω_2 on the basis of the $x_1, x_2, \ldots, x_{n+1}$ versions of this signal. Number of these versions is $n+1$.

According to such an approach the restoring signal x must be treated as a random quantity X with realizations x, characteristic of which is the $n+1$ random quantity $X_1, X_2, \ldots, X_{n+1}$. Expediently the set of these quantities is to
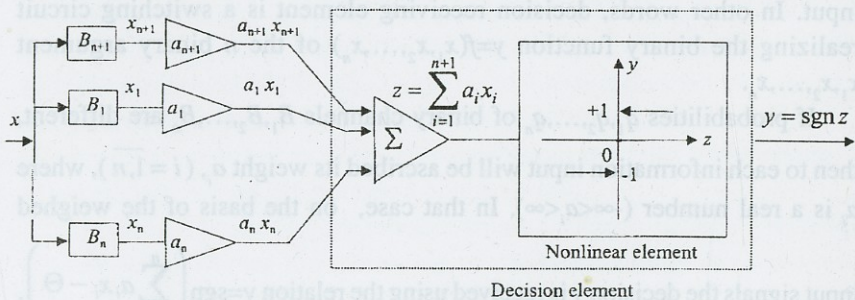
Fig.1. The model of threshold organ

be considered a random vector. In other words, regulated combination of the column $n+1$ must be considered:

$$\vec{X} = \begin{bmatrix} x_1 \\ x_2 \\ \vdots \\ x_{n+1} \end{bmatrix} = (X_1, X_2, \dots X_{n+1})'$$

where $\ll{}\gg$ is a symbol of transposition. Thus, each element X_i ($i = \overline{1, n+1}$) represents a component of the random vector.

Realization of the random vector $\vec{X}$ can be written as a vector of observation:

$$\vec{x} = (x_1, x_2, \dots x_{n+1})'$$

where the components of the vector are the realizations $x_1, x_2, \dots, x_{n+1}$ of the random quantities $X_1, X_2, \dots, X_{n+1}$.

Vector with the components $X_1, X_2, \dots, X_{n+1}$ can be described by the common function of distribution

$$f(x) = \mathrm{Prob}\{X_1 = x_1; X_2 = x_2; \dots X_{n+1} = x_{n+1}\},$$

where the probable meanings of x_i ($i = \overline{1, n}$) are -1 or $+1$, and $x_{n+1} \equiv -1$.

It is easy to see that for the class Ω_1 the vector has the following distribution

$$f_1(\vec{x}) = \prod_{i=1}^{n+1} q_i^{\frac{1-x_i}{2}} \cdot (1 - q_i)^{\frac{x_i+1}{2}}, \tag{1}$$

and for the class Ω_2

$$f_1(\vec{x}) = \prod_{i=1}^{n+1} q_i^{\frac{x_i+1}{2}} \cdot (1 - q_i)^{\frac{1-x_i}{2}}, \tag{2}$$

Given relations are just if $X_1, X_2, \dots, X_{n+1}$ components of the vector $\vec{X}$ are independent.

Mathematical expectation $\mu_i = M[X_i]$ for any arbitrary component X_i can be obtained by particular distributions of the quantities X_i. Combination of the aforesaid mathematical expectation $n+1$ can be written in the form of the mean value vector $\bar{\mu}$

$$\bar{\mu} = M[\bar{X}] = (\mu_1, \mu_2, ... \mu_{n+1}).$$

Namely, the centre of distribution of probabilities of the vector $\vec{X}$ for the class Ω_1 can be defined by the vector

$$\bar{\mu}_1 = (\mu_{11}, \mu_{12}, ..., \mu_{1n}, \mu_{1(n+1)}) \qquad (3)$$

and for the class Ω_2 by

$$\bar{\mu}_1 = (\mu_{11}, \mu_{12}, ..., \mu_{1n}, \mu_{1(n+1)}), \qquad (4)$$

where

$$\left. \begin{array}{l} \mu_{1i} = 1 - 2q_i \\ \mu_{2i} = 2q_i - 1 \\ i = 1, n+1 \end{array} \right\} \qquad (5)$$

Particular distributions of $X_i \cdot (\overline{1, n+1})$ define the dispersions σ_i^2 of these random quantities and the combined distribution of X_i and X_j components define their covariance σij:

$$\Sigma_{ij} = M[(X_i - \mu_i)(X_j - \mu_j)] = \begin{cases} \sigma_i^2, & for \ i = j \\ \sigma_{ij}, & for \ i \neq j \end{cases} \qquad (6)$$

It must be noted that the combination of the dispersions $\sigma_{ii} = \sigma_i^2$ and the covariances $\sigma_{ij} = \sigma_{ji}$ make the covariance matrix generalizing the notion of one-dimensional random quantity dispersion

$$\Sigma = \begin{bmatrix} \sigma_1^2 & \sigma_{12} & \sigma_{13} & \cdots & \sigma_{1n} \\ \sigma_{21} & \sigma_2^2 & \sigma_{23} & \cdots & \sigma_{2n} \\ \vdots & \vdots & \vdots & \cdots & \\ \sigma_{n1} & \sigma_{n2} & \sigma_{n3} & \cdots & \sigma_{n+1}^2 \end{bmatrix}$$

22

As we consider the case, when the components $X_1, X_2, \ldots, X_{n+1}$ of the vector X are not interdependent, hence $\sigma_{ij}=0$ for every $i \neq j$ and it represents a diagonal matrix Σ:

$$\Sigma = \begin{bmatrix} \sigma_1^2 & 0 & 0 & \ldots & 0 \\ 0 & \sigma_2^2 & 0 & \ldots & 0 \\ \vdots & \vdots & \vdots & \ldots & \vdots \\ 0 & 0 & 0 & \ldots & \sigma_{n+1}^2 \end{bmatrix}$$

It can easily be seen that the dispersions σ_i^2 are equal for both classes and it is defined by the expression

$$\left. \begin{aligned} \sigma_{(1)i}^2 &= \sigma_{(2)i}^2 \equiv \sigma_i^2 = 4q_i(1-q_i) \\ i &= 1, n+1 \end{aligned} \right\} \qquad (7)$$

Consequently, the covariance matrices are equal

$$\Sigma_1 = \Sigma_2 \equiv \Sigma. \qquad (8)$$

So, studying the threshold element we assume that the parameters and Σ are known and according to its working principle the threshold organ is considered to be a linear combination of observations

$$z = a_1 x_1 + a_2 x_2 + \ldots + a_{n+1} x_{n+1}$$

This expression is called a linear discriminant function. The vector of observations $\bar{x}$ is considered to belong to the class Ω_1 for $z>0$ and to the Ω_2 for $z<0$, and for $z=0$ the decision is not received.

Let us introduce to consider a random quantity Z defining it by the relation

$$Z = \sum_{i=1}^{n+1} a_i X_i \qquad (9)$$

or

$$Z = \sum_{i=1}^{n+1} Z_i, \qquad (10)$$

where

$$Z_i = a_i X_i \qquad (11)$$

23

If the observation $\bar{x}$ for the class Ω_1 is realized, then the sum (9) has the distribution

$$F_1(z) = \mathop{*}_{i=1}^{n+1} f_{1i}(z_i) \tag{12}$$

where $*$ - is a symbol of convolution, and

$$f_{1i}(z_i) = q_i^{\frac{a_i - z_i}{2a_i}} (1 - q_i)^{\frac{z_i + a_i}{2a_i}} \tag{13}$$

where z_1 gets the values $+a_i$ or $-a_i$.

Mathematical expectation of the random quantity Z can be computed by the formula

$$m_1 = \sum_{i=1}^{n+1} a_i \mu_{1i} = \sum_{i=1}^{n+1} a_i (1 - 2q_i) \tag{14}$$

Similarly, when the observation $\bar{x} = (x_1, x_2, \ldots, x_{n+1})$ belong to the class Ω_2, then distribution of probabilities of the random quantity Z is defined by the formula

$$F_2(z) = \mathop{*}_{i=1}^{n+1} f_{2i}(z_i) \tag{15}$$

where

$$f_{2i}(z_i) = q_i^{\frac{z_i + a_i}{2a_i}} (1 - q_i)^{\frac{a_i - z_i}{2a_i}} \tag{16}$$

and the probable values of z_i are $+a_i$ and $-a_i$.

If the observation $\bar{x}$ is of the class Ω_2, then mathematical expectation of the random quantity Z is defined by the formula

$$m_2 = \sum_{i=1}^{n+1} a_i \mu_{2i} = \sum_{i=1}^{n+1} a_i (2q_i - 1). \tag{17}$$

Comparing the formulae (14) and (17) we can easily conclude that

$$m_1 = -m_2,$$

and analyzing the formulae (13) and (16) we derive

$$\left.\begin{aligned} f_{2i}(z_i) &= f_{1i}(-z_i) \\ i &= 1, n+1 \end{aligned}\right\}, \tag{19}$$

Consequently,

$$F_2(z) = F_1(-z). \tag{20}$$

Dispersion σ_z^2 of the random quantity Z is equal in both cases and is defined by the formulae

$$\sigma_z^2 = \sum_{i=1}^{n+1} \sum_{j=1}^{n+1} a_i \sigma_{ij} a_j \tag{21}$$

Using (7) for $\sigma_{ij} = 0$ the formulae (21) gives

$$\sigma_z^2 = \sum_{i=1}^{n+1} 4 a_i^2 q_i (1 - q_i). \tag{22}$$

According to the heuristic points of view the weights $a_1, a_2, ..., a_{n+1}$ should be chosen so that the values of the mathematical expectations m_1 and m_2 be different as far as possible, and the dispersion be minimal.

It suffices to choose the generalized distance (Mahalanobis) [2] for a target function

$$\rho = \frac{(m_1 - m_2)^2}{\sigma_z^2}, \tag{23}$$

In our case it has the form:

$$\rho = \frac{\left[\sum_{i=1}^{n+1} a_i (\mu_{1i} - \mu_{2i}) \right]^2}{\sum_{i=1}^{n+1} \sum_{j=1}^{n+1} a_i \sigma_{ij} a_j}. \tag{24}$$

The weights a_i ($i = \overline{1, n+1}$) giving the maximum to this expression satisfy the following system

$$\left. \begin{array}{c} \dfrac{\partial \rho}{\partial a_i} = 0 \\[2mm] i = \overline{1, n+1} \end{array} \right\} . \tag{25}$$

Using (24) we arrive at

$$\frac{\mu_{1s} - \mu_{2s}}{\sum\limits_{j=1}^{n+1}\sigma_{sj}a_j} = \frac{\sum\limits_{i=1}^{n+1}a_i\left(\mu_{1i} - \mu_{2i}\right)}{\sum\limits_{i=1}^{n+1}a_i\sum\limits_{i=1}^{n+1}\sigma_{ij}a_j}. \tag{26}$$

Each vector $(a_1, a_2, ..., a_{n+1})'$ is the solution of the system of equations (26) if it satisfies the system

$$\left.\begin{array}{c}\sum\limits_{j=1}^{n+1}\sigma_{sj}a_j = k\left(\mu_{1s} - \mu_{2s}\right)\\ \\ s = \overline{1, n+1}\end{array}\right\} \tag{27}$$

where k is an arbitrary (free) constant.

Taking into account that in (23) $\sigma_{ij}=0$ for $i \neq j$ and $\sigma_{ii} = \sigma_i^2$ we get

$$\left.\begin{array}{c}a_s\sigma_s^2 = k\left(\mu_{1s} - \mu_{2s}\right)\\ \\ s = \overline{1, n+1}\end{array}\right\}$$

from where

$$\left.\begin{array}{c}a_s = k\dfrac{\mu_{1s} - \mu_{2s}}{\sigma_s^2}\\ \\ s = \overline{1, n+1}\end{array}\right\}. \tag{28}$$

Using (5) and (7) finally we get

$$\left.\begin{array}{c}a_i = k\dfrac{1 - 2q_i}{2q_i\left(1 - q_i\right)}\\ \\ i = \overline{1, n+1}\end{array}\right\} \tag{29}$$

If the existence of positive weights is desirable for $q_i<1/2$ and the negative weights for $q_i>1/2$, then the constant k must satisfy the condition $0<k<\infty$.

For such weights the distance r equals the absolute value of the difference of the characteristics m_1 and m_2

$$\rho = \left|m_1 - m_2\right| = \sum\limits_{i=1}^{n+1}\frac{\left(1 - 2q_i\right)^2}{q_i\left(1 - q_i\right)}, \tag{30}$$

26

where, as it was already mentioned, m_i ($i=1,2$) is a mathematical expectation of the sum Z for the class Ω_i.

Thus, if we choose the weights a_i according to (29) then there holds a theorem

$$\frac{\sigma_z^2}{|m_1 - m_2|} = 1.$$

$$(31)$$

Formula (30) shows that if probabilities of errors at the inputs do not equal 1/2, then increasing the number of threshold element inputs n the generalized distance ρ is monotonously increased and the probability of signal restoration error is reduced. In particular, generalized distance ρ for majority elements equals

$$\rho = \frac{(1-2q)^2}{q(1-q)} \cdot n,$$

$$(32)$$

where $q_1 = q_2 = ... = q_n \equiv q$ and $q_{n+1} = 1/2$.

Family of the dependences $\rho(q)$ for a number of meanings n is shown in Fig.2.
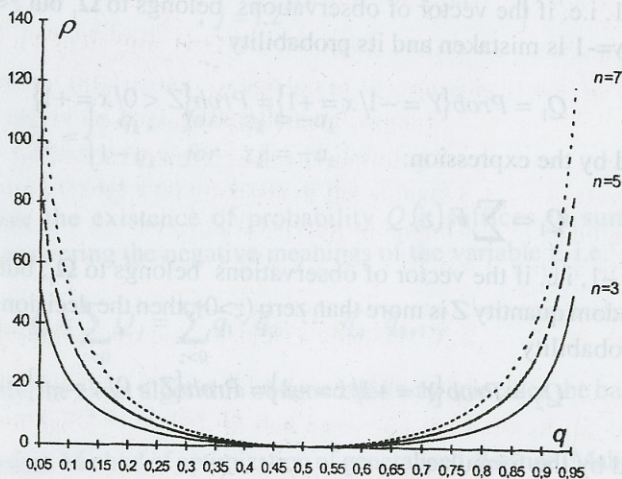

Fig.2. Dependence of generalized distance (Mahalanobis) on the probability of error of majority element inputs for some values of the number of the inputs.
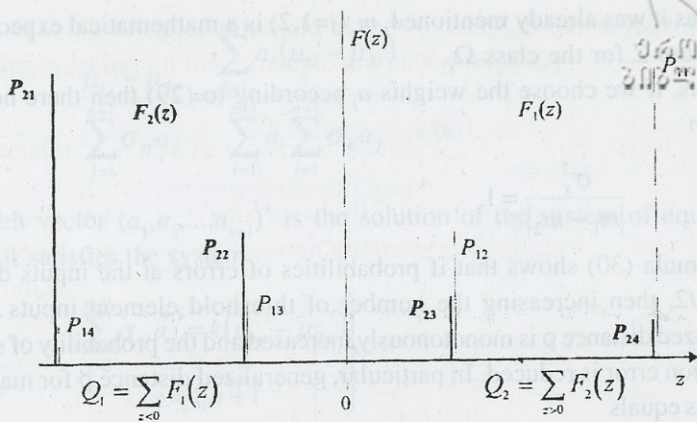
Fig.3. Discrete distributions $F_1(z)$ and $F_2(z)$ of the random sum Z for the classes Ω_1 and Ω_2.

Probability of error. Let us consider the Fig.3 define the probability of error of the threshold element. There are shown the two distributions ($F_1(z)$ and $F_2(z)$) of the random quantity Z for the origin $z=0$.

If $x=1$, i.e. if the vector of observations belongs to Ω_1 but $z<0$, then the decision $y=-1$ is mistaken and its probability

$$Q_1 = Prob\{Y = -1/x = +1\} = Prob\{Z < 0/x = +1\}$$

is defined by the expression:

$$Q_1 = \sum F_1(z). \tag{33}$$

If $x=-1$, i.e. if the vector of observations belongs to Ω_1, but realization of the random quantity Z is more than zero ($z>0$), then the decision is mistaken and its probability

$$Q_2 = Prob\{Y = +1/x = -1\} = Prob\{Z > 0/x = -1\}$$

is defined by the formulae

$$Q_2 = \sum_{z<0} F_2(z) = \sum_{z>0} F_1(-z) = \sum_{-z<0} F_1(-z) \equiv \sum_{w<0} F_1. \tag{34}$$

28

Probability (Q) of the signal restoration error of threshold decision organ can be defined by the formula of the complete probability

$$Q = q_{n+1} \cdot Q_1 + (1 - q_{n+1}) \cdot Q_2 = Q_1 = Q_2, \qquad (35)$$

where q_{n+1} is a priori probability of identification the class Ω_1, i.e. apriori probability that the signal x has the meaning $x = +1$.

Thus

$$Q = \sum_{z<0} F_1(z) = \sum_{z<0} \overset{n+1}{\underset{i=1}{*}} f_{1i}(z_i), \qquad (35)'$$

where the function $f_{1i}(z_i)$ is defined by (13) and there is to be introduced only that member which corresponds to the negative meaning of the variable z. The total number of discrete meanings of the variable z is 2^{n+1} as $z = \tilde{a}_1 + \tilde{a}_2 + \cdots + \tilde{a}_n + \tilde{a}_{n+1}$, where $\tilde{a}_i$ equals $+a_i$ or $-a_i$.

According to the formula (35)' each discrete quantity of the variable z is satisfied by the summand Q_j ($j = \overline{1, n+1}$) equal to the product of probabilities:

$$\left. \begin{aligned} Q_j &\equiv F_1(z) = \overset{n+1}{\underset{i=1}{*}} f_i(z_i) \equiv \tilde{q}_1 \cdot \tilde{q}_2 \cdot \; \cdots \; \cdot \tilde{q}_n \cdot \tilde{q}_{n+1} \\ &j = \overline{1, 2^{n+1}} \end{aligned} \right\},$$

where

$$\tilde{q}_k = \begin{cases} q_k, & for \quad z_k = -a_k \\ 1 - q_k, & for \quad z_k = -a_k \end{cases}.$$

To derive the existence of probability Q it suffices to sum up the summands answering the negative meanings of the variable z, i.e.

$$Q = \sum_{z<0} Q_j = \sum_{z<0} \tilde{q}_1 \cdot \tilde{q}_2 \cdot \; \cdots \; \tilde{q}_n \cdot \tilde{q}_{n+1}. \qquad (35)''$$

Evidently, the exact algorithm obtained this way coincides the basic result of [1].

Conclusion. Method of optimization of generalized distance (Mahalanobis) has been applied for the first time to define the weights of the threshold element inputs. Quite a new result (29) is obtained. Determination of

29

probability of error of the threshold element with the approaches of pattern recognition theory led us to the algorithm (35) with the weights estimated by optimization of Mahalanobis' distance.

REFERENCES

1. *J. Gogiashvili, K. Dalakishvili, O. Namicheishvili*. Thresold Redundancy of Binary Channels. Bull. Georg. Acad. Sci., **157**, 1, 1998, 38-41.
2. *P.C. Mahalanobis*. On the Generalized Distance in Statistics. Proceedings of the National Institute of Sciences of India. 12, 1936, 49-55.

ჭუჭუნა გოგიაშვილი, ოლეგ ნამიჩეიშვილი, გიორგი შონია

ოროგითი არხების წონთა ოპტიმიზაცია განზოგადებული (მაჰალანობისის) მანძილის მეთოდით ზღურბლური დარეზერვებისას

დასკვნა

ნაშრომში გამოყენებულია განზოგადებული (მაჰალანობისის) მანძილის ოპტიმიზაციის მეთოდი ზღურბლური კლემენტის შესასვლელთა წონების დასადგენად, რითაც ხსენებულ სიდიდეთა მნიშვნელობებისათვის სრულიად ახალი შედეგი მიიღება.

სახეთა გამოცნობის თეორიის მიდგომათა გამოყენება კი ზღურბლური კლემენტის შეცდომის ალბათობის დასადგენად იძლევა ალგორითმს, რომელშიც წონებად მაჰალანობისის მანძილის ოპტიმიზაციით განსაზღვრული სიდიდეები იხმარება.

THE NUCLEAR SPIN TEMPERATURE SHIFT IN DISORDERED STATES WITH PARAMAGNETIC IMPURITIES UNDER ULTRASOUND SATURATION CONDITIONS

Ts. Khutsishvili

Abstract : **The nuclear polarization in disordered dielectrics with two-level tunnelling systems under the ultrasound saturation conditions is investigated.**

It is shown that the nuclear inverse spin temperature became 40 times higher in the above mentioned conditions.

It is well known, that nuclear relaxation in solid states with magnetic impurities is caused by local field changes due to electron spin fluctuations. On the other hand the electron spin reorientations are caused due to electron-lattice interactions [1].
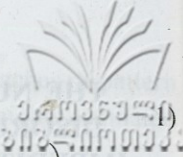
If the electron spin relaxation time is less than nuclear spin relaxation time, the nuclear spin polarization occurs when electron spin resonanse is saturated. In solid states the electron spin relaxation time is caused by electron spins interaction with phonons.

It is also well known, that disordered states at rather low temperatures (T<10 K) exhibits anomalous universal properties, caused by low laying excitations with constant density of states $P - 10^{46}J^{-1}$ m^{-3} [2]. The so-called two-level tunnelling systems (TLS) introduced by Anderson, et al and Phillips [3], are atoms and group of atoms, in two semiequal states, with tunnelling between them.

It was shown in [4], that TLS plays an important role in nuclear spin relaxation at low temperatures.

The aim of this article is to investigate the possibility of nuclear polarization under the ultrasound saturation conditions in disordered materials when the pin-lattice relaxation is caused by TLS.

Let's consider the amorphous dielectric with paramagnet impurities:

$$H = \omega_S \sum_i S_i^z + \omega_J \sum_i J_i^z + \sum_i \varepsilon_i l_i^z + H_{ph}$$

$$H_{ph} = \frac{1}{2} \sum_i B\left(J_i^+ S_i^- + J_i^- S_i^+\right)\left(l_i^z \cos\vartheta_i + \frac{1}{2}\left(l_i^+ + l_i^-\right)\sin\vartheta_i\right),$$

where

$$\cos\vartheta_i = -\frac{\Delta}{\varepsilon_i} = -\left[1 - \frac{\Delta_{oi}^2}{\varepsilon_i^2}\right]^{\frac{1}{2}},$$

$$\sin\vartheta_i = -\frac{\Delta_{oi}}{\varepsilon_i},$$

$\varepsilon_i = \left(\Delta_{oi}^2 + \Delta_i^2\right)^{\frac{1}{2}}$ is the TLS energy, Δ_i energy of asymmetry, Δ_{oi} tunnelling energy, $S_i^{\pm}, J_i^{\pm}, l_i^{\pm}$ electron, nuclear and TLS pseudospin operators projections, ω_S, ω_J Zeeman energies of electron and nuclear spin systems, B the superfine interaction constant.

The first three terms of Hamilton operator are the electron, nuclear and TLS subsystem energies, the forth term is the effective interaction between the nuclear electron and TLS subsystems. Concerning the dipole-dipole interaction among these systems it causes the spectral line broadening and spectral diffusion processes. The spin-lattice relaxation time is well known, so the spin lattice relaxation is taken into account in the final equations.

The whole system can be considered as three subsystems and interaction between them is caused by effective interaction operator.

The evolution equations of subsystems are derived using Zubarev's nonequilibrium statistical operator method [5] and have the form:

$$\frac{d\beta_J}{dt} = -\alpha\beta_J - \alpha\frac{\omega_s}{\omega_J}\beta_S - \alpha\frac{\omega_s}{\omega_J}\beta_D - \frac{1}{T_{JL}}(\beta_J - \beta_L), \tag{2}$$

$$\frac{d\beta_S}{dt} = -\delta\frac{\omega_J}{\omega_S}\beta_J - \delta\beta_S - \delta\beta_D - \frac{1}{T_{SL}}(\beta_S - \beta_L), \tag{3}$$

$$\frac{d\beta_D}{dt} = -\gamma\beta_J - \gamma\frac{\omega_s}{\omega_J}\beta_S - \gamma\frac{\omega_s}{\omega_J}\beta_D - \frac{1}{T_{DL}}(\beta_D - \beta_L), \tag{4}$$

here $\beta_S = \frac{1}{T_S}$, $\beta_J = \frac{1}{T_J}$, are the inverse temperatures of electron, nuclear and TLS subsystems, correspondingly. It is necessary to take into account,

32

that we consider the fast spectral diffusion in TLS so that the unit temperature is considered for TLS. Here

$$\alpha = \frac{\pi B^2}{16} P \frac{N_D}{N_J}$$

$$\delta = \frac{\pi B^2}{16} P \frac{N_D}{N_S}$$

$$\gamma = \frac{\pi B^2}{16} P \frac{\omega_J}{\omega_S}$$

P is the density of states of TLS, T_{JL}, T_{SL}, T_{DL} nuclear, electron and TLS lattice relaxation time, β_L the inverse temperature of lattice.

Due to the high rate of electron relaxation we consider $\beta_S = \beta_L$. If the saturation sound is applied at stationary case the following expression for nuclear inverse temperature is achieved (with the following initial conditions): $\beta_J(0) = \beta_L$, $\beta_D(0) = 0$:

$$\beta_J = 2 \frac{\omega_S}{\omega_J} \frac{\alpha T_{JL}}{1 + \frac{\omega_S}{\omega_J} \gamma T_{DL} + \alpha T_{JL}} \qquad (5)$$

In order to estimate the quantity of gained inverse nuclear spin temperature let us consider the following parameters for the sample: $\hbar \sim 10^{-34}$ J.sec, $\omega_S \sim 10^{11}$ Hr, $\omega_J \sim 10^{-3} \omega_S$, $N_D \sim 10^{-5} N_J$, $P \sim 10^{20}$ J^{-1}, $B \sim 10^8$ Hr, $\frac{1}{T_{JL}} \sim 10^{-2}$ sec^{-1} [4].

In this case α, γ and $\frac{1}{T_{DL}}$ parameters are

$$\alpha \sim 2 10^{-4} \text{ sec}^{-1}, \ \gamma \sim 2 10^{-2} \text{ sec}^{-1}, \ \frac{1}{T_{DL}} \sim 3 10^{-2} \text{ sec}^{-1}$$

and the inverse nuclear spin temperature is:

$$\beta_J \sim 40 \beta_L$$

So the nuclear inverse spin temperature became 40 times higher.

Tbilisi I. Javakhisvili State University

33

3.

REFERNCES

1. À.Àbragam. The Principles of Nuclear Magnetism. Oxford. 1961.
2. J.L.Black. J.In Classy Metals. Ionic Structure, Electronic Transport and Crystallization, edited by H.J. Guntherodt and H.Beck, Springer, Berlin 1981.
3. W.A.Anderson. Phys. Mag. **25**,1.1972
   W.A.Phillips, J. Low Temp. Phys. **7**,351.1972
4. L.L.Buishvili. L.Zh.Zakharov. A.I. Tugushi. N.D.Fokina. Physika. **168**, 1991.
5. E .Aleksandrov. Jadernaia Magnitnaia Relaksatsia. Moscow,1979 (Russian).

ც. ხუციშვილი

ბირთვული სპინური ტემპერატურის წანაცვლება პარამაგნიტურ მინარევების მქონე მოუწესრიგებელ მყარ სხეულებში

დ ა ს კ ვ ნ ა

შესწავლილია ბირთვების პოლარიზაცია მოუწესრიგებელ დიელექტრიკებში ტუნელური ორდონიანი სისტემების ულტრაბგერით გაჯერების პირობებში. ზუბარევის არაწონასწორული სტატისტიკური ოპერატორის მეთოდით დადგენილია მოძრაობის განტოლებები ბირთვული, ელექტრონული და ტუნელური ორდონიანი სისტემების ქვესისტემებისათვის. ნაჩვენებია, რომ ზემოთ აღნიშნულ პირობებში ბირთვული სპინური ტემპერატურის შებრუნებული სიდიდე 40-ჯერ გაიზარდა.

34

ON THE QUASISTABLE SYSTEM OF TWO METASTABLE HELIUM ATOMS

S.Dibo, T.Kereselidze, I.Noselidze

ABSTRACT: The behaviour of the $^3\Sigma_u^+$ term of a system of two metastable helium atoms at medium and small internuclear distances is investigated. The energy of the system composed by two triplet helium atoms is shown to have a minimum at $R=1.5a_0$ and a maximum at $R=2.0a_0$. The minimum is located 10.8eV above the energy of the non-interacting atoms. The possibility of coupled system formation is discussed.

It is well known that the total energy of doubly charged ion of helium quasimolecule He_2^{++} in the ground state has a minimum at the internuclear distance $R=1.33a_0$, a maximum at $R=2.17a_0$ and tends to the energy of two noninteracted He^+ ions at $R\to\infty$ [1-5]. Because of the strong Coulomb repulsion of the nuclei, the bottom of the well is 8.66eV above the value of the energy of two isolated He^+ ions. Calculations show that the potential well contains five quasidiscrete vibrational levels [1]. According to the estimates of [3] the lifetimes of the levels to decay due to the tunnel effect amount to the following: for the ground vibrational level 10^{10} sec, for the upper level 10^{-12} sec. The height of the potential barrier is 1.50eV.

Thus, in the decay of the quasimolecule He_2^{++} into two He^+ ions, an energy about 10eV is released. It is a large energy on a chemical scale (For comparison we notice that in the decay of one molecule of the trotyl 9.86eV is released [6]). However, since the quasimolecule He_2^{++} is electrically charged, it is not possible to accumulate such a gas in significant quantities. Therefore, the question arises as to whether this property of the He_2^{++} quasimolecule is preserved if it is completely neutralized by the addition of two

electrons. In other words, could two helium atoms in any electron state form a quasistable system with a large (on a chemical scale) decay energy? This system could be a good accumulator of energy. The existence and magnitude of maxima in the bound states of He_2 are important factors in the determination of the composition of helium plasmas and afterglow.

Two helium atoms in the ground state have one purely repulsive term [7,8]. Therefore they do not form a stable system (or, consequently, a quasistable one either). Some of the energy terms, which correspond to a helium atom in the ground state and a helium atom in an excited state at infinity, lead to the formation of a quasistable molecule, with a maximum decay energy from a fraction of an electronvolt to one electronvolt [9-14].

The next terms energetically are the quasimolecular terms corresponding to two metastable helium atoms at infinity. If two singlet helium atoms approach each other, then a single term $^1\Sigma_g^+$ is obtained. If one of the atoms is in the triplet spin state, then the number of terms is doublet, and they differ in parity. In this case we have $^3\Sigma_g^+$ and $^3\Sigma_u^+$ terms. If both metastable helium atoms are in triplet spin states, then we have three terms: $^5\Sigma_g^+$, $^3\Sigma_u^+$ and $^1\Sigma_g^+$ with respective total spin $s = 2, 1, 0$.

The behaviour of the $^1\Sigma_g^+$ terms as a function of the internuclear distance R has been studied in [15]. It was obtained that these terms have a minimum and a maximum in the internuclear region $R < 3a_0$. The minima are located below the energy of the noninteracting atoms. The heights of the maxima are less than 1.5 eV.

In the present paper we investigate the behaviour of $^3\Sigma_u^+$ terms of a system of two metastable helium atoms at medium and small internuclear distances. We will determine a location of the minimum of the potential energy with respect to the energy of two noninteracting metastable helium atoms, moreover we will estimate an energy released in the decay of the quasimolecule He_2.

The Schrödinger equation for the four electrons in an axially symmetric Coulomb field of the two fixed nuclei a and b with charges $Z_a = Z_b = 2$ is

$$\left[\sum_{k=1}^{4} \left(-\frac{1}{2} \Delta_k - \frac{2}{r_{a_k}} - \frac{2}{r_{b_k}} \right) + \sum_{j<i=1}^{4} \frac{1}{r_{ij}} \right] \Psi = E(R)\Psi. \tag{1}$$

36

Here r_{a_k} and r_{b_k} are the distances of the k-th electron from the respective nuclei a and b, $r_{ij} = |\vec{r}_{ai} - \vec{r}_{aj}| = |\vec{r}_{bi} - \vec{r}_{bj}|$, $E(R) = \widetilde{E}(R) - 4/R$ is the electron energy and $\widetilde{E}(R)$ is the total energy of the quasimolecule (here and below we use atomic units $e = m = \hbar = 1$).

We neglect in zero approximation the repulsive interaction between the electrons and treat the neglected part of the potential energy in (1) as a perturbation. The simplification results because the approximate Schrödinger equation is separable into four equations

$$\left(-\frac{1}{2}\Delta_k - \frac{2}{r_{a_k}} - \frac{2}{r_{b_k}} \right) \varphi(\vec{r}_k, R) = \varepsilon(r)\varphi(\vec{r}_k, R), \tag{2}$$

where $k = 1,2,3,4$. Each of these equations describes an electron motion in the field of two fixed nuclei with charges $Z_a = Z_b = 2$ (He_2^+-like quasimolecule).

The excited $^3\Sigma_u^+$ states of helium molecule He_2 are obtained by lifting two electrons to exited terms of He_2^+-like quasimolecule (these terms pass into the levels of He^+ ions with principal quantum number $n=2$ at the separated atoms limit), and leaving two other electrons in the terms which pass into the levels of He^+ ions with $n=1$ at R. There are two terms $1s\sigma_g$ and $2s\sigma_u$ of the He_2^+-like quasimolecule which transform into the levels of the He_2^+ ions with $n=1$ at $R \to \infty$. There are two terms $1s\sigma_g$ and $2p\sigma_u$ of the H_2^+-like quasimolecule which transform into the levels of rhe He_2^+ ions with n=1 and four terms $2s\sigma_g$, $3p\sigma_u$, $3d\sigma_g$, $4f\sigma_u$, - which transform into the levels of He^+ ions with $n=2$ [16] (we classify the terms of the He_2^+-like quasimolecule by the quantum numbers of the united atoms).

For $^3\Sigma_u^+$ states of the quasimolecule the wavefunctions can in the independent particle approximation be written as Slater's determinants:

$$D_1 = det|\varphi_g\alpha, \varphi_g\beta, \psi_g\alpha, \psi_u\alpha|, \qquad D_1^{'} = det|\varphi_u\alpha, \varphi_u\beta, \psi_g\alpha, \psi_u\alpha|,$$
$$D_2 = det|\varphi_g\alpha, \varphi_g\beta, \psi_g\beta, \psi_u\beta|, \qquad D_2^{'} = det|\varphi_u\alpha, \varphi_u\beta, \psi_g\beta, \psi_u\beta|,$$
$$D_3 = det|\varphi_g\alpha, \varphi_g\beta, \psi_g\alpha, \psi_u\beta|, \qquad D_3^{'} = det|\varphi_u\alpha, \varphi_u\beta, \psi_g\alpha, \psi_u\beta|, \tag{3}$$
$$D_4 = det|\varphi_g\alpha, \varphi_g\beta, \psi_g\beta, \psi_u\alpha|, \qquad D_4^{'} = det|\varphi_u\alpha, \varphi_u\beta, \psi_g\beta, \psi_u\alpha|.$$

where φ_g, φ_u and ψ_g, ψ_u are the wavefunctions of $1s\sigma_g$, $2p\sigma_u$ and $2s\sigma_u$, $3p\sigma_u$ states of H_2^+-like quasimolecule respectively, α corresponds to "spin up",

37

and β corresponds to "spin down". The determinants D_1, D_1' and D_2, D_2' are the eigenfunctions of the z-component of the total spin operator $\hat{S}_z$ with the eigenvalues $s_z = +1$ and $s_z = -1$, respectively. The linear combinations $(D_3 + D_4)$ and $(D_3' + D_4')$ are also eigenfunctions of the operator $\hat{S}_z$ with the eigenvalues $S_z = 0$.

Besides these determinants there are eight determinants which correspond to the $^3\Sigma_u^+$ states of the quasimolecule
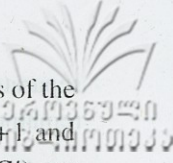
$$D_5 = det|\varphi_g\alpha, \varphi_u\alpha, \psi_g\alpha, \psi_g\beta|, \qquad D_5' = det|\varphi_g\alpha, \varphi_u\alpha, \psi_u\alpha, \psi_u\beta|,$$
$$D_6 = det|\varphi_g\beta, \varphi_u\beta, \psi_g\alpha, \psi_g\beta|, \qquad D_6' = det|\varphi_g\beta, \varphi_u\beta, \psi_u\alpha, \psi_u\beta|,$$
$$D_7 = det|\varphi_g\alpha, \varphi_u\beta, \psi_g\alpha, \psi_g\beta|, \qquad D_7' = det|\varphi_g\alpha, \varphi_u\beta, \psi_u\alpha, \psi_u\beta|, \qquad (4)$$
$$D_8 = det|\varphi_g\beta, \varphi_u\alpha, \psi_g\alpha, \psi_g\beta|, \qquad D_8' = det|\varphi_g\beta, \varphi_u\alpha, \psi_u\alpha, \psi_u\beta|.$$

The determinants D_5 (or D_5'), D_6 (or D_6'), $(D_7 + D_8)$ (or $D_7' + D_8'$) are eigenfunctions of the z-component of the total spin operator with the eigenvalues $s_z = +1, -1, 0$, respectively.

Substituting instead of ψ_g and ψ_u in (3) and (4) $\tilde{\psi}_g$ and $\tilde{\psi}_u$ - the wavefunctions of the $3d\sigma_g$ and $4f\sigma_u$ states of the H_2^+-like quasimolecule - we will obtain sixteen new determinants, which correspond to $^3\Sigma_u^+$ states of the quasimolecule. We represent these determinants as $\tilde{D}_1, \tilde{D}_2, \cdots \tilde{D}_8$ and $\tilde{D}_1', \tilde{D}_2', \cdots \tilde{D}_8'$.

Besides determinants considered above there are sixteen more determinants for the $^3\Sigma_u^+$ states of the quasimolecule

$$G_1 = det|\varphi_g\alpha, \varphi_g\beta, \psi_g\alpha, \tilde{\psi}_u\alpha|, \qquad G_1' = det|\varphi_u\alpha, \varphi_u\beta, \psi_g\alpha, \tilde{\psi}_u\alpha|,$$
$$G_2 = det|\varphi_g\alpha, \varphi_g\beta, \tilde{\psi}_g\alpha, \psi_u\alpha|, \qquad G_2' = det|\varphi_u\alpha, \varphi_u\beta, \tilde{\psi}_g\alpha, \psi_u\alpha|,$$
$$G_3 = det|\varphi_g\alpha, \varphi_g\beta, \psi_g\beta, \tilde{\psi}_u\beta|, \qquad G_3' = det|\varphi_u\alpha, \varphi_u\beta, \psi_g\beta, \tilde{\psi}_u\beta|,$$
$$G_4 = det|\varphi_g\alpha, \varphi_g\beta, \tilde{\psi}_g\beta, \psi_u\beta|, \qquad G_4' = det|\varphi_u\alpha, \varphi_u\beta, \tilde{\psi}_g\beta, \psi_u\beta|,$$
$$G_5 = det|\varphi_g\alpha, \varphi_g\beta, \psi_g\alpha, \tilde{\psi}_u\beta|, \qquad G_5' = det|\varphi_u\alpha, \varphi_u\beta, \psi_g\alpha, \tilde{\psi}_u\beta|, \qquad (5)$$
$$G_6 = det|\varphi_g\alpha, \varphi_g\beta, \psi_g\beta, \tilde{\psi}_u\alpha|, \qquad G_6' = det|\varphi_u\alpha, \varphi_u\beta, \psi_g\beta, \tilde{\psi}_u\alpha|,$$
$$G_7 = det|\varphi_g\alpha, \varphi_g\beta, \tilde{\psi}_g\alpha, \psi_u\beta|, \qquad G_7' = det|\varphi_u\alpha, \varphi_u\beta, \tilde{\psi}_g\alpha, \psi_u\beta|,$$
$$G_8 = det|\varphi_g\alpha, \varphi_g\beta, \tilde{\psi}_g\beta, \psi_u\alpha|, \qquad G_8' = det|\varphi_u\alpha, \varphi_u\beta, \tilde{\psi}_g\beta, \psi_u\alpha|.$$

Here G_1, G_2 (or G_1', G_2') and G_3, G_4 (or G_3', G_4') are the eigenfunctions of the z-component of the total spin operator $\hat{S}_z$ with the eigenvalues $s_z = +1$, and $s_z = -1$, respectively, and $(G_5 + G_6)$ (or $G_5' + G_6'$) and $(G_7 + G_8)$ (or $G_7' + G_8'$) are the eigenfunctions of the operator $\hat{S}_z$ with the eigenvalues $s_z = 0$.

At last there are sixteen more determinants, which take part in the determination of the wavefunctions of $^3\Sigma_u^+$ states:

$$
\begin{aligned}
&\tilde{G}_1 = det\left|\varphi_g \alpha, \varphi_g \alpha, \psi_g \alpha, \tilde{\psi}_u \beta\right|, \qquad
&&\tilde{G}_1' = det\left|\varphi_g \alpha, \varphi_u \alpha, \psi_u \alpha, \tilde{\psi}_u \beta\right|, \\
&\tilde{G}_2 = det\left|\varphi_g \alpha, \varphi_g \alpha, \psi_g \beta, \tilde{\psi}_u \alpha\right|, \qquad
&&\tilde{G}_2' = det\left|\varphi_g \alpha, \varphi_u \alpha, \psi_u \beta, \tilde{\psi}_u \alpha\right|, \\
&\tilde{G}_3 = det\left|\varphi_g \beta, \varphi_g \beta, \psi_g \alpha, \tilde{\psi}_u \beta\right|, \qquad
&&\tilde{G}_3' = det\left|\varphi_g \beta, \varphi_u \beta, \psi_u \alpha, \tilde{\psi}_u \beta\right|, \\
&\tilde{G}_4 = det\left|\varphi_g \beta, \varphi_g \beta, \psi_g \beta, \tilde{\psi}_u \alpha\right|, \qquad
&&\tilde{G}_4' = det\left|\varphi_g \beta, \varphi_u \beta, \psi_u \beta, \tilde{\psi}_u \alpha\right|, \\
&\tilde{G}_5 = det\left|\varphi_g \alpha, \varphi_g \beta, \psi_g \alpha, \tilde{\psi}_u \beta\right|, \qquad
&&\tilde{G}_5' = det\left|\varphi_g \alpha, \varphi_u \beta, \psi_u \alpha, \tilde{\psi}_u \beta\right|, \\
&\tilde{G}_6 = det\left|\varphi_g \alpha, \varphi_g \beta, \psi_g \beta, \tilde{\psi}_u \alpha\right|, \qquad
&&\tilde{G}_6' = det\left|\varphi_g \alpha, \varphi_u \beta, \psi_u \beta, \tilde{\psi}_u \alpha\right|, \\
&\tilde{G}_7 = det\left|\varphi_g \beta, \varphi_g \alpha, \psi_g \alpha, \tilde{\psi}_u \beta\right|, \qquad
&&\tilde{G}_7' = det\left|\varphi_g \beta, \varphi_u \alpha, \psi_u \alpha, \tilde{\psi}_u \beta\right|, \\
&\tilde{G}_8 = det\left|\varphi_g \beta, \varphi_g \alpha, \psi_g \beta, \tilde{\psi}_u \alpha\right|, \qquad
&&\tilde{G}_8' = det\left|\varphi_g \beta, \varphi_u \alpha, \psi_u \beta, \tilde{\psi}_u \alpha\right|.
\end{aligned}
\tag{6}
$$

Here $(\tilde{G}_1 - \tilde{G}_2)$ (or $(\tilde{G}_1' - \tilde{G}_2')$) and $(\tilde{G}_3 - \tilde{G}_4)$ (or $(\tilde{G}_3' - \tilde{G}_4')$) and $(\tilde{G}_5 - \tilde{G}_6) + (\tilde{G}_7 - \tilde{G}_8)$ (or $(\tilde{G}_5' - \tilde{G}_6') + (\tilde{G}_7' - \tilde{G}_8')$) are the eigenfunctions of the operator $^3\Sigma_u^+$ with the eigenvalues $s_z = 1, -1, 0$, respectively.

Thus, there are sixteen determinants for each projection of the total spin. The linear combinations of these determinants define the desired wavefunctions of the quasimolecule. For instance, for $s_z = 1$ we have

$$
\psi_i = \left(\alpha_i D_1 + \alpha_i' D_1'\right) + \left(\tilde{\alpha}_i \tilde{D}_1 + \tilde{\alpha}_i' \tilde{D}_1'\right) + \left(c_i G_1 + c_i' G_1'\right) + \left(d_i G_2 + d_i' G_2'\right) +
$$
$$
+ \left(b_i D_5 + b_i' D_5'\right) + \left(\tilde{b}_i \tilde{D}_5 + \tilde{b}_i' \tilde{D}_5'\right) + \tilde{c}_i\left(\tilde{G}_1 - \tilde{G}_2\right) + \tilde{c}_i^1\left(\tilde{G}_1' - \tilde{G}_2'\right)
\tag{7}
$$

where $i = 1, 2, 3, \ldots 14$. The expansion coefficients in (7) and the energy terms of the quasimolecule are determined by solving the system of linear homogeneous equations.

In (7) seven wavefunctions correspond to the states when two electrons with $n=1$, or two electrons with $n=2$, are at the nucleus a or b at the

separated atom limit. Therefore we are not interested in these states. For the remained states we can write at $R \to \infty$.

$$\Psi_i = a_i \left[(D_1 - D_1') + (\tilde{D}_1 - \tilde{D}_1') \pm \left((G_1 - G_1') + (\tilde{G}_1 - \tilde{G}_1') \right) \right] +$$
$$+ b_i \left[(D_5 - D_5') + (\tilde{D}_5 - \tilde{D}_5') \pm \left((\tilde{G}_1 - \tilde{G}_2) + (\tilde{G}_1 - \tilde{G}_2') \right) \right],$$

(8)

where $i = 1, 2$.

In (8) the signs "$\pm$" correspond to $2s$ and $2p$ states of the electrons in the separated helium atoms. Therefore taking into consideration that when $R \to \infty$ [16,17]

$$\varphi_{gu} \to \frac{1}{\sqrt{2}} \left(\varphi^a{}_{000} \pm \varphi^b{}_{000} \right) = \frac{1}{\sqrt{2}} \left(\varphi^a{}_{1s\sigma} \pm \varphi^b{}_{1s\sigma} \right),$$

$$\Psi_{gu} \to \frac{1}{\sqrt{2}} \left(\varphi^a{}_{100} \pm \varphi^b{}_{100} \right) = \frac{1}{2} \left[\left(\Psi^a{}_{2s\sigma} \pm \Psi^b{}_{2s\sigma} \right) + \left(\Psi^a{}_{2p\sigma} \pm \Psi^b{}_{2p\sigma} \right) \right],$$

$$\tilde{\Psi}_{gu} \to \frac{1}{\sqrt{2}} \left(\varphi^a{}_{010} \pm \varphi^b{}_{010} \right) = \frac{1}{2} \left[\left(\Psi^a{}_{2s\sigma} \pm \Psi^b{}_{2s\sigma} \right) - \left(\Psi^a{}_{2p\sigma} \pm \Psi^b{}_{2p\sigma} \right) \right],$$

(9)

and substituting (9) into (8) after simple but cumbersome calculations we will obtain at the sign "+" in (8)

$$\Psi_i = a_i \left[\det \left| \psi^a{}_{1s\sigma} \alpha \psi^a{}_{2s\sigma} \alpha \psi^b{}_{1s\sigma} \beta \psi^b{}_{2s\sigma} \alpha \right| - \det \left| \psi^b{}_{1s\sigma} \alpha \psi^b{}_{2s\sigma} \alpha \psi^a{}_{1s\sigma} \beta \psi^a{}_{2s\sigma} \alpha \right| \right] +$$
$$+ b_i \left[\det \left| \psi^a{}_{1s\sigma} \alpha \psi^a{}_{2s\sigma} \alpha \psi^b{}_{1s\sigma} \alpha \psi^b{}_{2s\sigma} \beta \right| - \det \left| \psi^b{}_{1s\sigma} \alpha \psi^b{}_{2s\sigma} \alpha \psi^a{}_{1s\sigma} \alpha \psi^a{}_{2s\sigma} \beta \right| \right]$$

(10)

where $i = 1, 2$ and $\varphi^{a,b}_{n,n,m}$ and $\psi^{a,b}_{nlm}$ are, respectively, Coulomb parabolic and spherical wavefunctions centered on the nuclei a and b.

Owing to the degeneracy of the energy levels of the quasimolecule at $R \to \infty$ in the independent particle approximation the coefficients in (10) are $a_1 = b_1$ and $a_2 = -b_2$. It is easy to see that when $a_1 = b_1$, wavefunction (10) describes two noninteracting triplet helium atoms, and when $a_2 = -b_2$, (10) describes noninteracting triplet and singlet helium atoms.

In the present study we consider a simplified model. It is assumed in this model that the inner electrons of the quasimolecule form a "rigid" system with the electron shell of He_2^{++}, while the outer electrons move in the averaged field of the nuclei and the inner electrons. The total energy of the electrons is composed of the electron energy of the quasimolecule He_2^{++} and

the energy of the outer electrons, which is determined.

We represent the wavefunctions $\Psi_{1,2}(1,2,3,4)$ in the form

$$\Psi_1 = X_1(1,2)Y_1(3,4)(\alpha(1)\beta(2) - \alpha(2)\beta(1))\alpha(3)\beta(4)/\sqrt{2},$$
$$\Psi_2 = X_2(1,2)Y_2(3,4)\alpha(1)\beta(2)(\alpha(3)\beta(4) - \alpha(4)\beta(3))/\sqrt{2}, \quad (11)$$

where $X_{1,2}(1,2)$ are the wavefunctions of the quasimolecule He_2^{++}

$$X_1(1,2) = A_1\varphi_g(1)\varphi_g(2) + B_1\varphi_u(1)\varphi_u(2),$$
$$X_2(1,2) = \left(\varphi_g(1)\varphi_u(2) - \varphi_g(2)\varphi_u(1)\right)/\sqrt{2}, \quad (12)$$

and $Y_{1,2}(3,4)$ are the wavefunctions of the outer electrons of the quasimolecule He_2

$$Y_1(3,4) = C_1\left(\psi_g(3)\psi_u(4) - \psi_g(4)\psi_u(3)\right) + D_1\left(\tilde{\psi}_g(3)\tilde{\psi}_u(4) - \tilde{\psi}_g(4)\tilde{\psi}_u(3)\right) +$$
$$+ E_1\left(\psi_g(3)\tilde{\psi}_u(4) - \psi_g(4)\tilde{\psi}_u(3)\right) + F_1\left(\tilde{\psi}_g(3)\psi_u(4) - \tilde{\psi}_g(4)\psi_u(3)\right),$$
$$Y_2(3,4) = A_2\psi_g(3)\psi_g(4) + B_2\psi_u(3)\psi_u(4) + C_2\tilde{\psi}_g(3)\tilde{\psi}_g(4) + D_2\tilde{\psi}_u(3)\tilde{\psi}_u(4) +$$
$$+ E_2\left(\psi_g(3)\tilde{\psi}_u(4) + \psi_g(4)\tilde{\psi}_u(3)\right) + F_2\left(\psi_u(3)\tilde{\psi}_u(4) + \psi_u(4)\tilde{\psi}_u(3)\right).$$

$$(13)$$

In (12) the coefficients A_1 and B_1 are determined in the two states approximation [18]

$$A_1 = \left[\frac{1}{2}\left[1 - \frac{2\varepsilon_g - 2\varepsilon_u + V_{gg} - V_{uu}}{\left((2\varepsilon_g - 2\varepsilon_u + V_{gg} - V_{uu})^2 + 4V_{gu}^2\right)^{1/2}}\right]\right]^{1/2},$$

$$(14)$$

$$B_1 = -\left[\frac{1}{2}\left[1 + \frac{2\varepsilon_g - 2\varepsilon_u + V_{gg} - V_{uu}}{\left((2\varepsilon_g - 2\varepsilon_u + V_{gg} - V_{uu})^2 + 4V_{gu}^2\right)^{1/2}}\right]\right]^{1/2},$$

where $\varepsilon_g = \varepsilon_{1s\sigma}(R)$ and $\varepsilon_u = \varepsilon_{2p\sigma}$, (R) are the energy terms of the H_2^+-like quasimolecule and

$$V_{gg} = \left\langle\varphi_g(1)\varphi_g(2) \mid r_{12}^{-1} \mid \varphi_g(1)\varphi_g(2)\right\rangle$$
$$V_{uu} = \left\langle\varphi_u(1)\varphi_u(2) \mid r_{12}^{-1} \mid \varphi_u(1)\varphi_u(2)\right\rangle$$
$$V_{gu} = \left\langle\varphi_g(1)\varphi_g(2) \mid r_{12}^{-1} \mid \varphi_u(1)\varphi_u(2)\right\rangle$$

$$(15)$$

are the matrix elements of the Coulomb repulsion between electrons in the H_2^+-like quasimolecule. Substituting (11) in (1), multiplying on the left by $X_1(1,2)\left(\psi_g(3)\psi_u(4)-\psi_g(4)\psi_u(3)\right)$, $X_1(1,2)\left(\tilde{\psi}_g(3)\tilde{\psi}_u(4)-\tilde{\psi}_g(4)\tilde{\psi}_u(3)\right)$,...

and integrating over the coordinates of the electrons we obtain a finite system of linear homogeneous equations. The obtained system of equations was solved on a computer. The matrix elements in the equations were calculated by using the numerical wavefunctions for H_2^+-like quasimolecule [16].

The curve of the total energy for system of two triplet helium atoms is shown in the Figure. The energy of the noninteracting atoms is chosen as the zero point. As it is seen from the Figure, the curve for $r=1.5a_0$ has a minimum, and that for $r=2.0a_0$ a maximum. The minimum is located 10.8eV above the energy of the noninteracting atoms. The calculations showed that the quasimolecule formed from the triplet and singlet helium atoms has purely repulsive term.
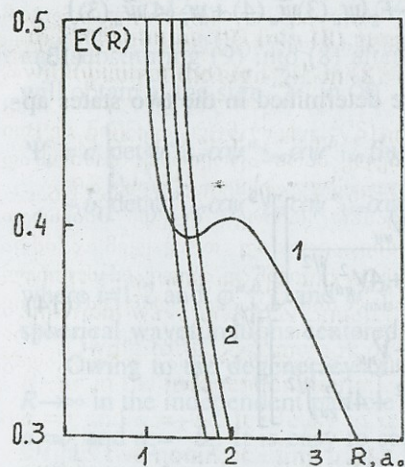
Fig. Behaviour of the $^3\Sigma_u^+$ term of two metastable triplet helium atoms as a function of the internuclear distance R in the region $R \leq 3a_0$ (curve 1). Curves 2 correspond to the systems $He(1S^2)+He^+$ and $He(1S^2)+He(1s,nl)$

We now investigate the question: can the well lead to the formation of a coupled system of two helium atoms? For this, we compare the calculated curve with the energy terms of the systems $He(1s^2)+He^+(1s)$ and determine the internuclear distances R at which intersection of the terms takes place. This system has two terms $^3\Sigma_g^+$ and $^3\Sigma_u^+$. These terms intersect the term $^3\Sigma_u^4$ in the region of the minimum, from which it follows that at internuclear distances $R \gtrsim 1.5a_0$ the term $^3\Sigma_u^+$ acquires a "width" due to the possibility of autoionization transition to the term $^2\Sigma_u^+$ of the system He_2^+. The autoionization transition to the term $^3\Sigma_g^+$ is considerably less probable, since it requires a change in the parity of the outgoing electron.

42

In addition to these terms, the term $^3\Sigma_u^+$ intersects in the region of the minimum with a whole band of terms that correspond at infinity to two helium atoms, one of which is single-electron-excited (see the Figure). So, it is clear that in order to answer to the above stated question it is necessary to study in detail all the intersections the $^3\Sigma_u^+$ has near to the minimum and to determine the probabilities for the corresponding transitions. It will be subject of the following study.

Tbilisi I. Javakhishvili State University

REFERENCES:

1. H.Yagsawa, H. Sato, H.Watanabe. Phys.Rev.A**16**,1352(1977)
2. J.S.Cohen, J.N.Bardesley. Phys.Rev.A18,1004(1978)
3. T.M.Kereselidze, O.B.Firsov. Sov.Phys.-JETP **38**,49(1974)
4. J.C.Browne, J.Chem.Phys. **42**,1428(1965)
5. H.Conroy, B.L.Bruner. J.Chem.Phys. **47**,921(1967)
6. E.Yu.Orlova. Chemistry and Technology of the Explosives. Leningrad, 1973 (Russian)
7. P.E. Phillipson. Phys. Rev. **125**,1981(1962)
8. D.J.Klein, C.E.Rodriguez, J.C.Browne. J.Chem. Phys. **47**,486(1967)
9. L.Lenamon, J.C.Browne, J.C.Olson. Phys.Rev. A8,2380(1973)
10. H.J.Kolcer, H.H.Mickels. J.Chem. Phys.**50**,1762(1969)
11. A.L.Smith. J.Chem. Phys.**49**,4817(1968)
12. D.R.Scott, E.M.Greenawalt, J.C.Browne, F.A.Matsen. J.Chem. Phys. **44**,2981(1966)
13. J.C.Browne. Phys.Rev., **138**,9(1965)
14. R.Poshista, F.A.Matsen. Phys.Rev., **132**,307(1963)
15. T.M.Kereselidze, Sov.Phys.-JETP **42**,33(1976)
16. D.R.Bates, R.H.G.Reid. Advances in Atomic and Molecular Physics V.IV.New York and London. Academic Press, 1968
17. T.M.Kereselidze, B.I.Kikiani. Sov. Phys.-JETP 60,423(1984)
18. L.D.Landau, E.M.Lifshitz. Quantum Mechanics: Non-Relativistic Theory. New York: Pergamon,1977

ს. დიბო, თ. კერესელიძე, ი. ნოსელიძე

ჰელიუმის ორი მეტასტაბილური ატომის კვაზისტაბილური სისტემის შესახებ

დასკვნა

ცნობილია, რომ ჰელიუმის ორჯერ იონიზებული მოლეკულა He_2^{++} კვაზი-სტაბილური სისტემაა, რომლის დაშლისას ორ H_2^+ იონად გამოიყოფა დაახლოებით 9 ელ-ვოლტი ენერგია. ქიმიურ მასშტაბში ეს დიდი ენერ-გიაა. ამიტომ აღნიშნული სისტემა, შესაძლოა, ყოფილიყო ენერგიის კარ-გი აკუმულატორი. იმის გამო, რომ He_2^{++} კვაზიმოლეკულა დამუხტულია, მისი დაგროვება მნიშვნელოვანი რაოდენობით არ ხერხდება.

წინამდებარე სტატიაში განხილულია საკითხი: ხომ არ შეიძლება ორი ელექტრონის დამატებით He_2^{++} კვაზიმოლეკულა გავხადოთ ნეიტრალური ისე, რომ მან შეინარჩუნოს დაშლის დიდი (ქიმიურ მასშტაბში) ენერგია? ამ კითხვაზე პასუხის გასაცემად გამოთვლილია ჰელიუმის ორი მეტასტა-ბილური ატომისგან შემდგარი სისტემის ენერგეტიკული თერმები ბირთვებ-შორის საშუალო და მცირე მანძილებზე. მიღებულია, რომ ტრიპლეტურ მდგომარეობაში მყოფი ჰელიუმის ორი ატომისაგან შემდგარი კვაზიმოლე-კულის $^3\Sigma_u^+$ ენერგეტიკულ თერმს გააჩნია მინიმუმ R = 1.5a_0 ბირთვებ-შორის მანძილზე და მაქსიმუმ, როდესაც R = 2.0a_0. მინიმუმ მოთავსებუ-ლია იზოლირებული ატომების ჯამურ ენერგიაზე მალცა 10,8 ელ-ვოლტ-ით. ეს ნიშნავს, რომ ორი He(^3S) ატომისაგან შემდგარი კვაზიმოლეკულის დაშლისას გამოიყოფა არანაკლებ 10 ელ-ვოლტი ენერგია.

გამოკვლეული ენერგეტიკული თერმ მინიმუმის არეში გადაიკვეთება თერმების მთელი სერიით, რასაც გარდა ზემოთ განხილული დაშლის არხისა, მივყავართ დისოციაციის ისეთი არხების არსებობასთან, რომ-ლებიც ხასიათდება დაშლის მცირე ენერგიებით. ამრიგად, სტატიაში დასმულ კითხვაზე ცალსახა პასუხის გასაცემად აუცილებელია, ჩატარდეს დამ-ატებითი კვლევა, რაც იმას ნიშნავს, რომ უნდა შეფასდეს თერმების გადაკვეთით განპირობებული პრედისოციაცის ალბათობები.

INVESTIGATION OF DIRECT NUCLEAR PROCESSES INVOLVING THE LIGHTEST NUCLEI

J. Mebonia, P. Saralidze , K. Salukadze ,
G. Skhirtladze, M. Abusaini*

ABSTRACT. We offer a unified microscopic unitary approach of investigating direct nuclear processes involving the lightest nuclei. We prove, that having specific kinematic conditions the mechanism of compound processes may be brought to consecutive three-body processes. While constructing three-particle amplitudes it is necessary to save their unitary properties, then the possibility of multiple scattering may be neglected. The solution of complex many-particle problems can be simplified in this case. Concrete calculations for elastic and quasi-elastic processes have been carried out: $N+d \rightarrow N+d$, $N+d \rightarrow N+N+N, d+d \rightarrow d+N+N, t+d \rightarrow t+N+N$. The obtained results satisfy the agreement of theory with experiment, that indicates the ability of the offered approach to be used even for investigation of the other complex processes.

1. Introduction

Three-body problem in final state represents a powerful facility to provide valuable information on the basic nuclear problems. Here arise basic principle difficulties associated with many-particle problems. We mean both writing the correct equations and solving them. Therefore, Faddeev integral equations [1] contributed not only to high progress of three-body theory, but also gave the possibility to find more consecutive approach to complex processes.

The so-called reactions of quasi-elastic scattering (RQS) play an important role among three-body (fragments) nuclear problem in the final state in nonrelativistic energies region (further only such cases would be examined). Systematic investigation of RQS for the last ten years brought significant successes. Improvement of measurement methods made the kinematic region of observation wider, that allowed us to obtain more reliable experimental results . Faddeev equations made possible to substantiate various

45

approximate methods of investigation, which helped to carry out more precise numerical calculations.

The overwhelming majority of RQS proceeds in many-fragment processes. As a rule, coming into the corresponding matrix elements of two fragment off-shell amplitudes are defined via experimental data of their free scattering. It is possible, when the off-shell effects are completely neglected, or when phenomenological potential of two fragments is applied. However, it is quite possible, that at not very low energies, the effect of microscopic description of interacting fragments such as many-particles consisting of nucleons will become essential. It is clear, that investigation of RQS on the basis of microscopic description of mechanism of reaction should be started with processes involving the lightest nuclei. These processes are: $d+d{\rightarrow}d+p+n$, $t+d{\rightarrow}t+p+n$, etc.

Before studying these reactions at microscopic level, it is necessary to work out the method on simpler process. Thus, such process is nucleon-deuteron scattering with two possible channels in the final state: $N+d{\rightarrow}N+d$, $N+d{\rightarrow}3N$.

The purpose of present paper is a unified theoretical microexamination of RQS, that involves the lightest nuclei, such as processes $N+d{\rightarrow}N+d$, $N+d{\rightarrow}3N$, $d+d{\rightarrow}d+p+n$, $t+d{\rightarrow}t+n+p$. The starting point of our approach is the statement, that in all the cases with proper selection of kinematic conditions three-body mechanism can play the determining role.

2. Elastic scattering

With the discovery of Faddeev equations Nd elastic scattering came to be studied first [2-10]. The problem can be solved in closed form for any realistic nucleon-nucleon potential. These potentials allowing to obtain the same results for physical two-nucleon amplitudes in general can be brought various off-shell amplitudes. Therefore, the solution of Faddeev's equations with high accuracy for various energies requiring to involve various partial off-shell amplitudes, comparing theoretical and experimental results may show an additional advantage of individual NN potentials. In this respect, besides differential cross section useful information gives the so-called polarizing asymmetry (analyzing power).

There is another important possibility, connected with the investigation of Nd scattering. Here we can reliably examine various approximate methods of three-body solution. The main advantage of each after being mathematically and physically grounded the solution must be conveniency and simplicity. One of these methods, three-body impulse approximation was suggested in [11]. Its concrete realization has been carried out by two various variants. The first is three-body unitary impulse approximation (TUIA) [12], which represents an outcome of unitary expansion of scattering amplitudes. TUIA does not include additional parameters, except the parameter of infinitesimal with the accuracy of which the approximate T-matrix satisfies the condition of three-body unitarity. The second variant is three-body impulse approximation with cut-off (TIAC) [13]. Although it represents the result of intuitive approach and theoretically is less substantiated, still it is simple and it was found to be quite effectively applied to RQS [14,15].

In TIAC it is proved, that in individual cases when particle 1 scatters on bond system (2,3) the principal contribution may be carried by the mechanism of single-collision of two-particle. In this case the third particle must be far enough from the "events". That leads to cutting-off of the Fourier-transform radial function of bond state $\varphi(r)$: $\Psi(r) \rightarrow \Psi(q,r)$,

where
$$\Psi(q,r) = \sqrt{2/\pi} \int_R^\infty r^2 dr \varphi(r) \frac{\sin(qr)}{qr} \qquad (1)$$

the cut-off radius must be no less than the Debroill wave length λ of relative motion of particle 1 and (2,3) and it is easily connected with magnitude of corresponding impulse $\bar{\omega}_1$ (Fig.1).

$$R = \frac{C}{|\bar{\omega}|} \qquad (2)$$
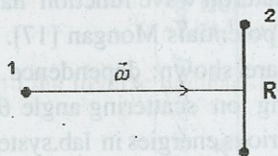
Fig.1

where C - constant, defines the performance of inequality $\lambda \leq R$.

Later the practical equivalent of two variants was proved [16]. Therefore,

taking the perspective of generalization into account, in present paper we use technically more convenient TIAC, as effective alternative of theoretically more substantiated TUIA.

On the basis of the stated above the differential cross section of Nd elastic scattering in the centre mass system is defined as follows:

$$\frac{d\sigma}{d\Omega} = (2\pi)^4 \frac{2m^2}{27} \sum_{spins} |M|^2, \tag{3}$$

where

$$M = \hat{A} \sum_{\alpha\beta=12.31} \int d\bar{q} \Psi_d^*(\bar{p}) t_{\alpha\beta}(\bar{\xi}, \bar{\eta}, \varepsilon) \Psi_d(\bar{P}_0) \tag{4}$$

$$\bar{p} = -\frac{\bar{k}}{2} - \bar{q}, \qquad\qquad \bar{p}_0 = -\frac{\bar{k}_0}{2} - \bar{q}$$

$$\bar{\xi} = \bar{k} + \frac{\bar{q}}{2}; \qquad\qquad \bar{\eta} = \bar{k}_0 - \frac{\bar{q}}{2} \tag{5}$$

$$\varepsilon = \frac{3}{4m}(\bar{k}^2 - \bar{q}^2) - Q$$

where $\hat{A}$ - operator of antisymmetrization by identical particles; $t_{\alpha\beta}$ - two-nucleonic T-matrix; Ψ_d-overall wave function of deuteron; m-mass of nucleon; Q- binding energy of deuteron; $\bar{k}(\bar{k}_0)$-impulse of incident nucleon before(after)scattering; the summation in (3) occurs by spin projections of nucleon and deuteron before and after scattering ; in explicit form they appear after partial expansion of Ψ_d, $t_{\alpha\beta}$.

We use unit system $\hbar = C = 1$, where in detailed calculations the two-body off-shell T-matrix and the radial part of deuteron wave function have been constructed using nonlocal and separable potentials Mongan [17]. In Figs. 2-4 there the results of our calculations are shown: dependence of differential cross section of Nd elastic scattering on scattering angle $\theta_{c.m}$ with corresponding experimental data for three various energies in lab.system 9 , 14.1 and 18 mev. The solid curve and left scale correspond to calculation of TIAC , the dashed curve and right scale are analogous to calculation without cut-off. Experimental points (left scale) were taken from [7,18]. In calculations we have restricted to $\ell = 0$ phases, i.e. we have taken into account only terms $^1S_0$, $^3S_1$.
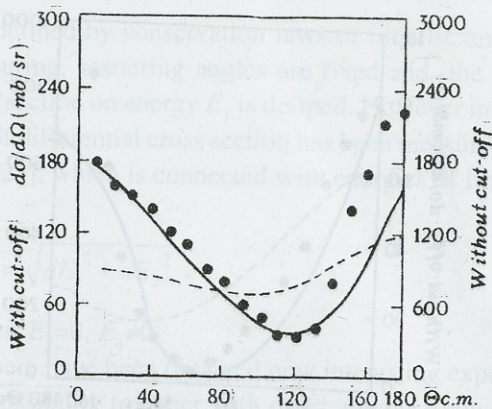
48

Fig.2. Dependence of differential cross section of elastic scattering of d(n,n)d on scattering angle $\theta_{c.m}$ in system of centre mass at energy of incident neutrons E= 9 mev in lab, system-Where the solid curve and left scale ale corresponding to calculation by TIAC, dashed curve and right scale are-analogous to calculation without cut-off Experimental data (left scale) were taken from Ref. [1 8].

It is easy to note, that the cut-off significantly improves the agreement of theory with experiment, especially by magnitude. However, the quantitative discrepancy still remains. But these discrepancies were expected, since we are examining an approximate method to solve the problem. Moreover , it
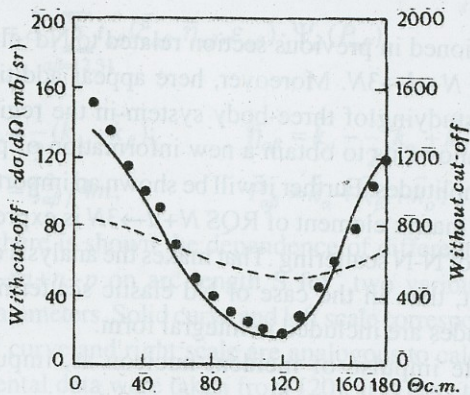
Fig. 3. The same as fig. (2), but for energy E=14.1 mev. Experimental data were taken from Ref. [7].

4.
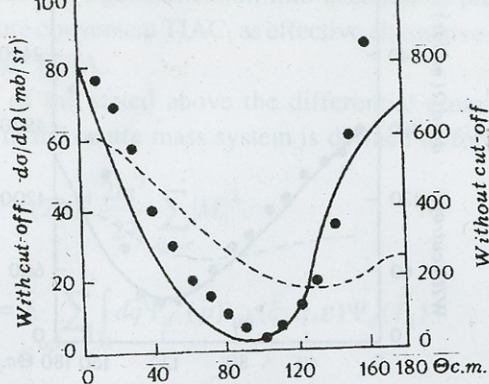
Fig. 4. The same as fig. (2), but for energy E=18 mev. Experimental data were taken from Ref. [8].

should be noted , that although we consider scattering at low energies, still other phases ($\ell \succ 0$) might noticeably affect on final results, as those phases are defined by off-shell T-matrix elements. Finally it should be noted that precise Faddeev's calculations, of course, give better agreement of theory with experiment.

3.Reaction of quasi-elastic scattering $N+d \rightarrow 3N$

All the mentioned in previous section related to Nd elastic scattering is true for reaction $N+d \rightarrow 3N$. Moreover, here appear additional possibilities connected with studying of three-body system in the region of continuous spectrum. This allows us to obtain a new information of properties of two-body off-shell amplitudes. Further it will be shown an important circumstance, that in TIAC the matrix element of RQS $N+d \rightarrow 3N$ is expressed via half-off-shell amplitudes of N-N scattering .That makes the analysis of N-N interaction more transparent, than in the case of Nd elastic scattering, where the NN off-shell amplitudes are included in integral form.

Let's denote impulse of incident nucleon as, impulses of scattered nucleons $\vec{k}_1, \vec{k}_2, \vec{k}_3$. Usually experiments are carried out in complanar geometry and dependence of differential cross section on scattering angles of two final nucleons and on energy of one of them is observed. The rest kinematic

50

magnitudes are defined by conservation laws of impulse and energy. As a rule, while measuring, scattering angles are fixed and the dependence of differential cross section on energy E_1 is defined. However in previous years the dependence of differential cross section has been measured on so - called arc length S [19-23], which is connected with energies of final particles, as follows:

$$dS = \sqrt{dE_1^2 + dE_2^2} \; . \tag{6}$$

where $S=0$, when $E_2=0$, $E_1 \neq 0$.

As a result there have been obtained new interesting experimental data, which give the possibility together with other already known data to draw important theoretical conclusions.

Theoretical analysis of dependence of differential cross section of RQS $N+d \rightarrow 3N$ on energy E_1 within the scope of TIAC has been carried out in [14]. Here we continue this analysis for new experimental data-dependence of differential cross section on arc length S. In TIAC it is may be written as follows:

$$\frac{d^3\sigma}{d\Omega_1 d\Omega_2 dS} = \frac{8}{3}\pi^4 m^3 \frac{k_1 k_2^2}{K_o} \frac{dE_1}{dS} \frac{\sum_{spins} |M|^2}{|2k_2 - k_o \cos(\theta_2) + k_1 \cos(\theta_1 + \theta_2)|}, \tag{7}$$

where

$$M = \hat{A} \sum_{\alpha\beta=12,31} t_{\alpha\beta}(\vec{\xi}_{\alpha\beta}, \vec{\eta}_{\alpha\beta}, \varepsilon_{\alpha\beta}) \cdot \Psi_d(\vec{P}_{\alpha\beta}) \tag{8}$$

$$\vec{\xi}_{\alpha\beta} = \frac{1}{2}(\vec{k}_\alpha - \vec{k}_\beta); \qquad \vec{\eta}_{\alpha\beta} = \vec{k}_o - \frac{1}{2}(\vec{k}_\alpha + \vec{k}_\beta);$$
$$\varepsilon_{\alpha\beta} = \xi_{\alpha\beta}^2 / 4m; \qquad \vec{P}_{\alpha\beta} = \vec{k}_\alpha + \vec{k}_\beta + \vec{k}_o. \tag{9}$$

In Figs. 5-6 there is shown the dependence of differential cross section of reaction $n+d \rightarrow n+n+p$ on arc length S for two various collections of fixed kinematic parameters. Solid curve and left scale correspond to calculation by TIAC, dashed curve and right scale are analogous to calculation without cut-off. Experimental data were taken from [20]. It is easy to note, that here the features of differential cross section theoretically pass better, than in case of Nd elastic scattering. It might be attributed, as it has already been
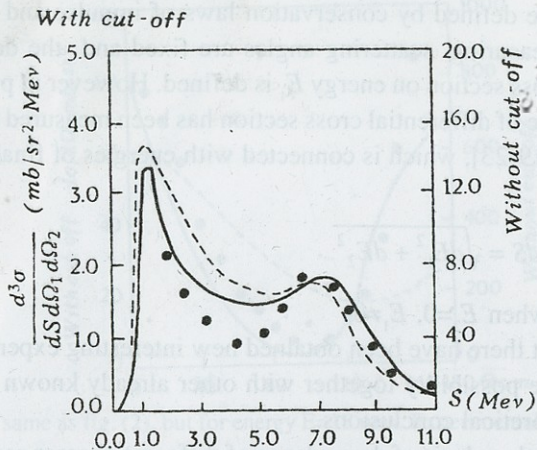
Fig. 5. Dependence of differential cross section of d(n,2n)p on arc length S at energy of incident neutrons E_0=13 mev in lab, system, and scattering angles of final neutrons $\theta_1 = 17°$, $\theta_2 = 90°$. Where the solid curve and left scale are corresponding to calculation by TIAC, the dashed curve and right scale are analogous to calculation without cut-off. Experimental data (left scale) were taken from Ret. [20].
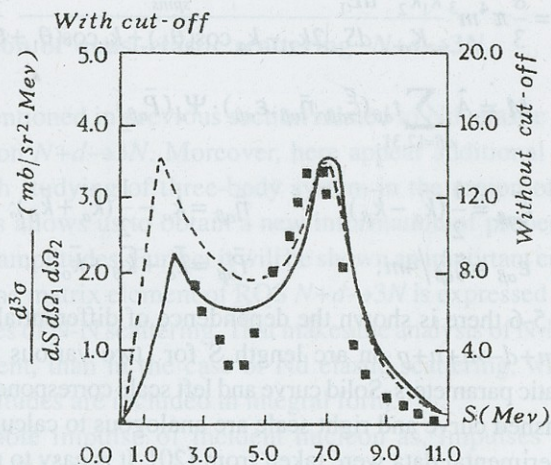

Fig. 6. The same as fig. (5) but for angles $\theta_1 = 25°$, $\theta_2 = 90°$.

mentioned above, that the matrix element of RQS(8) is defined immediately via half-off-shell amplitude of N-N scattering. Therefore, the contribution of high phases $\ell > 0$ here could be less important. However the statement of previous section, that the cut-off basically affects the magnitude of cross section, is proved as well in the present case.

4. Reaction of quasi-elastic scattering $d+d{\to}d+N+N$

As mentioned above, the process of Nd scattering represents great interest, because it serves to be a testing ground for understanding the mechanism of more complicated RQS involving three composite fragments. We consider, that the same role for processes involving four fragments could be played reaction $d(d,dN)N$, which in any way represents an interesting problem in the region of direct nuclear reaction.

Theoretical investigation of RQS $d(d,dN)N$ basically is introduced in two directions [24-33]. Some authors try to reduce mechanism of reactions to two-particle examination on basis of routine impulse or Bohrn approximation [28-32]. In this case there is obtained wider quasi-elastic peak and several times increased cross section. The agreement of theory with experiment is achieved by taking into account possible "distortions", introduction of the cut-off parameter or just normalized factor. More interesting is developed in [33] four-particle approach for $d(d,dN)N$ reaction, based on the known system of integral equations Alta, Graccberger and Candas [34]. However, due to technical difficulties of selected approach concrete calculations have been carried out in the simplified variant. At relatively low energies (~20 mev) the form of experimental cross section is transferred well, however their magnitude is increased by 2-3 times. As the energy goes up (~50 mev) the agreement of theory with experiment is improved by magnitude, but deteriorated by form .

From the theoretical point of view in the present paper the suggested approach for $d(d,dN)N$ takes an interim place between approaches which are mentioned above. We consider, that although $d(d,dN)N$ reaction represents a real four-particle problem in nonrelativistic region of scattering , nevertheless while carrying out specific kinematic conditions decisive role can be played by three-body mechanism. Such condition would be carried out in the region

of the so-called quasi-elastic kinematics, when one of the final nucleons in lab. system represents "spectator", carrying low kinetic energy in comparison to an average kinetic energy of nucleon in deuteron. We can consider that this nucleon-spectator either does not take part in the process, or its role is insignificant. Then the mechanism of $d(d,dN)N$ reaction could be reduced to two consecutive three-body processes: deuteron-projectile as unified particle quasi-elasticity scatters on two-nucleon system nucleus-target, occuring amplitude of Nd collision could be described within the scope of three-body scattering (it is easy to show, that the breakup of deuteron-projectile in the region of quasi-elastic kinematics is slightly probable).

Let's assign to nucleons of deuteron-projectile numbers 1, 2, to nucleons of deuteron-target 3 ,4. Then on the basis of what has been mentioned above it is clear, that the cut-off radius for wave function of deuteron-target R_1 is defined by impulse of relative motion of deuterons $\bar{\omega}_1$, the cut-off radius for wave function of deuteron-projectile R_2 is defined by impulse of relative motion of deuteron-projectile and the nucleon of deuteron-target $\bar{\omega}_2$, with which interaction occurs (Fig.7) .

$$\begin{array}{cc} \underset{\displaystyle 2}{\overset{\displaystyle 1}{\big|}} \quad \bar{\omega}_2 \atop R_2 \qquad \xrightarrow{\bar{\omega}_1} & \underset{\displaystyle 4}{\overset{\displaystyle 3}{\big|}} \quad R_1 \end{array} \tag{15}$$
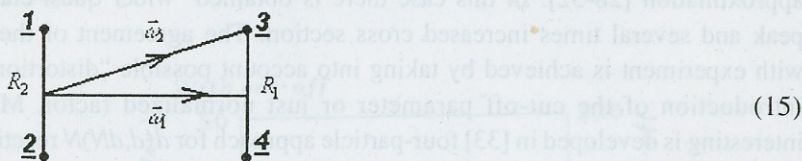
Fig.7

Experiments by $d(d,dN)N$ reaction usually are carried out in complanar kinematics and the dependence of differential cross section on energy of final deuteron E_d (or nucleon's E_3) at fixing scattering angles of deuteron θ_d and one nucleon θ_3 are studied. The corresponding expression can be written as follows:

$$\frac{d^3\sigma}{d\Omega_3 d\Omega_d dE_d} = (2\pi)^4 \cdot \frac{4m^3 k_d k_3^2}{9K_o} \cdot \frac{\sum\limits_{spins}|M|^2}{\left|2k_3 - k_o\cos(\theta_3) + k_d\cos(\theta_3 + \theta_d)\right|} \tag{10}$$

where $M = \hat{A} \cdot \sum_{\substack{\alpha=1.2 \\ \beta=3.4}} \Psi_d(\vec{P}_\beta) \cdot \int \Psi_d^*(\frac{1}{2}\vec{k}_d - \vec{q}) \cdot t_{\alpha\beta}(\vec{\xi},\vec{\eta},\varepsilon_\beta) \cdot \Psi_d(\frac{1}{2}\vec{k}_o - \vec{q})d\vec{q}$ (11)

$$\vec{p}_\beta = \vec{k}_\beta + \vec{k}_d - \vec{k}_o; \qquad \vec{\xi}_\beta = \frac{1}{2}(\vec{k}_d - \vec{k}_\beta - \vec{q}); \qquad \vec{\eta}_\beta = \vec{k}_o - \frac{1}{2}(\vec{k}_d + \vec{k}_\beta + \vec{q})$$

$$\varepsilon_\beta = \frac{1}{4m}\left\{2k_d^{\,2} + \vec{k}_\beta(\vec{k}_\beta + \vec{q} - \vec{k}_o) - 3q^2 - \vec{k}_o(\vec{k}_o - \vec{q})\right\} - Q \qquad (12)$$

$\vec{k}_o, \vec{k}_d$ are impulses of incident and scattered deuterons ; $\vec{k}_\beta$ -impulse of final nucleon, with which the deuteron-projectile interacts. All the other designations, as well as the calculation procedure of the previous sections remain valid.

In Figs. 8,9 there is shown the dependence of differential cross section of $d(d,dN)N$ reaction on energy E_d for various collections of fixed kinematic parameters. Solid curve and left scale correspond to calculation by TIAC, dashed curve and right scale are analogous to calculation without cut-off. Experimental data (left scale) were taken from [32,33]. We consider, that we have achieved quite a good agreement of theory with experiment ,that is
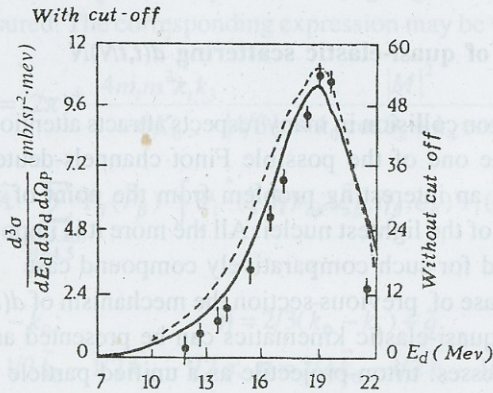
Fig. 8. Dependence of differential cross section of $d(d,dn)p$ on energy of final deutrons E_d at energy of inci deutrons in lab, system E_o=27.5 mev and scattering angles $\theta_1 = 19°$, $\theta_v = 50.7°$ Where the solid curve left scale are corresponding to calculation by TIAC, dashed curve and right scale are analogous to calculi without cut-off. Experimental data (left scale) were taken from Ref.[33].

55
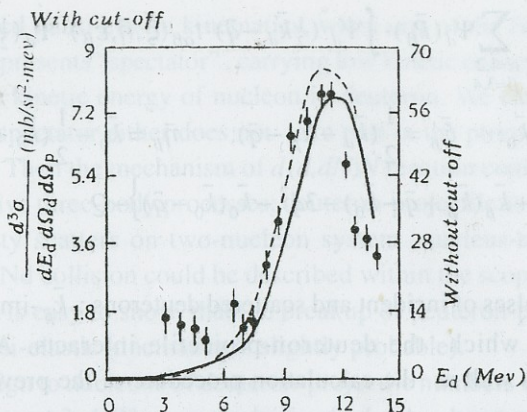
Fig. 9. The same as fig. (8), but at $E_0 = 20{,}7$ mev, $\theta_d = 19°$, $\theta_n = 50.7°$. Experimental data were taken from Ref. [32].

in accord with analogous preliminary results for other kinematic parameters [35]. It was unexpected, that matrix element (11) includes two-nucleon off-shell amplitudes, that could even at low energies be dependent on high phases $\ell \succ 0$.

5. Reaction of quasi-elastic scattering $d(t,tN)N$

Triton-deuteron collision in many respects attracts attention of physicists. Here we examine one of the possible Finot channels-deuterons breakup, which represents an interesting problem from the point of view of quasi-elastic scattering of the lightest nuclei. All the more it is important to test the suggested method for such comparatively compound case

As in the case of previous section the mechanism of $d(t,tN)N$ reaction in the region of quasi-elastic kinematics can be presented as a set of two consecutive processes: triton-projectile as a unified particle scatters quasi-elastically on two-nucleon nucleus-target system, appearing amplitude of NT of collision is explained within the scope of single elastic scattering of the nucleon on each nucleon of triton.

Let's assign to nucleons of triton-projectile numbers 1, 2 and 3, to nucleons of deuteron-target 4, 5. Let's denote $\bar{\omega}_1$ - impulse of relative motion

of colliding nuclei. $\bar{\omega}_2$ - impulse of relative motion of triton and one of the nucleons of nucleus-target (Fig. 10) . Then on the basis of what has been mentioned above it is clear, that the cut-off radius for deuteron wave function is defined by impulse $\bar{\omega}_1$. Moreover we must cut-off the wave function of motion of one triton's nucleon (e.g. 1), with which nucleon of nucleus-target (e.g. 4) interacts relatively to other two nucleons (2,3). In the capacity of such function variation function of triton, which has right asymptotic was chosen [36]. Now the cut-off radius is defined by impulse $\bar{\omega}_2$.
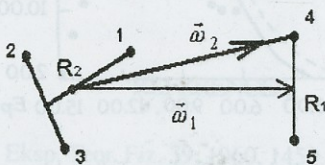
Fig. 10.

Experiments on $d(t,tN)N$ reaction are usually carried out in complanar kinematics and the dependence of differential cross section on energy of one of the final nucleons E_4 (or triton) and scattering angles of nucleon and triton θ_4, θ_t are measured. The corresponding expression may be written as follows:

$$\frac{d^3\sigma}{d\Omega_t d\Omega_4 dE_4} = (2\pi)^4 \cdot \frac{4 m_t m^2 k_t k_3}{6 K_0} \cdot \frac{|M|^2}{|4/3 k_t - k_0 \cos\theta_t + k_4 \cos(\theta_t + \theta_4)|} \quad (13)$$

where, $M = \hat{A} \cdot \sum_{\substack{\alpha=1,2,3 \\ \beta=4,5}} \Psi_d(\vec{P}_\beta) \cdot \int \Psi_t^*(\vec{\xi},\vec{\eta}) t_{\alpha\beta}(\vec{\xi}_\beta,\vec{\eta}_\beta,\varepsilon_\beta)\Psi_t(\vec{\xi},\vec{q})d\vec{\xi}d\vec{q}$ \quad (14)

$$\vec{p}_\beta = \vec{k}_t + \vec{k}_\beta - \vec{k}_0; \qquad \vec{\eta} = 2/3(\vec{k}_0 - \vec{k}_t) + \vec{q}$$

$$\vec{\xi}_\beta = 1/2\,\vec{k}_t - 1/3\,\vec{k}_0 - 1/2\,\vec{k}_\beta - 1/2\,\vec{q}; \quad \vec{\eta} = 2/3\,\vec{k}_0 - 1/2\,\vec{k}_t - 1/2\,\vec{k}_\beta - 1/2\,\vec{q}$$

$$\varepsilon_\beta = 1/m\left\{4/3 k_0^2 + k_t^2 + k_\beta^2 + \xi^2 + q^2 - 4/9 \vec{k}_0\vec{k}_t - 2/3 \vec{k}_0\vec{k}_t + \vec{k}_t\vec{k}_\beta - \vec{k}_t\vec{q} + \right.$$

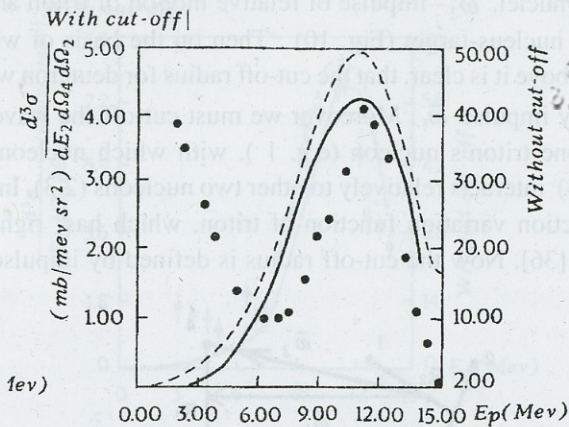$$\left. + 4/3 \vec{k}_0\vec{q} - \vec{k}_\beta\vec{q}\right\} - Q_t,$$

57

Fig. 11. Dependence of differential cross section of $d(t,tp)n$ on energy of final protons E_p at energy of incident tritons $E_0=35$ mev and scattering angles $\theta_p = 50°$, $\theta_t = 20°$. Where the solid curve and left scale are corresponding to calculation by TIAC, dashed curve and right scale are -analogous to calculation without cut-off .Experimental data (left scale) were taken from Ref. [36].

m_t - mass of triton; $\vec{k}_0, \vec{k}_t$ -impulses of incident and scattered tritons; Q_t - binding energy of triton; Ψ_t - tritons wave function. All the other designations, as well as the calculation procedure of previous sections remain valid.

In Fig.11 there is shown the dependence of differential cross section $d(t,tN)N$ reaction on energy of final proton E_p while values of other parameters are fixed. Solid curve and left scale correspond to calculation by TIAC, dashed curve and right scale are analogous to calculation without cut-off. Experimental data (left scale) were taken from [36]. The theory quite satisfactory describes the quasi-elastic region ($E_p \sim 6$-15 mev) of scattering. As regards to nonquasi-elastic region ($E_p \prec 6\ mev$), here it may seem that we must take into account the resonance mechanism of reaction. Although even in this case the agreement of theory with experiment could be achieved by form. It is necessary to introduce normalized coefficient [37].

Thus, the comparatively simple suggested theoretical approach TIAC allows to make unified microscopic description of processes of quasi-elastic scattering involving the lightest nuclei. It is interesting that the parameter of

58

cut-off, which represents a quantity of one order, practically unsignificantly depends on concrete reactions. The obtained results allow us to conclude, that with realization of specific physical conditions the mechanism of compound nuclear reaction could essentially be simplified if the possibility of multiple rescattering is neglected, but the unitary property of scattering amplitudes must be saved. That once again underlines the fundamental role of unitarity, while investigating many-particle problems.

Tbilisi I. Javakhishvili State University

REFERENCES:

1. L.D. Faddeev. Zh. Eksp. Teor. Fiz. **39**, 1960, 1459.
2. P. Doleschall. Nucl. Phys. **A 220**, 1974, 491.
3. M. Sawada. et al. , Phys.Rev. **C 27**, 1983, 1932.
4. T. Sasakawa, H.Okuno, S.Jshikawa, T.Sawada. Phys.Rev. **C 26**, 1982, 42.
5. W. Kluge, R.Schlufter, W.Ebenhoh. Nucl.Phys. **A 228,** 1974, 29.
6. W. Ebenhöh. Nucl.Phys. **A 191,** 1972, 97.
7. T.Takemiya. Progr.Teor. Phys. **74**, 1985, 301.
8. W.Glöckle, H.Witala. Nucl.Phys. **A 525,** 1991, 48.
9. J.Cub. et al., Few-Body Systems, **6**, 1989, 151.
10. W.Tornow. et al. Phys.Rev. **C 27**, 1983, 2439.
11. J.V.Mebonia. Phys.Lett, **B 48,** 1974, 196.
12. T.J.Kvaratskelia, J.V.Mebonia. Phys.Lett. **B 90,** 1980, 17.
13. O.L. Bartaia. J.V. Mebonia. Phys. Atomic nucl. **33**, 1981, 1987.
14. T.J.Kvaratskelia, J.V.Mebonia. J.Phys.G.:Nycl.Phys. **10,** 1984, 1677.
15. T.J.Kvaratskhelia, J.V.Mebonia. Repor. FS. GSSR, **110,** 1983, 285.
16. T.J.Kvaratskhelia, J.V.Mebonia, Repor. FS. GSSR, **136,** 1989, 53.
17. Th. Mongan. Phys. Rev. **178,** 1968, 1957.
18. P.Schwartz. et al. Nucl.Phys. **A398,** 1983, 1.
19. M. Karus. et al. Phys. Rev. **C31,** 1985, 112.
20. J. Strate. et al. Nucl. Phys. **A501,** 1989, 51.
21. G. Rauprich. et al. Nucl. Phys. **A535,** 1991, 313.
22. K. Gebhardt. et al. Nucl. Phys. **A561,** 1993, 232.
23. J. Zejma. et al. Phys. Rev. **C55,** 1997, 42.
24. P. Donovan. Rev. Mod. Phys. **37,** 1965, 501.
25. T. Tanabe. J. Phys. Soc. Jap. **25,** 1968, 21.
26. H. Bruchmann. et al. Z. Phys. **217,** 1968, 350.

27. W. Von Witsch. et al. Phys. Rev. **C2**, 1972, 2144.
28. B.E.Corey. et al. Nucl. Phys. **A174**, 1971, 478.
29. J.P. Burg. et al. Nucl. Phys. **A183**, 1972, 126.
30. V. Valkovic et al. Nucl. Phys. **A183**, 1972, 126.
31. D.J. Bonbrite. et al. Phys. Rev. **C8**, 1973, 114.
32. G.E. Djaloeis. et al. Nucl. Phys. **A273**, 1976, 29.
33. T.E. Mdlalose. et al. Nucl. Phys. **A457**, 1988, 273.
34. S.A. Sofianos. et al. Phys.Rev. **C32**, 1985, 400.
35. V.Sh.Jikia, TJ.Kvaratskhelia, J.V. Mebonia. Phys.Atomic nucl. **58**, 1995, 27.
36. J. Slaus. et al. Nucl. Phys. **A286**, 1977, 67.
37. S. Blagus. et al. Phys. Rev. **C44**, 1991, 325.

ჯ. მებონია, პ. სარალიძე, კ. სულაკაძე, გ. სხირტლაძე, მ. აბუსინი

პირდაპირი ბირთვული პროცესების შესწავლა მსუბუქი ბირთვების
გათვალისწინებით

დასკვნა

დამტკიცებულია, რომ მოცემული კინემატიკური პირობებისას მექანიზმში
რთულ პროცესებში შეიძლება დაიყვანიდ იქნეს სამ ნაწილაკობრიგ პრო-
ცესებზე, მაშინ უნიტარული თვისებები სამნაწილაკობრივი ამპლიტუდისა
ინახება და იმავდროულად მრავალჯერადი დაჯახებები შეიძლება უგ-
ულებელყვოთ და რთული პროცესების გადაწყვეტა მარტივდება.

NON-LINEAR α _ ω DYNAMO WAVES WITH TEMPERATURE DEPENDENT TURBULENT DISSIPATION AND α COEFFICIENTS

A.D.Pataraya, T.A.Pataraya, B.M. Shergelashvili

ABSTRACT. Non-linear α–ω dynamo waves are investigated, when in the Magnetohydrodynamic (MHD) equations the dependence of α and turbulent dissipation coefficients on the temperature is taken into account. The calculations are done in a local Cartesian coordinate system, in which gravity is ignored. The perturbed non-linear MHD equations are investigated also. In this case the zero, the first and the second order harmonics of Dynamo waves are taken into account when dynamo numbers are close to unity (Weakly Non-linear Dynamo Waves). In such ≈imation the stationary solution of the non-linear equation for amplitude is found and stability of this solution is investigated .

1. Introduction.

A comprehensive inroduction in the dynamo waves theory is presented in many papers [1-4]. Kinematic mean-field dynamo and linear α–ω dynamo waves were first treated in [1,5]. Non-linear dynamo waves were ≈imately investigated. For example, there was solved equation of induction, where α coefficient depends on magnetic field [6,7]. Then non-linear dynamo waves were investigated by means of equtions of induction and motion with force of Lorenz [8,9]. The aim of the present work is to self-consistently solve a set of equeations for non-linear dynamo waves, derived from the MHD equations of motion, continuity, magnetic induction and energy, where α and dissipation coefficients depend on the temperature. The problem was solved by using of perturbation theory, preserving the terms representing the zero, the first and the second harmonics of the dynamo waves. We consider the medium as an ideal gas $p=\rho RT/\mu$, where p and ρ are pressure and density, respectively; R is ideal gas constant and μ is the average particle mass and T is the temperature of medium. The structure of the paper is as follows: in section 2 the perturbation theory is discussed; in section 3 the non-linear

5.

dynamo waves equations are discussed taking into account only the first harmonics of the dynamo waves for the components of the magnetic field induction and zero order harmonics for the temperature; in the section 4 a fuller set of non-linear dynamo equations is given, including the terms of the first harmonics for the magnetic field induction, the second harmonics for the density and components of velocity and zero and the second harmonics for the temperature; in section 5 the results are discussed.

2. The Perturbation Theory

We investigate dynamo waves by means of the MHD Equations [1,4,10,11]: Equation of Induction

$$\frac{\partial \vec{B}}{\partial t} = rot[\vec{V}\vec{B}] - rot(\eta rot\vec{B}) + rot\vec{E}. \tag{1}$$

Equation of Motion

$$\frac{\partial \vec{V}}{\partial t} + (\vec{V}\nabla)\vec{V} = -\frac{\nabla p}{\rho} + \frac{[rot\vec{B}\vec{B}]}{4\pi\rho} - \rho^{-1}\nabla(2\rho v\vec{S}). \tag{2}$$

Equation of Energy

$$\frac{\partial e}{\partial t} + (\vec{V}\nabla)e = -\frac{p div\vec{V}}{\rho} + \frac{(\nabla \rho \chi \nabla e)}{\rho} + \frac{\eta(rot\vec{B})^2}{4\pi\rho} + 2vS^2 + Q. \tag{3}$$

Continuity equation

$$\frac{\partial \rho}{\partial t} + div(\rho\vec{V}) = 0. \tag{4}$$

Here $\vec{B}$ and $\vec{V}$ are magnetic field and velocity. In the equation (1) $\vec{E} = \alpha B_x \vec{i}_x$ for the α–ω dynamo wave, az'and $\vec{i}_x$ is a unit vector along the x axis. In the equations (2),(3) we write the components of tensor $\vec{S}$ in the following form:

$$S_{ij} = 0,5\left[\frac{\partial V_i}{\partial x_j} + \frac{\partial V_j}{\partial x_i} - \frac{2}{3}\delta_{ij}\frac{\partial V_l}{\partial x_l}\right]. \tag{5}$$

Here $x_1 = x$, $x_2 = y$, $x_3 = z$, $V_1 = V_x$, $V_2 = V_y$, $V_3 = V_z$.

The calculations are made in the local Cartesian coordinate system with

62

origin immovable in regard to the centre of the Sun. The z-axis is directed locally orthogonal to the Solar surface, the y-axis is directed toward north and is locally tangent to the meridian and the x-axis is directed toward west toroidally. In the MHD equations all the functions f can be given as follows: $f = f_0 + f'$. Here f_0 is unperturbed term of the function f band f' is the perturbed term. Let us consider the unperturbed term of the magnetic induction as equal to zero and the unperturbed velocity $\vec{V}_0 = (V_{x0} + yV_{xy} + zV_{xz})\vec{i}_x$, where V_0, V_{xy}, V_{xz} are constants.

In the equation (3) we include a cooling term Q of the form [10,11]:

$$Q = \sigma(e - e_0). \tag{6}$$

where σ is a thermal relaxation rate, e is the internal energy per unit mass and for the perfect gas $e = p/[(\gamma-1)\rho]$, and e_0 is unperturbed meaning of the function e. In the equations (1-3) we have taken into account the dependence of α and dissipative coefficients on the temperature: $\alpha = \alpha_0(1 + T'/T_0)^{n_4}$; magnetic diffusion $\eta = \eta_0(1 + T'/T_0)^{n_1}$; kinematic viscosity $v = v_0(1 + T'/T_0)^{n_2}$; temperature condactivity $\chi = \chi_0(1 + T'/T_0)^{n_3}$.

Note, that our further investigation for the Sun is valid only for thin spherical layer case, as it was supposed for linear dynamo waves [1,5]. Width of this layer is smaller than the local scale height in the lower convective zone. Hence, unperturbed density ρ_0 can be imately considered as constant. On the other hand for estimation of the unperturb pressure p_0 (temperature $T_0 = p_0\mu/(R\rho_0)$) we investigate the unperturbed equation (3)

$$\frac{\partial \rho_0}{\partial t} + (V_0 \nabla)\rho_0 = (\gamma-1)\rho_0 v_0 \left(V_{xy}^2 + V_{xz}^2\right) \tag{7}$$

Suppose that the pressure p_0 does not depend on the time. As it is known $p_0 \approx 10^{12}\ din/sm^2$, $v^0 \approx 10^{12}\ sm^2/sec$, $V_0 = \Omega R_\Theta$, $(V_{xy}^2 + V_{xz}^2) \leq \Omega^2$, $\rho_0 \approx 0.1\ gr/cm^3$. Here R_Θ is the radius of the Sun, Ω is angular frequency of the Sun rotation. Hence, from the equation (7) we can estimate the characteristic length l_0 of change of the pressure p_0: $l_0 \approx 5 \cdot 10^5 R_\Theta$. If we take into account dependence of p_0 only on the time, then we can estimate characteristic time t_0 of the pressure change as follows: $t_0 \approx 2 \cdot 10^5$ year. We have assumed, that y and z coordinates are satisfying following unequalities $|y| \ll R_\Theta$, $|z| \ll R_\Theta$, and time $t \ll 10^5$ year. Hence, we may consider p_0 as constant in the perturbed MHD equations, when the unperturbed equation (7) is valid. In the MHD

63

equations, we have considered perturbation functions of the temperature T', the density components ρ', x, y, z of the magnetic induction vector B'_x, B'_y, B'_z and velocity V'_x, V'_y, V'_z as follows:

$$T'/T_0 = U_0 + U_6 exp(i2\varphi) + C.C., \tag{8}$$

$$\rho'/\rho_0 = U_{14} exp(i2\varphi) + C.C., \tag{9}$$

$$B'_x = B_0 U_2 exp(i\varphi) + C.C., \tag{10}$$

$$B'_y = B_0 \Delta^{-1} k_z \omega U_4 exp(i\varphi) + C.C., \tag{11}$$

$$B'_z = - B_0 \Delta^{-1} k_y \omega U_4 exp(i\varphi) + C.C., \tag{12}$$

$$V'_x = U_8 exp(i2\varphi) + C.C., \tag{13}$$

$$(k_y V'_y + k_z V'z) \big/ \omega = U_{10} exp(i2\varphi) + C.C., \tag{14}$$

$$(k_y V'_y - k_z V'z) \big/ \omega = U_{12} exp(i2\varphi) + C.C., \tag{15}$$

$$\varphi = y k_y + z k_z + \delta\omega \int U_3 dt' + \delta\omega \int (1+U_0)^{0.5n_4} dt' + \varphi_0, \tag{16}$$

Here k_y, k_z are y,z components of the wave vector; $\omega=[0,5|\alpha_0\Delta|]^{0.5}$ is the frequency of the linear $\alpha-\omega$ dynamo wave; $\Delta=k_z V_{xy} - k_y V_{xz}$; $\delta=1$ when $\alpha_0\Delta>0$; $\delta=-1$ when $\alpha_0\Delta<0$; C.C. -means complex conjugate; $k^2=k_y^2+k_z^2$; B_0 is a constant quantity and is determined as a value of perturbed magnetic induction at $t=0$ moment; U_0, U_2, U_3 are real functions of the variable t; U_4, U_6, $U_8,\ldots$ are complex functions depending on the time; φ_0 is constant.

We have assumed, that all perturbed values f'in MHD equations do not depend on x coordinate $\delta f'/\delta x=0$. In the paper [12] the equations (1-16) are investigated supposing $\sigma_0=0$, $V'_x = V'_y = V'_z = 0$, $\rho'=0$. According to the equations (10-12) φ is the characteristic phase of oscillation of x,y,z components of the magnetic induction. For example, we have obtained the x component of the magnetic induction B'_x:

$$ReB'_x = 2B_0 U_2 \cos\varphi, \quad ImB'_x = 0 \tag{17}$$

From the equation (16) we can obtain the characteristic frequency of non-linear dynamo wave $\omega_n=-\partial\varphi/\partial t$:

64

$$\omega_n = \delta\omega[-U_3 - (1+U_0)^{0.5n_4}], \tag{18}$$

In equation (18) U_3 and U_0 are the non-linear terms. In case when $U_3 = U_0 = 0$, then for frequency of $\alpha-\omega$ linear dynamo waves ω_l we have:

$$\omega_l = -\delta\omega, \tag{19}$$

Taking into account the equation (17-19) we can suggest that the x, y, z components of perturbed magnetic induction oscillation (10-12) include only the first harmonics of dynamo waves. According to the equation (8) the expression for the perturbed temperature consists of terms with the zero and the second harmonics of dynamo waves, in contrast to the x, y, z components of perturbed velocity (13-15) and density (9), which depend only on the second harmonics of dynamo waves.

3. Non-linear Dynamo Waves without the Second Harmonics

Let us investigate dynamo waves taking into account only the perturbed terms of magnetic induction with the first order harmonics and pertubed temperature with the zero order harmonics. In this case with the help of the equations of magnetic induction (1) and energy (3),(7) we obtain the following set of coupled non-linear equations for the dynamo waves:

$$\frac{\partial U_2}{\partial \tau} = U_4 - \left\{ (1+U_0)^{n_1} N^{-1/2} + i\delta \left[(1+U_0)^{n_4/2} + U_3 \right] \right\} U_2. \tag{20}$$

$$\frac{\partial U_4}{\partial \tau} = i\delta 2 (1+U_0)^{n_4} U_2 - \left\{ (1+U_0)^{n_1} N^{-1/2} + i\delta \left[(1+U_0)^{n_4/2} + U_3 \right] \right\} U_4. \tag{21}$$

$$\frac{\partial U_0}{\partial \tau} = 2(\gamma-1)(1+U)^{n_1} N^{-1/2} F \beta^{-1} + p_m C_0 N^{-1/2} \left[(1+U_0)^{n_2} - 1 \right] - \sigma_0 U_0. \tag{22}$$

Here $\tau = \omega t$, $\beta = 8\pi\rho_0 / B_0^2$, $C_0 = \gamma(\gamma-1)(V_{xy}^2 + V_{xz}^2)/(k^2 V_T^2)$, $V_T^2 = \gamma p_0 / \rho_0$. is a square thermal velocity, $F = U_2^2 + d_0 |U_4|^2$, $d_0 = \omega^2 k^2 / \Delta^2$, $k^2 = k_x^2 + k_y^2$ $N = \omega^2 \eta_0^{-2} k^{-4}$ is the dynamo number from the $\alpha-\omega$ dynamo theory [1,4], $p_m = v_0 / \eta_0$ is a magnetic Prandtl's number [4], γ is a relative heat, $\sigma_0 = \sigma / \omega$.

3.1 The Linear Approximation. Investigating the equations (20-22) in the linear ≈imation first we have to assume that $U_0 = 0$, so that temperature is constant. Then we can write the solution of the equations in the following form:

65

$$U_2 = exp[\,(1 - N^{-1/2})\tau], \quad U_3 = 0, \tag{23}$$

$$U_4 = [1 + i\delta]U_2. \tag{24}$$

From the equations (23-24) we can see that for monotonically increasing functions U_2 and U_4 with time $t \lneq 0$ ($\tau > 0$) it is necessary $N > 1$ [1,4].

3.2 Non-Linear waves, when α Is Constant.

Let us investigate the equation (20-22) when $n_4 = 0$. From equations (20-22) we can obtain:

$$U_4 = (1 + i\delta)U_2, \tag{25}$$

$$U_3 = 0 \tag{26}$$

$$\frac{\partial U_2}{\partial \tau} = U_2 - (1 + U_0)^{n_1} N^{-1/2} U_2, \tag{27}$$

$$\frac{\partial^2 U_0}{\partial \tau^2} - n_1(1 + U_0)^{-1}(\frac{\partial^2 U_0}{\partial \tau^2})^2 + \{p_m C_0 N^{-1/2}(1 + U_0)^{-1}[(n_1 - n_2)(1 + U_0)^{-n_2} -$$
$$- n_1] + \sigma_0[1 - n_1 U_0(1 + U_0)^{-1}] - 2[1 - (1 + U_0)^{n_1} N^{-1/2}]\}\frac{\partial U_0}{\partial \tau} +$$
$$+ 2[1 - (1 + U_0)^{n_1} N^{-1/2}]\{p_m C_0 N^{-1/2}[(1 + U_0)^{n_2} - 1] - \sigma_0 U_0\} = 0. \tag{28}$$

Here $U_2 = U_{21} + U_2'$, $U_4 = U_{41} + U_4'$, $U_0 = U_{01} + U_0'$, where U_{21}, U_{41}, U_{01} are the stationary solutions of the equations (25-28) and U_2', U_4', U_0' are their perturbation terms. According to the (25-28) we can obtain:

$$U_{01} = N^{1/2n_1} - 1, \tag{29}$$

$$U_{21}^2 = 0.5\beta(\gamma - 1)^{-1}[\sigma_0(N^{1/2n_1} - 1) - p_m C_0 N^{-1/2}(N^{n_2/2n_1} - 1)] \tag{30}$$

In case $N \approx 1$ from the equation (28-30) we have:

$$U_{01} \approx (N-1)/(2n_1), \tag{31}$$

$$U_{21}^2 \approx \beta(n-1)[4n_1(\gamma-1)]^{-1}(\sigma_0 - p_m C_0 n_2). \tag{32}$$

Let us determine the time $t_1 > 0$ when the function U_2 achieves a stationary value. By using the conditions: $U_2|_{t=0} = 1$, $U_2|_{t=t_1} = U_{21}$ and the equations (25-32) we find:

66

$$t_1 = \omega^{-1}(N-1)^{-1} lg U_{21}^2 . \tag{33}$$

Let us investigate stability of stationary solutions (29-30) of equations (25-28). In the equations (25-28) following conditions are assumed: $|U_0''| \ll |U_{2,}''|$, $|U_2''| \ll |U_{21}|$, $|U_4''| \ll |U_{41}|$, and $U_0' \sim U_2' \sim U_4'$ $exp(q\tau)$. We have obtained q in the linear approximation:

$$q = \frac{1}{2} \left\{ -A_1 \pm (A_1^2 - 4A_2)^{1/2} \right\}. \tag{34}$$

where,

$$A_1 = p_m C_0 N^{-\frac{1+n_1}{2n_1}} \left[(n_1 - n_2) N^{\frac{n_2}{2n+1}} - n_1 \right] + \sigma_0 \left[1 - n_1 (1 - N^{-\frac{1}{2n_1}}) \right]. \tag{35}$$

$$A_2 = 2n_1 N^{-\frac{1}{2n_1}} \left[\sigma_0 (N^{\frac{1}{2n_1}} - 1) - p_m C_0 N^{-\frac{1}{2}} (N^{\frac{n_2}{2n+1}} - 1) \right]. \tag{36}$$

This stationary solution is the stable if:

$$Re\, q < 0. \tag{37}$$

From equation (34) we can see that condition (37) is valid, when $A_1 > 0$, $A_2 > 0$.

Let us analyse solutions (34) by unequality (37) in cases when a) $n_2 = 1$ and b) $N_1 \approx 1$.

a) In this case we obtain:

$$A_1 = (\sigma_0 - p_m C_0 N^{-1/2})[(1 - n_1) + n_1 N^{-\frac{1}{2n_1}}], \tag{38}$$

$$A_2 = 2n_1 (1 - N^{-\frac{1}{2n_1}})(\sigma_0 - p_m C_0 N^{-1/2}). \tag{39}$$

Hence, $Re\,(q) < 0$, when: 1) $n_1 > 0$; 2) $N > 1$; 3) $\sigma_0 > p_m C_0 N^{-1/2}$ and

$$(1 - n_1) + n_1 N^{-\frac{1}{2n_1}} > 0 \tag{40}$$

If $n_1 \leq 1$, then (40) satisfies always. If $n_1 > 1$, and $1 < N < \frac{n_1}{n_1 - 1}$, than (40) satisfies always.

b) When $N \approx 1$ we have

$$A_1 = \sigma_0 - p_m C_0 n_2, \tag{41}$$

$$A_2 = (\sigma_0 - p_m C_0 n_2)(N - 1). \tag{42}$$

From equations (31),(32),(41-42) with unequality (37) we obtain: 1) $\sigma_0 - p_m C_0 C_1^{-1} n_2 > 0$; 2) $N_1 > 1$, 3) $n_1 > 0$.

3.3 Non-Linear Waves, When α Depends on the Temperature.

Let us investigate the equations (20-22) when $n_4 \neq 0$. In this case we assume, that $U_2 = U_{22}' + U_2'$, $U_3 = U_{32}' + U_3'$, $U_4 = U_{42}' + U_4'$, $U_0 = U_{02}' + U_0'$, where U_{22}, U_{32}, U_{42}, U_{02} are the stationary solutions of the equations (20-22), and U_2', U_3', U_4', U_0' are their perturbaration terms. We have considered weakly non-linear waves i.e. $N_1 \approx 1$. In this case we obtain:

$$U_{02} = \frac{N-1}{2n_1 - n_4}, \tag{43}$$

$$U_{22}^2 = 0.5\beta(\gamma-1)^{-1}(\sigma_0 - p_m C_0 n_2)U_{02}, \tag{44}$$

$$U_{32} = 0, \tag{45}$$

$$U_{42} = (1 + i\delta)U_{22}. \tag{46}$$

We have investigated the stability of stationary solutions (43-46). For this reason we consider the linear aproximation $U_0' \sim U_2' \sim U_3' \sim U_4' \sim exp(q_1\tau)$. For q_1 we obtain the forth degree algebraic equation. Analysis of this equation leads to the following necessary and sufficient conditions for $Re(q_1) < 0$:

$$1) \; \sigma_0 - p_m C_0 n_2 > 0; \quad 2) \; N_1 > 1; \quad 3) \; 2n_1 > n_4. \tag{47}$$

4. Non-Linear Dynamo Waves with a Glance to The Second Harmonic

Let us investigate non-linear dynamo waves by means of the set of MHD equations (1)-(4), when we take into account the first harmonic for the magnetic field, the second harmonic for velocity and density, zero and second harmonics for temperature and we suppose that α is constant i.e. $n_4 = 0$. We consider the solutions of the equations (1-4) using the perturbation theory when $N_1 \approx 1$. Taking into account this conditions, we obtain stationary solution of the equations (1)-(4),(8-16) in the following form:

$$B_x' = B_m cos(\varphi), \tag{48}$$

68

$$B_x = B_m \omega k_z \Delta^{-1} 2^{-1/2} \cos(\varphi + \frac{\pi}{4}), \qquad (49)$$

$$B_z = -B_m \omega k_y \Delta^{-1} 2^{1/2} \cos(\varphi + \frac{\pi}{4}), \qquad (50)$$

$$\frac{T'}{T_0} = U_0 + U_T \sin(2\varphi + \varphi_T + \pi), \qquad (51)$$

$$\frac{\rho'}{\rho_0} = U_\rho \sin(2\varphi + \varphi_\rho + \pi), \qquad (52)$$

$$V_x' = \delta V_* U_v \sin(2\varphi + \varphi_v + \pi), \qquad (53)$$

$$V_y' = -\delta \omega k_y k^{-2} \rho/\rho_0, \qquad (54)$$

$$V_z' = -\delta \omega k_z k^{-2} \rho/\rho_0, \qquad (55)$$

$$U_3 = [-\frac{1}{4} + \frac{(\gamma - 1)(n_1 + 4b)b}{4\gamma(4b^2 + 1)}]\beta_m^{-1}, \qquad (56)$$

$$N - 1 = 2n_1 U_0 + [(\gamma^{-1} - 0,5) + \frac{(1 - \gamma^{-1})(n_1 + 4b)b}{4b^2 + 1}]\beta_m^{-1}. \qquad (57)$$

Here $\beta = 8\pi\rho_0/B_m^2$, where $B_m = 2B_0 U_{20}$, , U_{20} is stationary value of function U_2; $b = \chi_0/\eta_0 + \sigma_1/4\gamma$; $U_0 = (\gamma - 1)(\sigma_1\beta_m)^{-1}$; $V_* = (K_y V_{xy} + K_z V_{xz})/(K_y^2 + K_z^2)$,

$$\sin(\varphi\tau) = \frac{2b + 1}{(8b^2 + 2)^{1/2}}, \qquad (58)$$

$$\cos(\varphi\tau) = -\frac{2b - 1}{(8b^2 + 2)^{1/2}}, \qquad (59)$$

$$\sin(\varphi v) = -\frac{1}{A_v}\{(\gamma - 1)[(4p_m^2 n_2 + 1)(2b - 1) + 2p_m(2b + 1)(1 - n_2)] - \qquad (60)$$
$$- \gamma(4b^2 + 1)2p_m\},$$

$$\cos(\varphi v) = -\frac{1}{A_v}\{(\gamma-1)[(4p_m^2 n_2+1)(2b+1)-2p_m(1-n_2)(2b-1)]$$
$$-\gamma(4b^2+1)\}, \tag{61}$$

$$\sin(\varphi_\rho) = -\frac{a_1}{A_\rho}, \tag{62}$$

$$a_1 = -\gamma(4b^2+1)+(\gamma-1)(2b-1). \tag{63}$$

$$\cos(\varphi_\rho) = \frac{b_1}{A_\rho}, \tag{64}$$

$$b_1 = -2\gamma(4b^2+1)+(\gamma-1)(2b-1), \tag{65}$$

$$U_T = \frac{(1-\gamma^{-1})\beta_m^{-1}}{[2(4b^2+1)]^{1/2}}, \tag{66}$$

$$U_\rho = \frac{A_\rho \beta_m^{-1}}{2\gamma(4b^2+1)}, \tag{67}$$

$$U_v = \frac{A_v \beta_m^{-1}}{2\gamma\gamma(4b^2+1)(4p_m^2+1)}, \tag{68}$$

$$A_v = 0.5(4b^2+1)\{[2(\gamma-1)(4p_m^2 n_2+1)+\gamma(-4p_m b+2p_m-2b-1)]+$$
$$+[4(\gamma-1)p_m(1-n_2)+\gamma(-4p_m b-2p_m+2b-1)]^2\}^{1/2}, \tag{69}$$

$$A_\rho = \{[\gamma(4b^2+1)-(\gamma-1)(2b+1)]^2+(\gamma-1)^2(2b-1)^2\}^{1/2}. \tag{70}$$

We have investigated the stability of stationary solution (48-57). For this we consider the linear aproximation for the perturbed quantities $\sim exp(q\tau)$ and for the q we obtain:

$$q = \{\frac{3(\gamma-1)n_1}{2\sigma_1}-\frac{2-\gamma}{2\gamma}-\frac{(\gamma-1)(n_1+4b)b}{\gamma(4b^2+1)}\}\beta_m^{-1}. \tag{71}$$

Consequently, stationary solution (48-57) is the stable i.e. $q<0$ if $n_1>0$, $\sigma_1>0$, $b>0$.

70

5. Discussion

Propagation of a weakly non-linear $\alpha-\omega$ dynamo waves in the Solar lower convective zone is investigated. The analytical solutions for the components of magnetic field (48-50), the temperature (51), the components of velocity (53-54) and the density (52) are obtained. With the help of these equations we can study variation processes taking place on the Sun.

These approaches make possible to investigate nature of sound waves' frequency shift and splitting on the Sun (p-modes). During the research works we have considered the characteristic values of the environment in the non-perturbed state, which were following the processes described in (48-55) equations. With the help of the perturbation theory we have suggested possible excitation mechanism of the shift and splitting of p-modes' frequencies. Doppler effect was also taken into account.

The other important result of the solution is that it can explain Solar luminosity during the 22 year solar cycle period.

Abastumani Astrophysical Observatory
Tbilisi I. Javakhishvili State University

REFERENCES

1. E.N. Parker, Cosmocal Magnetic Fields. Oxford University Press, England 1979.
2. H.K. Moffat, Magnetic Field generation in Electrically Conducting Fluids, Cambridge.
3. F. Krause, K.H. Rudler, Mean-Field Magnetohydrodynamics and Dynamo Theory, Pergamen, Oxford, 1980.
4. E.R.Priest, Solar Magnetohydrodynamics. Reidel, Dordrecht:USA, London: England, 1982.
5. E.N. Parker, Astrophysical Journal. **122,**293,1955.
6. M. Stix, Astron. and Astrophysics. **20,**9,1072.
7. H. Yoshimra, Astrophysical Journal Suppl. **29,**467,1975.
8. M.R. Proctor E.J. Fluid Mech. **80,**769,1977.
9. N.O.Weiss, F. Cattaneo, C.A. Jones, Astrophysical Fluid Dynamics. **30,**305-341,1984.
10. S.A. Balbus, J.F. Hawley, Astrophysical Journal. **376,**214,1991.

11. A. Branderburg, A. Nordlend, R.F. Stein, U. Torkesson. Astrophys.J. **446**,741,1995.

12. A.D. Pataraya, T.A. Pataraya. ann. Geophysicae, **15**,97,1997.

ა. პატარაია, თ. პატარაია, ბ. შერგელაშვილი

არავერზივი α−ω დინამო ტალდა, ტურბოლენტური დისიპაციისა α კოეფიციენტების ტემპერატურაზე დამოკიდებულების შემთხვევაში

რეზიუმე

ნაშრომში გამოკვლეულია არაწრფივი α−ω დინამო ტალდები, როცა მაგნიტოჰიდროდინამიკურ (მჰდ) განტოლებებში მხედველობაშია მიღებული დისიპაციური და α კოეფიციენტების ტემპერატურაზე დამოკიდებულება. გამოთვლები ჩატარებულია ლოკალურ დეკარტის კოორდინატთა სისტემაში, რომელშიც გრავიტაცია უგულებელყოფილია. ასევე გამოკვლეულია შეუშფოთებული, არაწრფივი მჰდ განტოლებები. დინამო ტალდების ნულოვანი, პირველი და მეორე რიგის ჰარმონიკების გათვალისწინებული, როცა დინამო რიცხვები მიახლოებით ერთს უდრიან. ამ შემთხვევაში ნაპოვნი არაწრფივი განტოლებების სტაციონარული, ანალიზური ამონახსნები მაგნიტური ველის მდგენელების ტემპერატურის, სიჩქარის კომპონენტებისა და სიმკვრივისათვის, გამოკვლეულია მათი სტაბილურობა. ამ ამონახსნების საშუალებით ჩვენ შეგვიძლია ვიწინასწარმეტყველოთ მზეზე არსებული ცვალებადი პროცესები.

ზემოთ აღნიშნული მიახლოებები საშუალებას გვაძლევს გამოვიკვლიოთ მზის ბგერითი ტალდების (p-მოდების) სიხშირის წანაცვლებისა და გახლეჩის წარმოშობის მექანიზმები. ამისათვის საჭირო ამოვხსნათ მჰდ განტოლებათა სისტემა, სადაც შეუშფოთებელ მდგომარეობაში გათვალისწინებულია ნაშრომში მიღებული გარემოს მახასიათებელი პარამეტრების შესაბამისი გამოსახულებები, ხოლო ბგერითი ტალდები განიხილულია, როგორც შეშფოთება. ამ შემთხვევაში შესაძლებელია მივიღოთ მზის ბგერითი ტალდების სიხშირის წანაცვლებისა და გახლეჩის შესაბამისი გამოსახულებები, როცა გახლეჩის შემთხვევაში ასევე მხედველობაში მიღებული ლოპლერის ეფექტი.

ABOUT LOOSENING ACTION OF ANTIBONDING ELECTRONS WHILE PHOTOMECHANICAL EFFECT

A. Gerasimov, G. Chiradze, N. Kutivadze,
A. Bibilashvili, Z. Bokhochadze

Abstract. We have shown experimentally with the help of the example of spectral dependence and value of microhardness increase (photomechanical effect - PME) in Si that the more is the energetical difference of antibonding state of electron from its state in insulated atom the more will be the loosening action of electron situated on antibonding level.

The mechanism of photomechanical effect (PME) influence of the light upon microhardness (MH) of semiconductors was offered in [1÷5]. The essence of this mechanism is such that the change of MH happens because of the change of antibonding quasiparticles (aquases)[1] concentration by light that loosens chemical bonds between the atoms of the substance. It is well-known [6] that the more effective is the loosening action the more is the difference in electron energies between the initial state of substance insulated atoms and the corresponding energies of electrons in solid state energetical bands formed while reapproachement of these atoms to one another for certain distances, e.g. the more is the splitting of bands as bonding and antibonding ones, (Fig.1). The splitting processes of bands in the space K differ one from another and these bands are able to have some extremums of energy [7]. If the electrons (holes) will be situated in minimums with higher (lower) values of energy then their loosening action will be more than in case of electrons (holes) situated in minimums with lower (higher) value of energy. For this reason the action of light with quant

---

[1] Antibonding quasiparticles (aquases) are electrons on antibonding states and holes on bonding states. Conductivity band [6], tails of density of states and donor levels corresponding to it consist of antibonding states, and valency band, its tails of density of states and acceptor levels of bonding states [8].
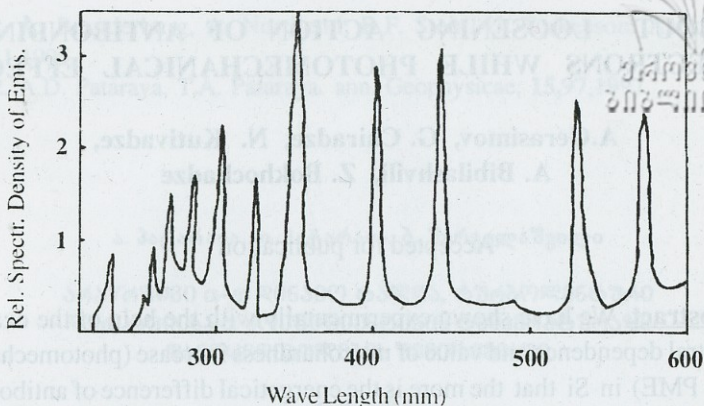
Fig. 1. UPH-lamp spectre.

energy sufficient for electron transition from valency (bonding) band to energetical minimums of conductivity (antibonding) band situated higher according to energetical scale must be more effective in PME.

The experimental results of spectral dependence of PME value are given below and they confirm the considerations declared above.

The investigations were carried out with a non-dislocational monocrystallic specimen of Si, of n-type conductivity, with specific resistance $\rho=200$ ohm cm, the preparation of specimen and methods of MH-measuring are given hereinafter [5]. We used the lazer ЛГН-4046 and ultraviolet(UV)-lamp with quant set $\eta v = 2 \div 6eV$ (Fig. 1, UV spectre) as the sources of light with different quant energies. The intensity of

Table

Emanation Source	Quants' Energy ev	φ, Photon Stream cm^{-2}sec^{-1}	Stationary Concentration of Electrons cm^{-3}	Capacity of Electrons ev	Rations		
					Φ_L/Φ_{UV}	Π_L/Π_{UV}	E_{UV}/Φ_L
Lazer	2	$1.6 \cdot 10^{17}$	$4 \cdot 10^{14}$	0.56	2.5	2.8	2.9
UV Lamp	2-6	$1.6 \cdot 10^{16}$	$1.4 \cdot 10^{14}$	1.64			

light was changed with the help of neutral filters. We have chosen such intensities of light situated on linear region of dependence of MH-change on light intensity [5] when there was reached the equal ΔH-change of MH (e.g. $\Delta H = H_D - H_L$, where H_D and H_L are the values of MH in the darkness and in the light, correspondingly) in case of loading 25g. The equal ΔH was taken in order to have the same depth of indenter-immersion. We have measured the photohall and calculated the stationary concentration of non-equilibrium electrons on the surface. The same values of photon stream ratio to stationary concentration of aquases for both sources of light (Table) indicate to identity of generative-recombinative conditions on the surface independently from emanation source. We give the results of measuring in Fig. 1 and they allow us to see that the influence of UV-light is more effective_than lazer emanation. Indeed, for equal ΔH in case of lighting by lazer the photon stream and stationary concentration of excited electrons are ~2,7 times
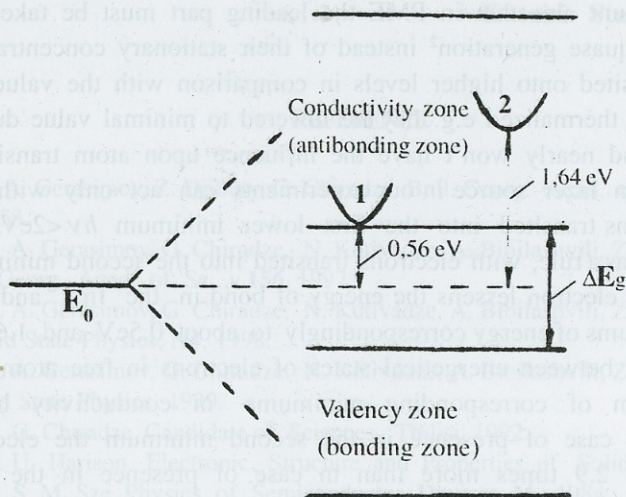
Fig 2. Schematical illustration of energetical states of electrons in insulated atom E_0 and in solid that is formed from a great quantity of atoms what causes the appearance of bonding (valency) and antibonding (conductivity) bands. In antibonding band there are shown illustratively the minimums for different lengths. E_g - the minimal width of forbidden band, $E_1 = 0.56$ eV, $E_2 = 1.64$ eV.

more than in case of lighting with UV-lamp, though if we'll take into account that this light is absorbed in thinner layer, the average coefficient of absorption for the given UV-light $\alpha = 10^5$ cm^{-1}, than lazer emanation $\alpha = 10^4$ cm^{-1}, the coercion of lazer emanation upon ΔH would have to be considerably greater, but the experiment shows us the inverse situation. We can explane it so that light quants $h\nu > 2,2$eV can transit the electrons into higher (second) minimum of conductivity (antibonding) band situated at a distance 2.2eV from the ceiling of valency band (Fig. 2). If we take into account that the number of quants able to transit electrons onto minimums situated higher is approximately only 1/4 of all photons emanated by UV-lamp (Fig.1), then the leading part will be taken by transitions into second minimum from which the electrons during ~10^{-11}sec (the time of interlinear transitions [7]) will transit to the lower minimum but during this time they help atoms whin their movement (the time needed for one gap of atom - of 10^{-13}sec rate) by loosening their bond strongly. We must take into account also that in PME the leading part must be taken by the temp of aquase generation[2] instead of their stationary concentration. Electrons transited onto higher levels in comparison with the values of minimums are thermalized e.g. they are lowered to minimal value during 10^{-14}sec [7] and nearly won't have the influence upon atom transition. The light from lazer source in our experiments can act only with the help of electrons transited into the first lower minimum $h\nu < 2$eV, and UV-light acts, as a rule, with electrons transited into the second minimum $h\nu > 2$eV. Each electron lessens the energy of bond in the first and the second minimums of energy correspondingly to about 0.5eV and 1.64eV (the difference between energetical states of electrons in free atom and on the bottom of corresponding minimums in conductivity band, Fig.2), e.g. in case of presence in the second minimum the electron loosens nearly 2.9 times more than in case of presence in the first minimum. Thus, in order to obtain the identical influences upon MH-

---

[2] This assumption is true because, in difference from the processes connected with atom migration where it's necessary to have the full release of atom, in case of PME each atom demonstrates the pressure of indenter and each decrease of chemical bond makes easier the transition of atom.

value of Si in case of lazer coercion we'll need the aquase concentration as many times more also, what we can observe during the experiment (Table), both for temp of aquase generation and for their stationary concentration. The fact that the ratio of aquase (photon stream) generation temp or concentration for two sources of emanation is less than the ratio of loosening capacities of electrons in the second and the first minimums, e.g. that during the experiment we observe aquase and photon stream concentration while $hv>2eV$ less than it is caused by the ratio of loosening capacities of electrons in the first and the second minimums, is connected with the circumstance that 1/4 of photons is transited to higher minimums by electrons that are able to make loosening more than electrons in the second minimum, and these photons have the weak influence but have the influence still upon loosening of chemical bonds.

Tbilisi I. Javakhishvili State University
Kutaisi State University

REFERENCE

1. A. Gerasimov, Z. Djibuty, G. Chiradze. Bull. Georg. Acad. of Sc., **142,** N1, 1991, 53.
2. A. Gerasimov, G. Chiradze, N. Kutivadze, A. Bibilashvili, Z. Bokhochadze. Bull. Georg. Acad. of Sc., v.**156,** 1997.
3. A. Gerasimov, G. Chiradze, N. Kutivadze, A. Bibilashvili, Z. Bokhochadze. J. Solid State Physics, N4, 1998.
4. A. Gerasimov, G. Chiradze, N. Kutivadze, A. Bibilashvili, Z. Bokhochadze. J.Solid State Physics, 1999.
5. G. Chiradze. Candidate of Sciences. Tbilisi, 1992.
6. U. Harison. Electronic Structure and Properties of Solids, M., **1**, p. 53;
7. S. M. Sze. Physics of Semiconductor Devices, M., 1984.
8. A. Gerasimov, G. Chiradze, N. Kutivadze, Z. Bokhochadze (in the given collection).

ა. გერასიმოვი, გ. ჩირაძე, ნ. კუტივაძე,
ა. ბიბილაშვილი, ზ. ბოხოჩაძე

ანტიდამაკავშირებელი ელექტრონების ქიმიური ბმის შემასუსტებელი ზემოქმედების შესახებ

დ ა ს კ ვ ნ ა

ნაშრომში მონოკრისტალური Si-ის მიკროსისალის სიდიდის შემცირების სპექტრალური დამოკიდებულების მაგალითზე (ფოტომექანიკური ეფექტი) ექსპერიმენტულად ნაჩვენებია, რომ ენერგეტიკულად რაც უფრო მეტად განსხვავდება ელექტრონის ანტიდამაკავშირებული მდგომარეობა იზოლირებულ ატომში მისი მდგომარეობისაგან, მით უფრო მეტია ელექტრონის ქიმიური ბმის შემასუსტებელი მოქმედება.

PHYSICAL NATURE OF THERMOMECHANICAL EFFECT

A. Gerasimov, G. Chiradze, N. Kutivadze,
A. Bibilashvili, Z. Bokhochadze.

Abstract. The physical mechanism of thermomechanical effect (reduction of microhardness according to the increase of temperature) is offered by us in the given work. On the basis of this mechanism we have explained all characteristic events of microhardness change caused by the temperature. The observation process is carried out using semiconductors with only covalent bonds Ge and Si. In such a way we have shown the role of electrons and holes excited by temperature in reduction process of microhardness that is appreciable especially for temperature less than the valua of Debay temperature.

The reduction of microhardness (MH) under the coercion of the temperature of solid is known as thermomechanical effect (TME) [1]. Heating is the cause of reduction of MH in covalent crystals that under the conditions of normal temperature are characterized by high hardness, fragility and low plasticity in comparison with metals, and these crystals gradually acquire the plastic properties [1–5]. As a rule, the reduction of MH is explained by thermal fluctuations that enlighten transition of dislocation in covalent crystals [6]. But this mechanism can't explain all observed particularities of change of MH while increase of temperature [7]. For example: great reduction of MH while certain temperatures, gradual reduction of MH anisotropy of 1st kind [8] together with heating. In the given work there is offered the new mechanism considering the dependence of MH on temperature, together with all characteristic events. The consideration is carried out for the example of semiconductors with only covalent bonds – Ge and Si.

---

[1] Electrons on loosening orbitals and holes on bonding ones are called the antibonding quasiparticles. Conductivity band [11], tails of state density corresponding to it, and donor levels consist of antibonding orbitals, what about valency band, its tails of state density and acceptor levels - they consist of bonding orbitals [12].

The offered mechanism is based on the new conception of atom transition in solids [9,10] which shows us that the probability of elementary migration act of atom is determined by means of probability $W=W_{aq} \cdot W_{ph}$, where $W_{aq}=A \cdot (n_{aq}/N_A)\alpha$ – is the probability of presence of certain quantity α of antibonding quasiparticles (aquases)[1] near the given atom, A – coefficient that weakly depends on temperature and aquase concentration, α –aquase quantity that is necessary for accomplishment of the given elementary migration act, W_{ph} – probability of presence of phonon with maximal energy near the given atom. During this process the way of aquase creation doesn't make any difference. These notions were used successfully for explanation of physical nature of light influence (PME) [12–14] and of electric field influence(EME) [15] upon MH. It was noticed that in case of the temperature set before, e.g. W_{ph}=const, change of MH correlates with aquase concentration [16].Proceeding from this we can suppose that together with phonons, the concentration of aquases created by temperature plays important role for reduction of MH while heating.

The typical dependencies of MH on the temperature of semiconductors Ge and Si are given in Fig.1 [1]. As we see, the relatively weaker dependence of MH on temperature (the low-temperatural region) is observed at first, and, beginning from certain temperatures, MH strongly depends on temperature (high-temperatural region). It's necessary to mention that the values of temperature of transition differ one from another within the interval $20°$ in various works. This fact is caused by different conditions of experiments of MH investigation (initial defects of specimen, way of preparation of investigated surface, form of indenter, influence of MH-anisotropy of 1-st and 2-nd kind, velocity of heating of investigated specimen). However,
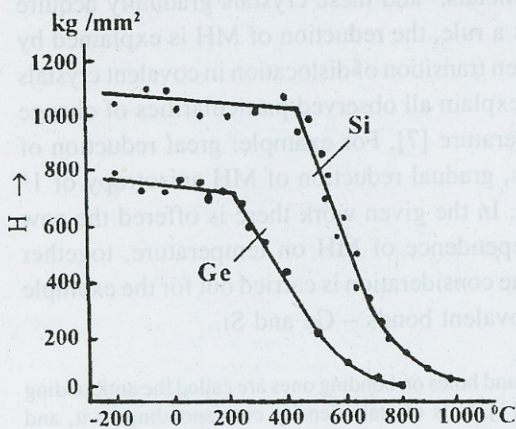
Fig. 1.

these temperatures coinside with Debay temperatures of the given material (e.g. with the temperature in case of which the whole energetical spectre of phonons is excited in the investigated material) within the interval of measuring exactness, and when the temperature becomes higher, the movement of defects is lightened considerably.

This assumption is supported also by experiments carried out in order to observe the temperatural dependence and defectness of specimen regions that are adjacent to the imprint [1]. We can observe considerable changes in this part of the specimen only in high-temperatural region what is caused by the mobility of defects.

Anisotropy of MH of the 1st type (change of MH in dependence with the orientation of indenter on the investigated hedre [8], is caused by the directedness of SP^3 in covalent bonds [17]) decreases with the increase of temperature [8]. It is well-known that because of electron migration from bonding band to the antibonding one not only the force of chemical bonds between atoms having near them aquases arisen during their thermal movement is reduced ,but also the spacial distribution of electron density of atom chemical bonds is changed. As a result, together with the increase of temperature in crystal there decreases the quota of directed P-states at the expense of S-states increase, e.g., the isotropization of bonds is accomplished. It is the cause of observed reduction of MH anisotropy together with the increase of temperature [8].

The influence of aquases upon TME is indicated also by the fact that, differently from PME and EME that take place in the thin nearsurfacial region of the specimen where aquases arise and concentrate as a result of the corresponding coercion [15,18], TME takes place in the whole volume of the crystal (in case of all loads of indenter, e.g. on all depths of indenter-immersion), because the formation of aquases as a result of coercion of temperature is accomplished uniformly in the whole investigated material.

In order to prove the mentioned considerations about TME we have carried out the comparative experiments with united methods concerning the temperature dependence of PME and TME for different intensities of light with the specimen of nondislocational monocrystallic Si of n-type with specific resistance p=200ohm cm. Methods of MH measuring are given in [14]. Investigation of TME and PME was carried out in case of different

6.

temperatures that were reached by means of heating of underlay with attached specimen. We have measured the temperature with the help of thermopair both in the darkness and in the lighting [14]. The process of unloading was accomplished after cooling of specimen in the darkness in order to evite the bloating of imprint [13, 18]. We must mention that we have chosen such values of intensity of white light I_1 and I_2 that are disposed on the linear region of dependence of MH on lighting intensity [13].

If the value of MH is reduced for ΔH in comparison with H measured in the darkness (for the same temperature) in case of the given temperature T_1 under the coercion of light with the certain intensity, then in order to obtain the same reduction without light it's necessary to heighten the temperature upto some certain value $T_2 > T_1$. Though, the comparison of aquase concentration in case of equal ΔH shows us that for light coercion the stationary concentration of aquases created by the light of the certain intensity is much greater than aquase concentration in case of the temperature that is necessary for obtaining the MH-reduction equal to the light one. This fact is explained so that according to [1], in order to reach the certain value of probability of migration act that determines the given value ΔH, the less is W_{aq} the more must be W_{ph}, e.g., the higher must be the temperature. Unfortunately, we weren't able to estimate the probability of phonon rise
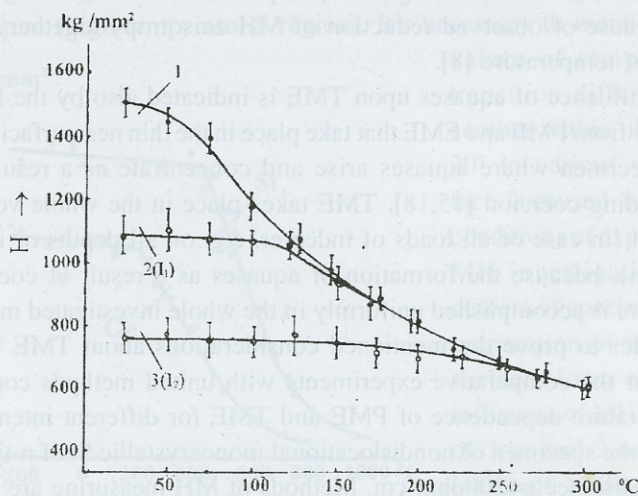
Fig. 2.

82
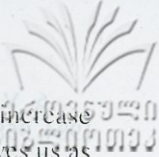
near the given atom in destroyed region of specimen but the trend of increase of this probability together with the temperature is evident what serves us as a qualitative approvement of the considerations that were given above.

The influence of aquases upon TME is approved by the fact that in case of simultaneous coercion of light and temperature MH is determined by the most concentration of aquases derived by light or temperature because under the condition of the certain temperature W_{ph} is the same both for PME and for TME. It's clear from the Fig. 2 that for the certain intensity I_1, while concentration of aquases created by light – $P_{light}=2\times10^{14}cm^{-3}$ is more than the equipose concentration of aquases created by temperature P_t, the value of MH is determined by P_{light}, and if $P_t \cong P_{light}$ for T= 150°C P_t begins to act upon the value of MH, and then, when $P_t>P_{light}$, T>200°C, MH is determined by $P_t>2\times10^{14}cm$. We observe analogue situation also while coercion by light with the intensity $I_2>I_1$, when $P_{light}=4\times10^{14}cm^{-3}$.

We may also conclude from the Fig.2, that in low-temperatural region phonons play less role than aquases, otherwise the inclination on curves of temperatural dependence of PME would have to be more, and higher the Debay temperature (high-temperatural region) they begin to play the considerable role, what explains, as we've mentioned above, the increase of temperatural dependence of TME in this region of temperature.

Tbilisi I. Javakhishvili State University
Kutaisi State University

REFERECES

1. V.I. Trefilov, Yu. V. Milman. Reports of the Academy of Sciences of USSR, techn. ser., **153**, 4, 1963, 824 (Russian).

2. S. S. Gorelyk, Yu. M. Litvinov. Reports of Academy of Sciences of USSR, techn. ser., **181**, 2, 1968, 327 (Russian).

3. A. K. Butylenko, Ukr. Phys. Journ. **2**, 1963, 100 (Russian).

4. S.S. Goreluk, Yu. M. Litvinov, M. G. Lozinsky. Electrotechnics, ser. Materials. **5**, 54, 1975 (Russian).

5. V.M. Glazov, V.B. Koltsov, A. R. Regel, V. Z. Kutsova, PhTS. **25**, 1991, 588 (Russian).

6. V. I. Trefilov, Yu. V. Milman, I.V. Gridneva. Non-organic materials, **20**, 6, 1984, 958 (Russian).

7. M. I. Valkovskaya, B. M. Pushkash, E. E. Maronchuk. Plasticity and fragility of semiconductor materials while testing for microhardness. Kishinyov, Shtyntsa, 1984, 100 (Russian).

8. P. D. Warren, S. G. Roberts, P.B. Hyrsh. Bulletin of the Academy of Sciences of USSR, Ser. physic., **51,** 4, 1987, 812 (Russian).

9. A. B. Gerasimov, V. B. Golubkov, E.R. Kutelia, V.P. Myneev, E.M. Mkrtchyan, A.A. Tsertsvadze. Letters to JTPh. **6,** 1980, 58 (Russian).

10. A.B. Gerasimov. Proceedings of the Fourth International Conference Materials, Science Forum. vols. **65-66,** New-York, 1990, 47.

11. W. Haryson. Electron Structure and properties of solids, M., 1, 384; (Russian).

12. A. Gerasimov, G. Chiradze, N. Kutivadze, A. Bibilashvili, Z. Bokhochadze (In the given collection).

13. A. Gerasimov, Z. Djibuti, G. Chiradze, Bulletin of the Georgian Academy of Sciences. **142,** 1, 1991, 53 (Russian).

14. G. Chiradze. Diss. cand. of phys.-mat. sciences. Tbilisi, 1992 (Russian).

15. A. Gerasimov, G. Chiradze, N. Kutivadze. Collection of Scientific Works. №2, Tbilisi, 1998 (Russian).

16. A. Gerasimov, Z. Djibuty, G. Chiradze. II Scientific conferene of professors and pedagogues staff. GSSR, Sukhumi, thes. of reports. 1991, 97 (Russian).

17. A. Gerasimov, G. Chiradze, N. Kutivadze, A. Bibilashvili, Z. Bokhochadze. Bulletin of the Georgian Academy of Sciences; **156,** 3, 1997, 59.

18. A. Gerasimov, G. Chiradze, N. Kutivadze, A. Bibilashvili, Z. Bokhochadze. Sol. St. Phys., **4,** 1998.

ა. გერასიმოვი, გ. ჩირაძე, ნ. კუტივაძე,
ა. ბიბილაშვილი, ზ. ბოხოჩაძე

თერმომექანიკური ეფექტის ფიზიკური ბუნება

დასკვნა

ნაშრომში მოცემულია თერმომექანიკური ეფექტის - მიკროსისალის
შემცირება ტემპერატურის მომატებით ფიზიკური მექანიზმი, რომლის საფუძ-
ველზეც ახსნილია მიკროსისალის ტემპერატურით გავლენით ცვლილების
თანამდევი ყველა დამახასიათებელი მოვლენა. აღნიშნული სამუშაო ჩატარე-
ბულია სუფთა კოვალენტური ბმის მქონე ნახევარგამტარებზე Ge და Si.
ნაჩვენებია ტემპერატურით აღგზნებული ელექტრონების და ხვრელების
როლი მიკროსისალის შემცირებაში, რაც განსაკუთრებით საგრძნობია
დების ტემპერატურებზე დაბალი ტემპერატურების შემოხვევაში.

THE PHYSICAL MECHANISM OF PHOTOMECHANICAL EFFECT

A. Gerasimov, G. Chiradze, N. Kutivadze,
A. Bibilashvili, Z. Bokhochadze

Abstract. The given work introduces the results of systematic investigations of photomechanical effect - PME (change of the value of material microhardness(MH) under the influence of the light) carried out with monocrystallic Si, using the uniform methods. We have studied the dependence of PME on spectral consistence and intensity of light, the residual PME (conservation of crystal softening during the certain interval of time), the influence of lighting upon MH-anisotropy and the temperatural dependence of PME. On the basis of carried out investigations and analysis of data we have ascertained the correlation between the values of PME and the corresponding concentration of non-equilibrium carriers excited by light (so-called antibonding quasiparticles). Leant upon this fact, we have offered the mechanism that can explain the decrease of MH because of lighting in covalent crystals as, on the whole, caused by weakening and isotropization of chemical bonds because of the presence of antibonding quasiparticles generated by light.

1. introduction

Sufficiently numerous works [1–9] are dedicated to the investigation of photomechanical effect (PME) [1], e.g., change of the value of material microhardness (MH) under the influence of light. But, unfortunately, the physical mechanism explaining the nature of this influence doesn't exist till now. Perhaps, it is caused partially by contradiction of experimental results obtained with the help of different methods, specimen and conditions of experiments. The knowledge of mechanism of PME is very important both from fundamental and from applied points of view.

We have considered the results of investigations of PME in Si with uniform methods that expose the physical nature of light influence upon MH.

As it is notorious, during the process of MH measuring the break of material takes place and causes the travel of the certain mass of observed substance under the pressure of indenter. If the coercion of light reduces

MH, it means that the displacement of this mass of substance will be made easier, and this fact is explained finally by the increase of atom mobility relatively to one another, e.g., by change of interatom interaction. In the works [10,11] there was offered the new conception of atom displacement in solids that describes the way of increase of atom mobility by light coercion. In order to facilitate the process of reading of this article, below we'll give the principal sense of the above-mentioned conception.

The use of the method of Linear Combination of Atom Orbitals (LCAO) in approaching of the strong connection for description of electron states in semiconductors gives us two meanings of energy [12]: states with the less energy – bonding states and states with the higher energy – antibonding states. The hybridization of atom orbitals having one S and three P states takes place while formation of covalent crystal from separate atoms. When they are transformed into bands, P-states of electrons conform to the ceiling of valency band that consists of bonding orbitals, and S-states of electrons conform to the bottom of conductivity band that consists of antibonding orbitals (Fig.1). Each travel of the electron from valency band to conductivity
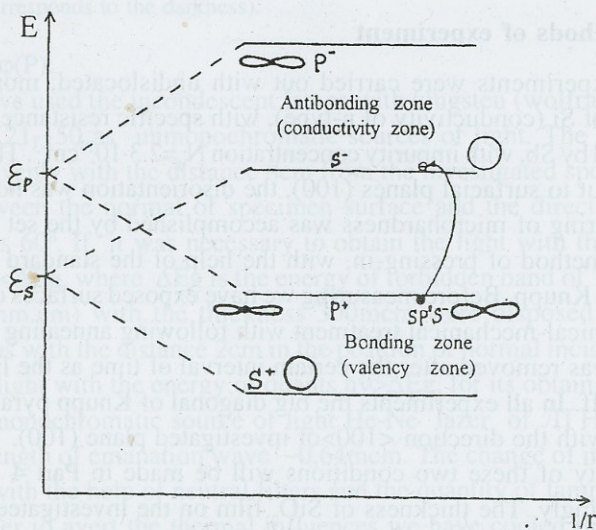
Fig. 1. Formation of energetical bands while rapprochement of atoms (r-internuclear distance), and change of energy and spacial distribution of electronic density of chemical bond as a result of electron translation from bonding band to antibonding one.

band, e.g., travel from bonding state to the antibonding one, is accompanied by the corresponding change of its quantum state, e.g., change of bond energy and space distribution of charge of those atoms that have near them the hole or free electron during the thermal movement. If we'll take into account that S-orbitals have spherical symmetry and P-orbitals have directed double-bell electron clouds, it means that the leaving of electron from P-state increases the specific weight of S-state near the given atom (Fig.1). Thus, the more conductivity electrons and holes formed because of excitation we find in crystal the more will be the reduction of bond energy and of the deal of hard directed P-bonds, and atoms will get the additional rate of freedom what leads to the increase of mobility of atoms relatively to one another [11]. It's necessary to mention that in case of defects creating the local energetical levels in forbidden band, the acceptor levels are bonding orbitals and donor levels-antibonding orbitals. Because of it the electrons in conductivity band and on donor levels and, also, the holes in valency band and on acceptor levels are antibonding quasiparticles (aquases). Below we give the experimental data that illustrate the leading role of aquases in PME.

2. Methods of experiment

The experiments were carried out with undislocated, monocrystallic specimen of Si (conductivity of n-type), with specific resistance $\rho = 200$ ohm cm, alloyed by Sb, with impurity concentration $N_d = 2.3 \cdot 10^{13} cm^{-3}$. The specimen were cut out to surfacial planes (100), the disorientation was not over 0.3^0. The measuring of microhardness was accomplished by the set „Durimet", using the method of pressing-in, with the help of the standard four-hedral pyramid of Knupp. Before measuring we have exposed surfaces of specimen to the chemical-mechanical treatment with following annealing in vacuum. The load was removed after the certain interval of time as the lighting was switched off. In all experiments the big diagonal of Knupp pyramid always coincides with the direction <100>of investigated plane (100). The ground for necessity of these two conditions will be made in Part 4 and Part 5, correspondingly. The thickness of SiO_2 film on the investigated surface of Si, measured with ellipsometric microscope, was about 30 A. The control experiments have shown that SiO_2 layer up to the 60A doesn't have influence upon the form of the curve that indicates to dependence of MH upon the
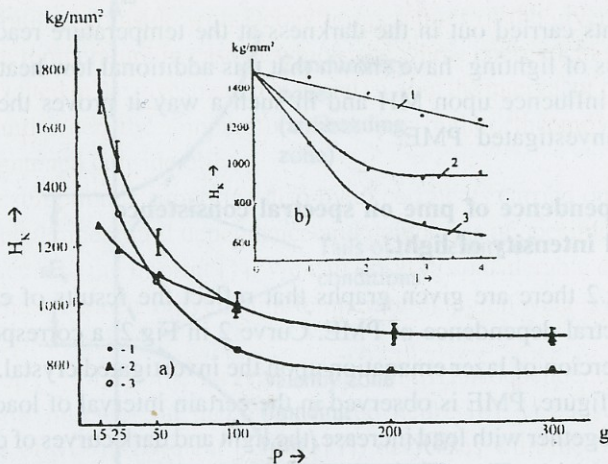
Fig. 2. a) Dependence of MH of Si on the load of indenter in the darkness (1), and while coercion by light quants , hv>ΔE$_g$ (2) and hv<ΔE$_g$ (3). The error of measuring is the same for all curves.

b) Dependence of MH of Si on lighting intensity while coercion by light quants, hv<ΔE$_g$ (1), hv>ΔE$_g$ (2), and by white light (3) (I-intensity of light sources in conventional units, O- corresponds to the darkness).

load-P:H=φ(P).

We have used the incondescent lamps with tungsten (wolfram) filament of type K21-150 as unmonochromatic sources of light. The lamps were disposed evenly with the distance 8cm from the investigated specimen. The angle between the normal of specimen surface and the direction of light stream was 60⁰. If it was necessary to obtain the light with the energy of quants hv<ΔEg, where ΔEg is the energy of forbidden band of Si, Si plates (ρ~150 ohm.cm) with the thickness 300mcm were disposed in front of these lamps with the distance 2cm in the position of normal incidence. What about the light with the energy of quants hv>ΔEg, for its obtaining we have used the monochromatic source of light He-Ne lazer of ЛГН-404B type with the length of emanation wave ~0,64mcm. The change of intensity was obtained with the help of neutral filters and the quantity of lamps.

In order to avert the thermal influences we have cooled the system of lamps, filters and the investigated crystal with the stream of air. The measuring of lightened surface temperature of investigated specimen and the control

89

experiments carried out in the darkness at the temperature reached during
the process of lighting have shown that this additional low heating doesn't
have any influence upon MH and in such a way it proves the unthermal
nature of investigated PME.

3. Dependence of pme on spectral consistence and intensity of light.

In Fig.2 there are given graphs that reflect the results of experiments
about spectral dependence of PME. Curve 2 in Fig.2, a corresponds to the
case of coercion of lazer emanation upon the investigated crystal. As we can
see in the figure, PME is observed in the certain interval of loads (<100g),
and then, together with load increase, the light and dark curves of dependence
$H=\varphi(P)$ coincide. The effect of considerable reduction of MH under the
influence of lighting exists in the depths of indenter-immersion that are not
over the thickness of crystal surfacial layer determined by the inverse value
of absorption coefficient $1/\alpha$, where, on the whole, the aquases are formed
(their concentration decreases farther exponentially). The Fig.2,b, curve 2
shows us the dependence of MH in Si on the intensity of the given emanation
and we can see that the linear abatement of MH turns into saturation. It is
caused by the reason that the thin nearsurfacial layer of crystal, where aquases
arise because of light absorption, is softened after the certain intensity so
greatly that it doesn't make contribution into the value of MH determined by
that part of material that in fact doesn't contain aquases.

The existence of PME is ascertained also in case of coercion by quants
with the energy $h\nu<\Delta E_g$ upon the investigated crystal (Fig.2, Curve 3). The
lighting of Si crystal with such a light leads to the reduction of its MH for all
loads used in practice [13]. Really, the reduction of MH because of the
intensity of lighting with energy of quants $h\nu<\Delta E_g$ (Fig.2,b, Curve 1) has a
linear nature. Therefore, in such a case the value of PME doesn't depend on
the depth of indenter immersion into the investigated crystal. So long as the
investigated Si crystal is transparent for the light $h\nu<\Delta E_g$, the observed PME
must be caused by the light absorption on defects that arise during the process
of imprint-formation, and because of the low coefficient of absorption the
emanation penetrates into the whole region of crystal broken by the indenter,
for any depth of indenter immersion during our experiments.
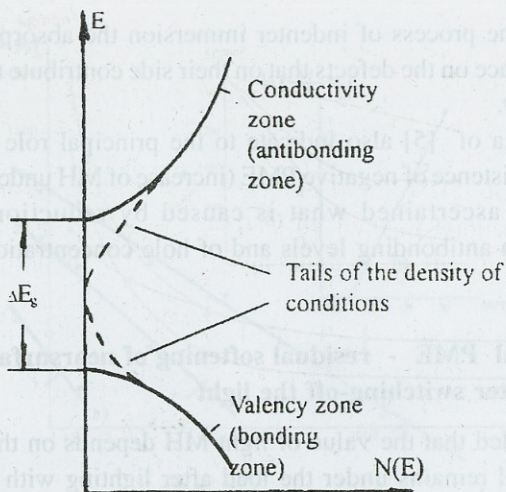
Fig.3. Tails of state density in the forbidden band of semiconductor with a high concentration of defects.

Really, the crystal is disregulated greatly at a touch of the indenter, there is formed the defect structure that stretches into the depth of crystal around the indenter. As we know [14], the greatly disregulated semiconductor has tails of state density in forbidden band (Fig.3), and they on their side must lead to the change of the nature of light optical absorption in the given region in comparison with the unbroken part of crystal. The tails of valency band consist of bonding orbitals, and the tails of conductivity zone consist of antibonding orbitals. The coercion upon such a structure with the quants of light $h\nu < \Delta E_g$ leads to the redistribution of electrons between the tails and to increase of aquase concentration in defect region, what is the reason of softening of this part of material.

The influence of aquases formed because of absorption on the defect part of crystal, in case if the concentrations of unequilibrium carriers generated while lighting of unbroken surface of crystal by lazer ray and by white light coincide, is displayed also in more effective coercion of the white light than - of light $h\nu > \Delta E_g$ (Fig.2,b, Curve 3). We can understand this fact if we'll take into account that because of the wide spectral consistence of white light together with absorption of light quants $h\nu > \Delta E_g$ on the regular part of

crystal during the process of indenter immersion the absorption of quants $hv < \Delta E_g$ takes place on the defects that on their side contribute to the increase of atom mobility.

The data of [5] also indicate to the principal role of aquases in PME, and the existence of negative PME (increase of MH under the influence of lighting) is ascertained what is caused by reduction of electron concentration on antibonding levels and of hole concentration on bonding levels.

4. Residual PME - residual softening of nearsurfacial layer after switching-off the light

It was revealed that the value of light MH depends on the time during which the crystal remains under the load after lighting with white light is switched off. If the load is removed in the moment of switching-off the lighting, we obtain the imprint with less sizes (consequently, MH has
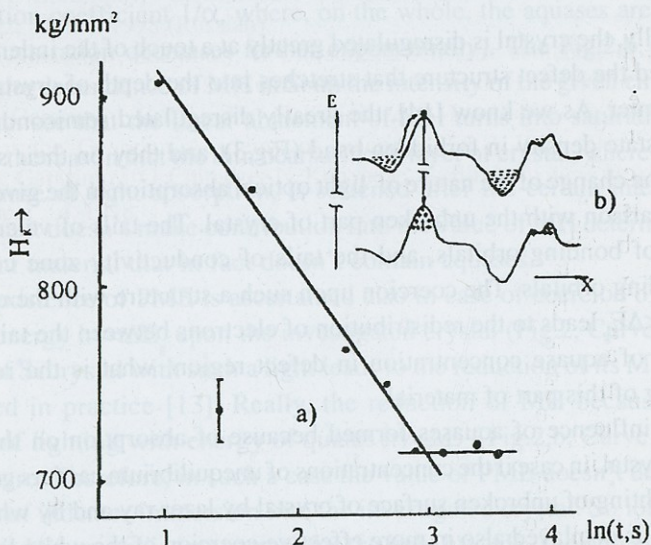
Fig.4. a) Reduction of values of light MH during the time when the specimen remains loaded after stopping the lighting.
b) Recombination transitions in nearsuperfacial region of crystal with heterogeneously bent bands. E-energy, X-coordinate along the surface.

92
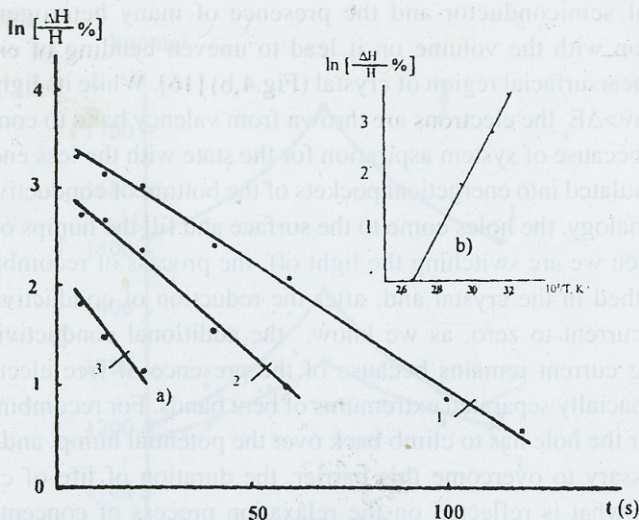
Fig.5. a) Temporal dependence of logarithm of relaxation for relatively changed MH after the stopping of lighting at different temperatures of the specimen: 1-25⁰, 2-50⁰, 3-75⁰.

b) Dependence of logarithm of relatively changed MH after the stopping of lighting on inverse temperature.

heightened values) than in case when the load is removed after the certain interval of time as the lighting is switched off, e.g. in the first case the elastic restoration of the imprint is accomplished. Under equal conditions of experiment this difference is more for small loads and great lightings [15]. The indicated temporal dependence of relaxation of MH is given in Fig.4a.

The residual PME can be observed also during the following experiment: if we first light up the crystal surface for 10 sec, then switch the light off and make imprints after the certain intervals of time. The temporal dependence of relative change of MH after stopping the lighting (relaxation of values of MH to its dark value) has the exponential nature (Fig.5,a). The both experiments indicate to residual influences of the light upon MH after stopping the lighting that we have mentioned as a residual PME[1]. This effect can be explained in such a way: as we know, the break of crystallic structure on the

---

[1]We have to mention that qualitatively analogue results were obtained [4] with the specimen GaAs and GaP, without the corresponding explanation of results.

surface of semiconductor and the presence of many heterogeneities in comparison with the volume on it lead to uneven bending of energetical bands in nearsurfacial region of crystal (Fig.4,b) [16]. While its lighting with the light $h\nu > \Delta E_g$ the electrons are thrown from valency band to conductivity band but because of system aspiration for the state with the less energy they are accumulated into energetical pockets of the bottom of conductivity band.

By analogy, the holes come to the surface and fill the humps of valency band. When we are switching the light off, the process of recombination is accomplished in the crystal and, after the reduction of conductivity at the constant current to zero, as we know, the additional conductivity at the alternating current remains because of the presence of free electrons and holes in spacially separated extremums of bent bands. For recombination the electron or the hole has to climb back over the potential hump, and, because it is necessary to overcome this barrier, the duration of life of carriers is prolonged what is reflected on the relaxation process of concentration of electrons and holes and, consequently, after stopping of lighting the nearsurfacial layer conserves the softening during some period [17]. The fact that together with load increase the value of relaxation effect is reduced and becomes unmeasurable can be explained so that the effect exists in the pressing depth of the indenter into ctystal, and the heterogeneous bending of nearsurfacial region bands approaches to this depth.

In order to prove these suppositions we have carried out the experiments concerning the residual PME at different temperatures of the investigated specimen, and they have shown that the relaxation of values of residual PME to its "dark" value has exponential nature, what depends not only on the time, but also on the temperature (Fig.5 a,b).

5. Anistropy of PME

As it is well-known [8], the value of MH depends on crystallographical orientation of the investigated surface (anisotropy of the 1st type) and on disposition of the indenter relatively to crystallographical directions on the given surface (anisotropy of the 2nd type). In case of Knupp pyramid when its big diagonal is orthogonal to <100> directions on (100) plane of monocrystallic Si, MH has relatively higher value ("hard" direction) than in case when the big diagonal of Knupp pyramid is parallel to <100> directions
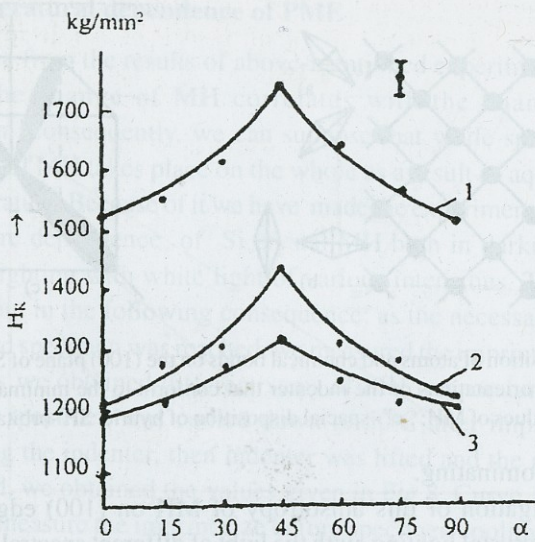
Fig.6. Dependence of values of MH on the (100) edge of Si, on angle that the big diagonal of Knupp pyramid makes with the direction <110> in the darkness (1) and while lighting (2,3) (2 - with light quants, $h\nu < \Delta E_g$, 3 - with light quants, $h\nu > \Delta E_g$).

("soft" direction). When the disposition of the crystal relatively to the immovable indenter is changed, periodically changes also the value of MH - from its minimum to maximum (Fig.6, Curve 1). Let's explain [19]: during the process of imprint-formation under the coercion of indenter in covalent crystal there happen break, pressing, tension and turn of chemical bonds. We can make analysis of indenter position and of chemical bonds spacial disposition. The Fig.7 a,b shows us two-dimensional analogue of disposition of atoms and directions of chemical bonds on the investigated (100) plane of monocrystal Si. However, in fact, the chemical bonds that unite atoms with one another make a certain angle with the surface (Fig.7c). We can see in this figure that, when the big diagonal of Knupp pyramid is disposed along the proection of chemical bonds onto (100) surface of Si monocrystal (Fig.7, a), the tension and turn of chemical bonds are dominating and the break is made easier, so the value of MH is minimal. If the big diagonal makes 45° angle relatively to the projection of chemical bonds onto (100) surface (Fig.7 b), then the value of MH is maximal, because the process

95
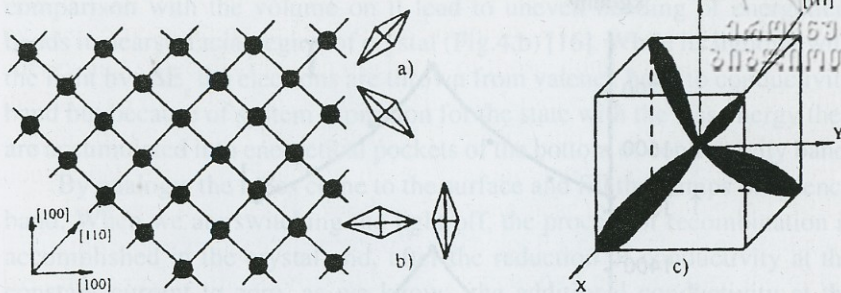
Fig.7. Disposition of atoms and chemical bonds on the (100) plane of Si monocrystal, and two different orientations of the indenter that conform to the minimal - „a" and the maximal - „b", values of MH: „c"- spacial disposition of hybrid SP^3-orbitals in Si crystal.

of pressing is dominating.

The investigation of this anisotropy of MH on (100) edge of Si monocrystal while crystal lighting with the light of different spectral consistences has shown that in case of coercion by quants of light $h\nu<\Delta E_g$ the value of MH-incidence is the same for all directions, e.g., initial anisotropy is conserved (Fig.6, Curve 2). It happens because the anisotropy of the initial crystal is greatly reduced in defect region where the quants $h\nu<\Delta E_g$ are absorbed. In case of coercion by quants of light $h\nu>\Delta E_g$ that is absorbed in unbroken region of crystal the value of MH-incidence for "hard" direction is more than for "soft" direction (Fig.6, Curve 3). As the anisotropy of MH on the edge of monocrystal is determined as the difference between maximal and minimal values of MH [18], on the basis of obtained results we can say that the lighting reduces anisotropy of MH [19]. It takes place because the pressing of directed chemical bonds is dominating for conformity to the maximal value of MH on the given edge of semiconductor, and, evidently, the light after accomplishing the travel of electrons causes the isotropization of sharply directed chemical bonds (Fig.1), and, as a result, the "light" curve is more smooth than the "dark" one. These considerations are proved by the fact that if we consider anisotropy of 2nd kind in case of residual PME while coercion by quants of light with the energy $h\nu>\Delta E_g$, the elastic restoration of imprint for "hard" directions is more than for "soft" directions.

6. Temperatural dependence of PME

As we see from the results of above-mentioned experiments concerning the PME, the change of MH correlates with the change of aquase concentration. Consequently, we can suppose that while specimen heating the reduction of MH takes place on the whole as a result of aquase formation by the temperature. Because of it we have made the experimental investigation of temperature dependence of Si crystal MH both in darkness and while coercion of lighting with white light of various intensities. The experiment was carried out in the following consequence: as the necessary temperature of investigated specimen was reached, we measured the imprint in dependence on conditions we obtained different steps of MH temperatural dependence under. If the specimen was cooled down to 50^0C after imprint-formation, without lifting the indenter, then indenter was lifted and the measuring was accomplished, we obtained the values given in Fig.8, Curve 1. If we lift the indenter and measure the imprint size before specimen cooling, it is less than in case mentioned above, e.g., its elastic restoration is accomplished. This fact, analogue to residual PME, gives us heightened values of MH, what
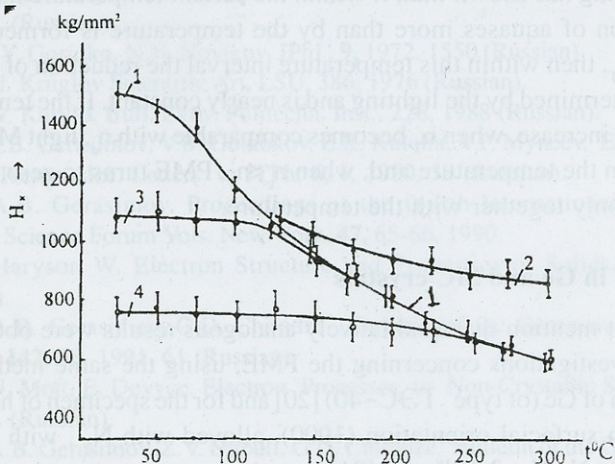
Fig.8. Temperatural dependence in Si of "dark" MH (1,2)-during the two different modes of imprint-formation: 1 - cooling with unlifted indenter, 2 - cooling with lifted indenter, and of "light", MH (3,4) measured in the 1st mode: 3 - at the intensity of white light I_1, 4 - at $I_2 > I_1$.

97

7.

leads to the quasi-saturation of MH by the temperature (Fig.8, Curve 2) that was observed by some authors [5]. From the graph (Fig.8, Curves 1,2) we can see that analogue to the case of light coercion, the concentration increase of aquases formed by the temperature leads both to reduction of MH together with the temperature and to mechanical unstableness of imprint frame that is displayed while increase of elastic restoration of its sizes.

During the investigation process of temperatural dependence of PME the temperature was measured while specimen lighting, and measuring of imprint size was made after specimen cooling with unlifted indenter. We can observe in the Fig.8, Curves 3,4, that at first the temperature doesn't have any influence upon light PME. But for each intensity, as the certain temperature is reached, the dependence of value of light MH on the temperature is displayed, and, if the increase of temperature continues, PME disappears. Also, together with the increase of lighting intensity, the point, where temperature and light curves coincide, is transited to the side of high temperatures.

The comparison of concentration of aquases created both by temperature and by lighting has shown that, if within the certain temperature interval the concentration of aquases more than by the temperature is formed by the light – $n_c > n_T$, then within this temperature interval the reduction of the value of MH is determined by the lighting and is nearly constant. If the temperature continues to increase, when n_T becomes comparable with n_c, light MH begins to depend on the temperature and, when $n_c < n_T$, PME turns to zero, and MH is changed only together with the temperature.

7. PME in Ge and SiC crystals

We must mention that qualitatively analogous results were obtained by us while investigations concerning the PME, using the same methods, for the specimen of Ge (of type ГЭС–40) [20] and for the specimen of hexagonal 6H-SiC with surfacial orientation (1000), alloyed with N_2, with impurity concentration $N_d - N_A = 3 \cdot 10^{18} cm^{-3}$ [21].

Conclusion

Thus, the clear correlation of MH reduction with aquase concentration indicates evidently that the change of MH because of lighting in crystals with mostly covalent bonds is accomplished on the whole because of weakening and isotropization of chemical bonds by antibonding quasiparticles, e.g.,quasiparticles created by excitation of electrons and holes.

REFERENCES

1. G.C. Kuczynsky, R.H. Hochman. Phys. Rev., **108**, 946, 1957.

2. P.P. Kuzmenko, N.N. Novikov, N.V. Goridko. Solid State Phys., **4**, 10, 1962, 2656 (Russian).

3. V.M. Beylin, Y.K. Vekilov. Solid State Phys., 5, 8, 1963, 2372 (Russian).

4. P.P. Kuzmenko, N.N. Novikov, N.Y. Goridko, L.I. Fedorenko. Solid State Phys., **8,** 6, 1966, 1732, (Russian).

5. V.A. Drozdov, L.A. Mozgovaya, A.L. Rvachyov. Rep.of Acad.of Scien.of USSR, **177,** 1, 1967, (Russian).

6. I.A. Domoryad - in: Radiation Physics of Non-Metallic Crystals. Minsk, 1970, 131. (Russian).

7. N.Y. Goridko, N.N. Novikov. JPhI . **9,** 1972, 1550 (Russian).

8. V.I. Kruglov Scientific Art. LSU, 386, 1976 (Russian).

9. I.V. Kurylo. Bull. Lvov. Politechn. Inst., 226, 1988 (Russian).

10. A.B. Gerasimov, V.B. Golubkov, E.R. Kutelia, V.P. Myneev, E.M. Mkrtchian, A.A. Tsertsvadze. Letters to JTPh; **6,** 1, 1980, 58 (Russian).

11. A.B. Gerasimov. Proceedings of the fourth International conference Materials Science Forum Vols. New-York, **47,** 65-66, 1990.

12. Haryson W. Electron Structure and Properties of Solids, M., **1,** 384 (Russian).

13. A.B. Gerasimov, G.D. Chiradze. Bulletin of the Georgian Academy of Sciences, **142,** 53, 1991, 61 (Russian).

14. N. Mott, E. Devyce. Electron Processes in Non-Crystallic Substances, 1, M., 1982. (Russian).

15. A.B. Gerasimov, Z.V. Djibuti, G.D. Chiradze. Bulletin of the Georgian Academy of Sciences; **142,** 1, 1991, 53 (Russian).

16. Problems of Radiation Technology of Semiconductors. red. L.S.Smyrnova. Nauka; Novosybirsk, 1980, 149 (Russian).

17. A.B. Gerasimov, G.D. Chiradze, N.G. Kutivadze, A.P. Bibilashvili, Z.G. Bokhochadze. Solid State Phys., **4,** 1998 (Russian).

18. P.D. Warren, S.G. Roberts, P.B. Hyrsh. Bull. of Acad. of Scien. of USSR, Ser. Phys. **51**, 4, 1987, 812. (Russian).

19. A. Gerasimov, G. Chiradze, N. Kutivadze, A. Bibilashvili, Z. Bokhochadze. Bulletin of the Georgian Academy of Sciences. **157**, 3, 1998, 396.

20. G.D. Chiradze. Autoref.of Dis. Cand. Phys. Mat. Sciences. Tbilisi, 1992 (Russian).

21. A. Gerasimov, G. Chiradze, N. Kutivadze, A. Bibilashvili, Z. Bokhochadze. Bulletin of the Georgian Academy of Sciences. **156**, 3, 1997.

ა. გერასიმოვი, გ. ჭირაძე, ნ. კუტივაძე, ა. ბიბილაშვილი,
ზ. ბოხოჩაძე

ფოტომექანიკური ეფექტის ფიზიკური ბუნება

დასკვნა

ნაშრომში მოცემულია ფოტომექანიკური ეფექტის - ფმე (მიკროსისა-ლის ცვლილება განათების გავლენით) სისტემატური კვლევის შედეგები, ჩატარებული მონოკრისტალურ Si-ის ნიმუშებზე, ერთიანი მეთოდიცით. გამოკვლეულია ფმე-ის დამოკიდებულება სინათლის სპექტრალურ შე-მადგენლობასა და ინტენსივობაზე, ნაჩჳენ ფმე (სინათლის გამორთვის შემდეგ კრისტალის დარბილების შენარჩუნება გარკვეული დროის განმავლობაში), განათების გავლენა მიკროსისალის ანიზოტროპიაზე და ფმე-ის ტემპერატურული დამოკიდებულება.

ჩატარებული კვლევების და ექსპერიმენტული მონაცემების ანალიზის საფუძველზე დადგენილია კორელაცია ფმე-ის სიდიდესა და სინათლით აღგზნებული შესაბამისი არაწონასწორული მატარებლების (ე.წ. ანტიდა-მაკავშირებელი კვაზინაწილაკები) კონცენტრაციას შორის. აღნიშნულის საფუძველზე მოცემულია მექანიზმი, რომლის თანახმად, განათების გავ-ლენით კოვალენტურ კრისტალებში მიკროსისალის შემცირება გამოწ-ვეულია, ძირითადად, სინათლით წარმოქმნილი ანტიდამაკავშირებელი კვა-ზინაწილაკების ხარჯზე, ქიმიური ბმების იზოტროპიზაცითა და შესუსტე-ბით.

ACCUMULATION OF CHARGE IN MIS-STRUCTURE WITH DIELECTRIC AL₂O₃ UNDER THE COECTION OF IONIZING RADIATION

A.Bibilashvili , A.Gerasimov , M.Merabishvili

Abstract. The influence of γ- and electronic irradiation upon the parameters of MIS-structures with dielectric Al_2O_3 obtained with the help of catalytic plasmatic anodizing has been investigated. Comparison of parameters of MIS-structures with dielectric Al_2O_3 obtained by means of catalytic plasmatic anodizing of Al and with generally accepted dielectric SiO_2 after ionizing radiation is given shows that MIS-structure with dielectric SiO_2 is more susceptible to ionizing radiation than the structures with Al_2O_3. The offered model of charge accumulation in dielectric Al_2O_3 after the influence of radiation considers the presence of traps of electron and hole types in the dielectric and, also, the recombination effects on these traps.

The nature of MIS-structure electrophysical properties change for given conditions of irradiation is defined not only by the type but also by properties of dielectric component and, because of it, the way of its obtaining has a great importance. There aren't made many investigations on radiation changes of electric properties in MIS-structure on the basis of dielectric Al_2O_3 though this material is perspective for microelectronics, as it is indicated in [1].

In the given work we have compared the results of coercion of various radiation types upon the parameters of MIS-structures with dielectric Al_2O_3 obtained with the help of plasmatic anodizing and with generally accepted dielectric SiO_2.

Methods of Experiment. In the process of obtaining MIS-structures we used Si of n-type with the orientation (100) and specific resistance 4.5 Om·cm as an underlay. Dielectric Al_2O_3 on Si-underlay was obtained by the method of catalytic plasmatic anoding of Al [2]. Al was sprayed onto the surface of Si processed to the 14th class of purity using the method of resistive evaporation in vacuum $6.6·10^{-4}$ Pa. Y was sprayed onto structures Si-Al using the method of electron-radiate evaporation with the temperature 373K.

Then we have placed the obtained Si-Al-Y structures into low-temperatural oxygen plasma (the temperature of the pattern was not over 313K). The process of Y-Al oxidation is accomplished during the feeding of positive removal relatively to plasma onto the pattern. The oxide Y_2O_3 serves as a catalyst that accelerates the oxidation process nearly 50 times. After the process Y_2O_3 is etched out in concentrated nitric acid. Ellipsometric measuring has shown that the thicknesses of different films of Al_2O_3 is in the interval 90-120 nm. Dielectrical films of SiO_2 with thickness 100-120nm are obtained by thermal oxidation of Si in "moist" and "dry" oxygen with the temperature 1432K. In order to finish the creation of MIS-structures we have sprayed the contact platforms of Al with the diameter 1.5 mm onto the surface of dielectrics through the stencil.

The obtained MIS-structures were exposed to electronic and γ-irradiation. The energy of electrons during irradiation process was 3 MeV, the intensity - $2.5 \cdot 10^{12} cm^{-2} s^{-1}$. The source of γ-irradiation was InGa - circuit of reactor with the intensity $1.2 \cdot 10^6$ r/hour. While irradiation different tensions were removed onto metallic electrodes of MIS-structures. The temperature of patterns was not over 350 K for all types of radiation.

The investigation of space distribution of radiation-induced charge in dielectric was carried out by the method of layer-by-layer etching out of dielectrical films after electronic irradiation with integral stream $10^{15} cm^{-2}$. 1 per cent hydrate of hydrofluoric acid was used for etching of oxide layer of SiO_2, and for etching of Al_2O_3 used the boiling concentrated orthophosphoric acid. The velocity of etching in both cases was ~1 nm/s. Thicknesses were measured with ellipsometer on each stage of etching.

The electrophysical characteristics of MIS-structures were studied using the method of declining of high-frequent volt-faradic curves. We have determined the charge in oxide volume according to the tension shear of experimental curves relatively to the theoretical C-V characteristics in points corresponding to the plane zones and to the middle of forbidden band of Si, strictly speaking, the charge on rapid surfacial states. It is well-known [3,4] that the distribution of density of surfacial states according to energies in the system Si-SiO_2 has a minimum in the middle of forbidden band of Si and surfacial states are neutral both for p-type and for n-type of Si when the level of Fermi is placed in the middle of forbidden band [5]. Because of it, if

the charge in the oxide will be calculated according to the points of the middle of forbidden band of Si, then the error that is conditioned by surfacial states will be minimal.

Results and their Consideration. The results of investigation of radiation-induced charge distribution in dielectrics after electronic irradiation are shown in Fig.1. The graphs indicate that after the irradiation in the same patterns distribution of the charge brought out by radiation doesn't depend on tension at the gate, and the differences in changes of plane zone tensions while different tensions at the gate are explained by the quantity of captured charge.
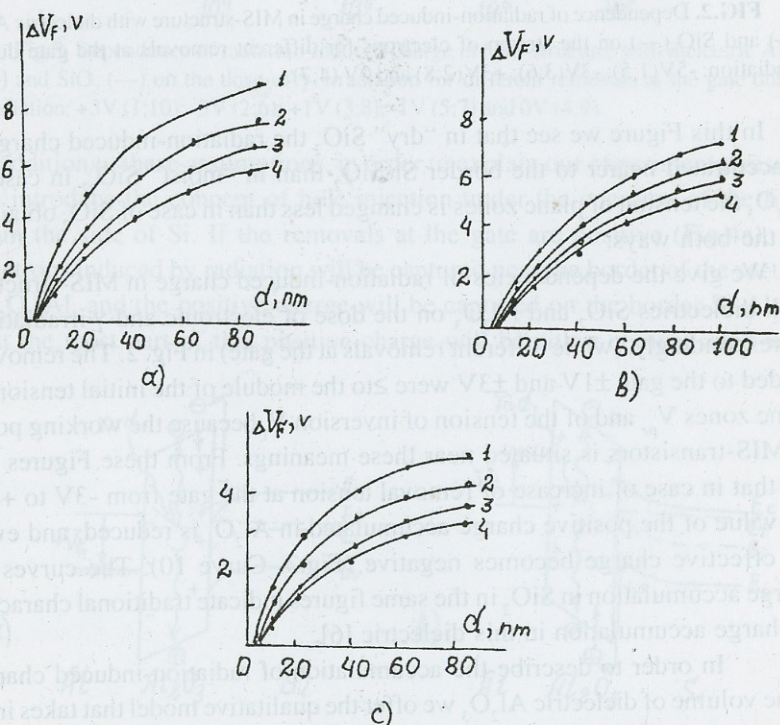
Fig.1. Change of tension of plane zones according to thickness in dielectric SiO_2 ("dry", (a) and "moist", (b)) and Al_2O_3(c) for different removals at the gate during electronic irradiation: +5V (1); -5V (2); 0V (3) and without irradiation (4).
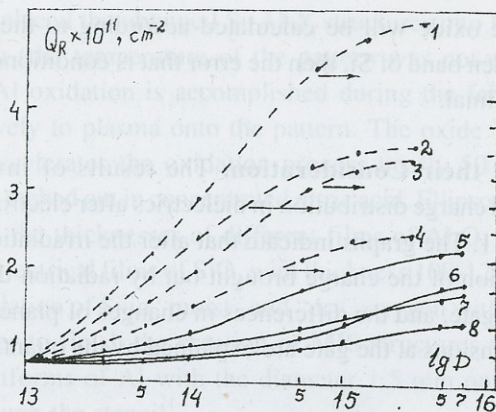
FIG.2. Dependence of radiation-induced charge in MIS-structure with dielectric Al_2O_3 (—) and SiO_2 (—) on the stream of electrons for different removals at the gate during irradiation: -5V(1;5); -3V(3;6); +3V(2;8) and 0V (4;7).

In this Figure we see that in "dry" SiO_2 the radiation-induced charge is concentrated nearer to the border $Si-SiO_2$ than in "moist" SiO_2, in case of Al_2O_3 the tension of plane zones is changed less than in case of SiO_2 obtained by the both ways.

We give the dependencies of radiation-induced charge in MIS-structure with dielectrics SiO_2 and Al_2O_3 on the dose of electronic and γ-irradiation, correspondingly, (while different removals at the gate) in Fig. 2. The removals feeded to the gate $\pm1V$ and $\pm3V$ were $\geq$to the module of the initial tension of plane zones V_{pz} and of the tension of inversion V_i because the working point of MIS-transistors is situated near these meanings. From these Figures we see that in case of increase of removal tension at the gate from -3V to +3V the value of the positive charge accumulated in Al_2O_3 is reduced, and even the effective charge becomes negative (Fig.3, Curve 10). The curves of charge accumulation in SiO_2 in the same figures indicate traditional character of charge accumulation in this dielectric [6].

In order to describe the accumulation of radiation-induced charge in the volume of dielectric Al_2O_3 we offer the qualitative model that takes into account the assumptions of Harari [7] about the presence of electron and hole traps in Al_2O_3, about their space distribution, about the processes of electronic recombination induced by the field near the surface of Si section.

104
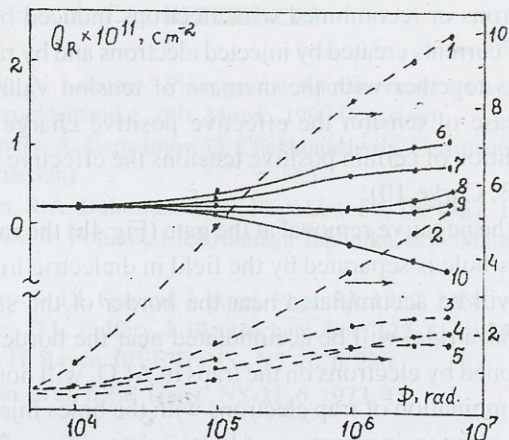
Fig.3. Dependence of radiation-induced charge in MIS-structure with dielectric Al_2O_3 (—) and SiO_2 (---) on the dose of γ- irradiation for different removals at the gate during irradiation: +3V (1;10); -3V (2;6); +1V (3;8); -1V (5;7) and 0V (4;9).

In addition to these assumptions, in order to explain our experimental results we introduce the concept of hole injection under the coercion of the field from the side of Si. If the removals at the gate are positive (Fig.4a), the electrons induced by radiation will be captured near the border of the section Al_2O_3-Al, and the positive charge will be captured on the border Si-Al_2O_3. But the most part of this positive charge will be either compensated with
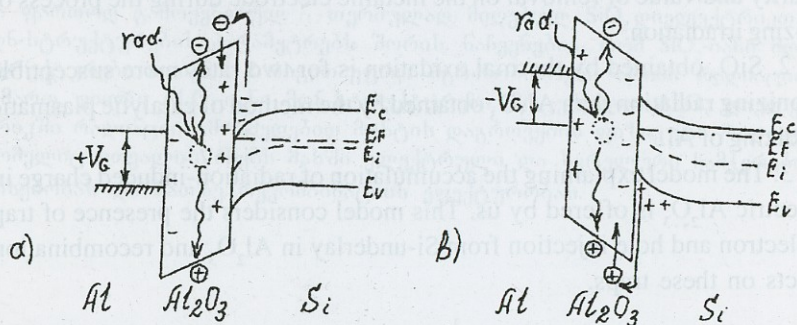
FIG.4. Schematic model of accumulation of radiation-induced charge in dielectric during ionizing irradiation: a) positive removal at the gate, and b) negative removal at the gate.

captured electrons or recombined with electrons induced by the field from Si. The ratio of currents created by injected electrons and by radiation-induced holes increases together with the increase of tension value. e.g. together with the increase of tension the effective positive charge is reduced and under the condition of certain positive tensions the effective charge becomes negative (Fig.3, Curve 10).

In case of the negative removal at the gate (Fig.4b) the radiation-induced couple electron-hole is separated by the field in dielectric in such a way that the electrons will be accumulated near the border of the section $Si-Al_2O_3$, and the holes, as a rule, will be accumulated near the border $Al-Al_2O_3$. The charge conditioned by electrons on the traps in Al_2O_3 will not be displayed as a result of recombination of trap electrons with the holes injected from Si, or - as a result of compensing capture of holes injected from Si onto the traps near the border Al_2O_3 - Si. In case of increase of negative removal at the gate the hole injection is increased and we observe the increase of the accumulated positive charge (Fig.2, Curve 5; Fig.3, Curve 6).

Thus, we can conclude that in Al_2O_3 obtained by plasmatic anoding of Al there exist the traps of electron- and, also, of hole types, and in SiO_2 there are only hole traps [8].

Conclusions. 1. The value of radiation-induced charge and its disposition relatively to the border of the section dielectric-semiconductor depend on polarity and value of removal on the metallic electrode during the process of ionizing irradiation.

2. SiO_2 obtained by thermal oxidation is for two rates more susceptible to ionizing radiation than Al_2O_3 obtained by the method of catalytic plasmatic anodizing of Al.

3. The model explaining the accumulation of radiation-induced charge in dielectric Al_2O_3 is offered by us. This model considers the presence of trap of electron and hole injection from Si-underlay in Al_2O_3 and recombination effects on these traps.

<div align="right">

Tbilisi I. Javakhishvili State University

</div>

REFERENCES
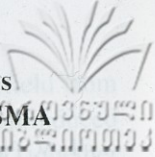
1. V. Parrhutic, V. Labunov. Plazmennoe Anodirovanye - Phyzika, Tekhnika, Primenenye v microelectronike, 280. Minsk, 1990 (Russian)

2. A. Bibilashvily, A. Gerasimov, G. Chakhunashvily. Certificate of Authorship N551972, 1976 (Russian)

3. S.A. Nelson, R.A. Buhrman. Appl. Phys.Lett. **50**, 16, 1987, 1095-1097.

4. G. Kuznetsov, V. Polunin. Electronnaya Tekhnika, ser. "Materialy", **4**, 1977, 105-108 (Russian)

5. J.H. Westbrook, J.J. Gilman. J. Appl. Phys. **33**, 1962, 2360.

6. J.J.H. Reche, D.L. Pulfery. J. Electrochem. Soc. **122**, 11, 1975, 1553.

7. E. Harari, S.H. Rayce, IEEE TraNS., NS-20, 6, 280.

8. F.B. McLean. et al. IEEE Trans., NS-21, 6, 1973, 47.

ა.ბიბილაშვილი, ა.გერასიმოვი, მ.მგრაბიშვილი

Al_2O_3 დიელექტრიკიან მდნ-სტრუქტურაში მუხტის დაგროვება მაიონიზირებელი რადიაციის მოქმედებით

დასკვნა

მოცემულია γ და ელექტრონული გასხივების მოქმედების შედეგები Al_2O_3 დიელექტრიკიან მდნ-სტრუქტურის პარამეტრებზე, როცა დიელექტრიკი Al_2O_3 მიღებულ იქნა კატალიზური პლაზმური ანოდირებით. მოცემულია რადიაციის გავლენის შედარება ზემოთ აღნიშნულ Al_2O_3 დიელექტრიკიან და ფართოდ გამოყენებულ – თერმულად მიღებულ SiO_2 დიელექტრიკიან მდნ-სტრუქტურების პარამეტრებს შორის. ნაჩვენებია, რომ SiO_2-იანი მდნ-სტრუქტურები თითქმის 2 რიგით უფრო მგრძნობიარენი არიან რადიაციის მიმართ, ვიდრე Al_2O_3-იანი მდნ-სტრუქტურები. მოცემულია Al_2O_3 დიელექტრიკში რადიაციის მოქმედებით მუხტის დაგროვების ფიზიკური მოდელი, რომელიც ითვალისწინებს მასში ელექტრული და ხვრელური ჩამჭერების არსებობას და მათზე რეკომბინაციის ეფექტურობას.

INVESTIGATION OF CONTACT OF Ti-Ge/GaAs SCHOTTKY BARRIER OBTAINED BY ION-PLASMA METHOD

A.Bibilashvili, A.Gerasimov, Z.Samadashvili

<u>Abstract</u>. The height of potential barrier (φ_b) and of perfectness coefficient (n) depends on per cent consistence of alloy (Ti-Ge) and on modes of photon treatment for contact with Schottky Barrier Ti-Ge/GaAs. We have established the optimal production process for obtaining contacts with Schottky Barrier, of high quality and stableness. The photon treatment with impulse power 5 kwt the alloy 4at%Ge – Ti is shown to be useful to give us the contacts with higher quality and stableness. We have observed experimentally that, because of chemical activity of Ti to oxygen, in contact layer there exists oxygen, and its contents is decreasable with the help of photon treatment.

The devices with Schottky Barrier (SB) bases are used widely for production process of integrated microcircuits (IMC) on GaAs [1,2]. The quality and stableness of SB define the parameters of IMC on GaAs and for this reason investigation of characteristics of new contact systems is very actual. Alloys of various materials can be the perspective material for creation of stable and high-quality contacts on GaAs SB. During this process one of alloy compounds must be a shallow donor that is surface-active in GaAs and must have a high solubility in it [3]. The second compound of alloy must have a low solubility with the first compound and for it that's obligatory not to form intermetallic fusion with GaAs [4,5].

The alloy Ti-Ge is perspective from this point of view because Ge is a shallow donor in GaAs and has a high solubility in it, Ti is inert regarding to GaAs and Ge, and the formation of intermetallic phases is difficult to arise [6].

In the given work there are investigated electrophysical parameters of Schottky Barrier Contact (SBC)-GaAs on the bases of Ti-Ge alloys obtained with the help of ion-plasma method.

Methods of experiment

We have used as a body epitaxial structures of n-type GaAs, of crystallographic orientation (100), with concentration of charge carriers $10^{17}cm^{-3}$. Films of alloy were plated using the method of ion-plasma spraying of mosaic target. The target consists of sheets of iodic Ti and of especially pure Ge disposed on it mosaically. For target spraying Ar ions were used. Before alloy plating we polished the surfaces of GaAs chemically following the well-known standard technology. The treatment of Ti-Ge/GaAs contacts was carried out using the photon method. The photon treatment was accomplished on a special unit that allowed to vary impulse power within the interval $0\div19$ kwt. and duration of light impulse – $0.1\div10$ sec (with the step 0,1sec), the range of emanation spectrum was $0,4\div3,5$mcm.

The values of barrier heights and of coefficients of contact perfectness for Ti-Ge/GaAs were defined by the method VAC. Investigation of element consistence of its change that is corresponding to the depth of surface structure was carried out using the method of Auger-Electron Spectroscopy (AES) on the set of PHI-450 type with coaxial analyzer of "cylindrical mirror".

Results and discussion

During the process of Ti-Ge alloy plating the mixture ratio was calculated according to the formula:

$$C_i = \alpha_i S_i / \sum \alpha_j S_j \cdot 100\%,$$

where S_i is the area engaged by i^{th} compound, α_i - coefficient of spraying of ith compound, C_i – its concentration.

The films of alloy with Ge contents 4at% and 12at% were plated. The thickness of films was $150 \div 160$nm. The error of mixture calculation was not over 2%.

N	Pesidual Pressure in Chamber, Pa	Pressure of Worcing Gaz, Pa	Current of discharge, A	Voltage on Target, kV	Current of Target, mA	Volocity of Plating, nm/min
1	$2 \cdot 10^{-3}$	$7 \cdot 10^{-2}$	4	1	15	5
2			5	2	30	12
3			5	3	40	14
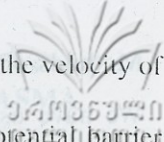
..able shows the working modes of spraying unit and the velocity of alloy deposition.

In Fig.1 there are given the graphs of dependence of potential barrier height and of perfectness coefficient for SB contact of Ti-Ge/GaAs 4at% and 12at% Ge in alloy obtained in the mode 3 (table), on time of photon annealing, while impulse power 5 kwt and 7 kwt.
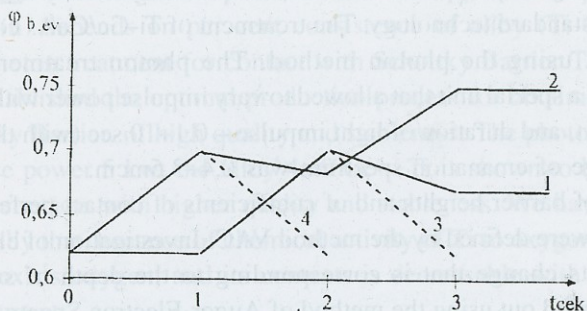
a)
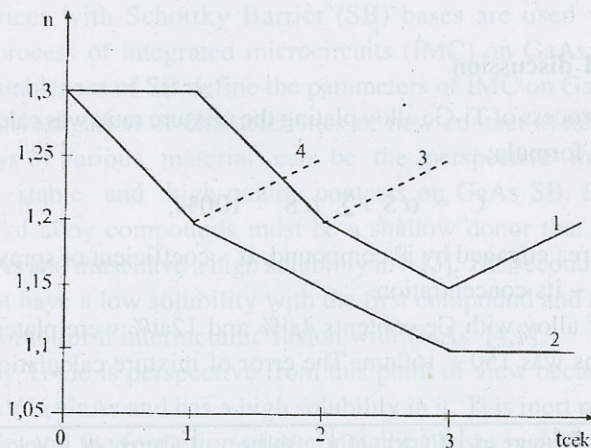
b)

Fig.1. Influence of photon coercion upon the height of potential barrier φ_h (a) and upon perfectness coefficient n (b), while different percent contents of Ge in Ti film: 4at%Ge –1; 2, 12at%Ge – 3; 4, and powers of photon treatment: 5 kwt – 1; 3, 7 kwt – 2; 4.

a)

b)
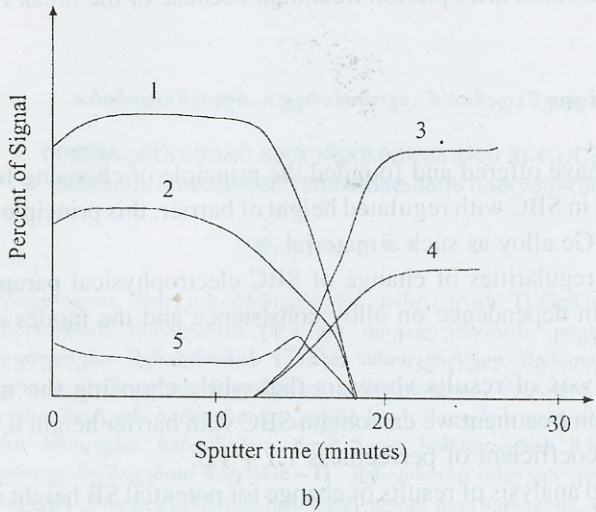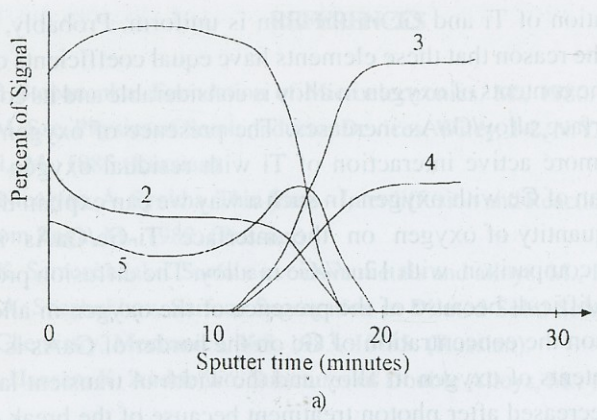
Fig.2. Profiles of element distribution according to the depths of contact systems Ti-Ge/GaAs obtained by the method of ion-plasma spraying: a) Ti – 4at%Ge; b) Ti - 12at%Ge. 1 – Ti; 2 – Ge; 3 – Ga; 4 – As; 5 – O.

As we see in Fig.1, we obtain more qualitative and stable contacts while 4at%Ge in alloy, after photon treatment of contact with impulse power 5 kwt.

Fig.2 gives typical AES profiles of elements distribution corresponding to the depth of contact systems Ti-Ge/GaAs 4at% and 12at%. As we can see,

the distribution of Ti and Ge in the film is uniform. Probably, this fact is caused by the reason that these elements have equal coefficients of spraying. However, the contents of oxygen in alloy is considerable and its concentration on the interface alloy/GaAs increases. The presence of oxygen in alloy is caused by more active interaction of Ti with residual oxygen in vacuum chamber than of Ge with oxygen. In such a way we can explain the presence of a great quantity of oxygen on the interface Ti-Ge/GaAs in case of 4at% Ge in comparison with 12at% Ge in alloy. The diffusion process of Ge in GaAs is difficult because of the presence of the oxygen in alloy [3], and for this reason the concentration of Ge on the border of GaAs is decreased.

The contents of oxygen in alloy and the width of transient layer Ti-Ge/GaAs are decreased after photon treatment because of the break of bond Ti – oxygen.

Conclusions

1.   We have offered and founded the principle of choosing for contact material used in SBC with regulated height of barrier; this principle allows us to choose Ti-Ge alloy as such a material.

2.   The regularities of change of SBC electrophysical parameters are investigated in dependence on alloy consistence and the modes of photon treatment.

3.   Analysis of results show us that while choosing the modes for impulse photon treatment we can obtain SBC with barrier height $0.62 \div 0.75$ eV and with coefficient of perfectness $1.1 \div 1.3$.

Compared analysis of results of change for potential SB height value and for value of perfectness coefficient allows us to use the offered technology for production of stable digital IC on GaAs.

Tbilisi I. Javakhishvili State University

112

REFERENCES

1. I.P. Stepanenko. Foundation of Microelectronics, M., 1980. (Russian).

2. S.M. Sze, Physics of Semiconductor Devices, Wiley, **1-2**, N.Y., 1881., Transl. from Engl., M., 1985 (Russian).

3. E. Nicolyan, A. Synkha. Thin films – Interdiffusion and Reactions, N.Y., 1978., Transl. from Engl., M., 1982. (Russian).

4. V.K. Semenchenko. Surface events in metals and alloys. M., 1977 (Russian).

5. A.A. Shezbukhov, Surface Segregation in Diluted Solid Solutions. Surface, Physics, Chemistry, Mechanics, №8, 1983, 13-25. (Russian).

6. M. Hansen, K. Andrienko. Structures of Double Alloys, M., 1968 (Russian).

ა.ბიბილაშვილი, ა.გერასიმოვი, ზ.სამადაშვილი

ᲘᲝᲜᲣᲠ-ᲙᲚᲐᲮᲛᲣᲠᲘ ᲛᲔᲗᲝᲓᲘᲗ ᲛᲘᲦᲔᲑᲣᲚᲘ Ti-Ge/GaAs
ᲨᲝᲢᲙᲘᲡ ᲑᲐᲠᲘᲔᲠᲘᲐᲜᲘ ᲙᲝᲜᲢᲐᲥᲢᲔᲑᲘᲡ ᲒᲐᲛᲝᲙᲕᲚᲔᲕᲐ

დასკვნა

შესწავლილია შოტკის ბარიერიანი კონტაქტის Ti-Ge/GaAs პოტენცია-ლური ბარიერის სიმაღლის (φ_b) და იდეალურობის კოეფიციენტის (ნ) დამოკიდებულება შენადნობის (Ti-Ge) პროცენტულ შემადგენლობაზე და ფოტონური დამუშავების რეჟიმებზე. დადგენილია, მაღალი ხარისხის და სტაბილური შოტკის ბარიერიანი კონტაქტის მიღების ოპტიმალური ტექნო-ლოგიური პროცესი. ნაჩვენებია, რომ 5კევ სიმძლავრის მქონე იმპულსის ფოტონური დამუშავებით 4ატ%Ge – Ti შენადნობი იძლევა უფრო ხარისხიან და სტაბილურ კონტაქტებს. ექსპერიმენტულად დამუხრილია, რომ ჭანგბადის მიმართ ტიტანის ქიმიური აქტივობის გამო, კონტაქტურ ფენაში არსებობს ჭანგბადი, რომლის შემცვლობა ფოტონური დამუშავების შემდეგ მცირდება.

8.

INELASTIC PROCESSES IN SLOW COLLISIONS BETWEEN ALKALI METAL IONS AND INERT GAS ATOMS.

B. Kikiani, R. Lomsadze, N. Mosulishvili

Abstracts. The energy dependences of the absolute cross sections of ionization (σ_i), charge trasfer (σ_c) and electron loss (σ_s) processes at the collisions of atomic particles with closed electron shells (Li^+, Na^+, K^+ - He, Ne, Ar) in the energy range 1-7 keV, have been determined. For interpretation of experimental results modern theoretical representation are used.

Introduction. Measurements of the absolute cross sections of the inelastic processes of alkali metal ions and inert gas atoms collisions in the region of several hundred and thousand electron volt energy are connected with experimental difficulties. In these cases colliding particles are characterized by closed electron shells and processes realized on a small internuclear distances R. The projectile ions are scattered through relatively large angles and this is accompanied by the formation of much more energetic secondary particles (target gas ions and free electrons) than is usual. The energies of these particles may reach tens of electron volts. This circumstance has not been considered in the earlier papers, which must raise doubts about the reliability of the measurements themselves and the conclusions drawn from them. On the other hand, these data are necessary for solution of many fundamental and applied problems (plasma and upper atmosphere physics, astrophysics and etc.).

The energy dependence of the absolute total cross sections of the processes of ionization σ_i, charge transfer σ_c and projectile ions electron loss (stripping) σ_s during collisions of alkali metal ions and inert gas atoms in the energy range 1-7 keV were determined in this work. Cross sections σ_i and σ_c were measured by an improved transverse electric field ("condenser") method, and σ_s, by recording double charged primary ions, produced as a result of collisions, using mass spectrometric system.

An estimate for the uncertainty in the absolute values of cross sections given below is about 15%.

Experimental arrangement and measurement methods.

The main parts of the used mass spectrometer arrangement are (Fig.1): surface ionization type ions source I; magnetic mass analysers M_1, M_2; accelerating and focusing (quadrupole lenses) system L_1; collimating slits S_0 - S_8; collision chambers C_1, C_2; valves G_1, G_2 for admission target gas in these chambers; ionization manometers P_1, P_2 and detectors of projectile ions F_1, F_2. Target gas pressure in the chambers (about 10^{-4} torr) corresponds to single collisions condition. Differential pumping system D secured vacuum about 10^{-6} torr in other parts of the arrangement. The standard transverse field method [I] involves collection with the aid of an electric field of plane condeenser K, of target gas ions and electrons generated by the passage of projectile ions through a gaseous target. Absolute cross sections of production of these particles σ_+ and σ_- are connected with cross sections σ_i, σ_c, σ_s by the following way:

$$\sigma_+ \cong \sigma_i + \sigma_c, \qquad \sigma_- \cong \sigma_i + \sigma_s$$

In view of the characteristic features of the investigated pairs of particles mentioned above, the standard method was modified. For fixed of the homogeneous part of field ("collision length") the condenser electrod was divided by small parallel sections (1-10 sections) and charge distribution was studied on them. In front of the electros a grid g is placed to suppress
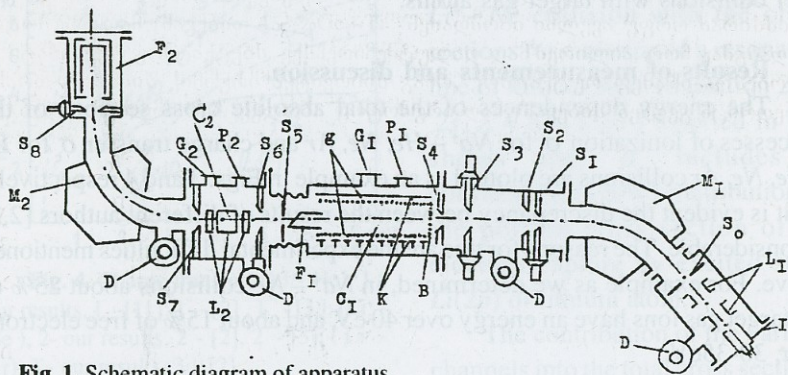
Fig. 1. Schematic diagram of apparatus.

115
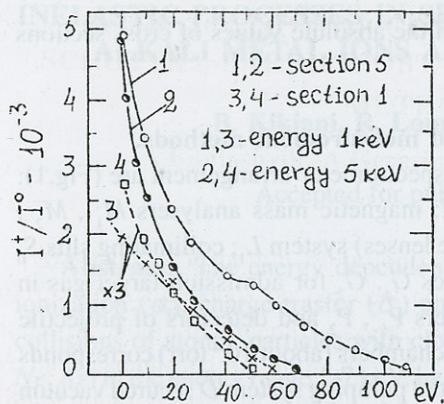
Fig.2. The dependence of the currents of positive ions scattering on the sections 1 and 5 from stopping potential.

secondary electron emission from the surface of sections. This grid is used to receive an information about energetical spectrum of scattering particles by "stopping potential" method too. In Fig.2 a dependence of the current of ions scattering on the section located as close as posible to the energy slit (S_4) of chamber C_1 (section 1, curves 3 and 4) and on the middle section (section 5, curves 1 and 2) from stopping potential for $K^+ + Ar$ pair at energy $E = 1$ keV and $E=5$ keV is ploted (curves 1,3 and 2,4 respectively). Considerable difference between these curents is connected with the high probability of the hit of scattering projectile ions on the middle section. That's way, section "I" was chosen as a measuring and hence additional electrod system is mounted to provide homogeneity of the field in this region (electrods B in Fig.1).

Absolute cross sections of the stripping processes σ_s were measured in separate experiments by mass spectrometer analyzis M_2 of projectile ions beam after passing through the collision chamber C_2, filled with the target gas. The electric lens L_2 (Fig.2) provides the focusing of the projectile ions after collisions with target gas atoms.

Results of measurements and discussion.

The energy dependences of the total absolute cross sections of the processes of ionization σ_i for $Na^+ - He, Ne, Ar$ and charge transfer σ_c for $Li^+ - He, Ne, Ar$ collisions are plotted as an example in Figs. 3 and 4 respectively. As it is evident the discrepancy between the results of different authors [2,3] is considerable. The reasons for this are the experimental difficulties mentioned above. For example as we determined, in $Na^+ - Ne$ collisions about 25% of the target gas ions have an energy over 40 eV, and about 15% of free electrons over, 30-35eV.

116
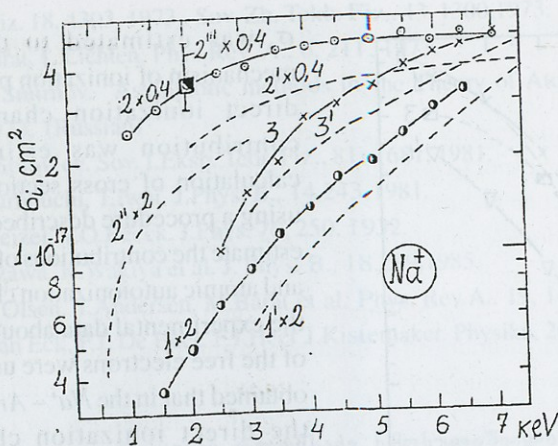
Fig.3. Ionization: (Na$^+$- He), 1 - our results, 1' -[2]; (Na$^+$- Ne), 2- our results, 2' - [2]; 2'' - [3]; 2''' - [10]; (Na$^+$- Ar), 3- our results, 3' - [2].

The interpretation of our results by plotting schematic correlation diagrams of diabatic terms of the colliding system [4] and the use of model representations [5,6] expresses certain conclusions about the mechanisms of the relevant processes. It was found that in $Li^+ - Ar$ collisions an electron is captured mainly into graund state of lithium atom Li(2s), at internuclear distance R~1.5 a.u. For $Li^+ - Ne$ pair the charge transfer is realized through intermediate state $Li^+ - Ne(2p^5\ 3s)$ at relatively large distances R .
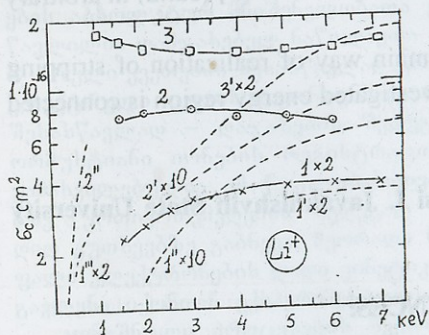
Fig. 4. Charge transfer: (Li$^+$- He), 1 - our results, 1' - [11]; 1'' - [2]; 1''' - [3]; (Li$^+$- Ne), 2- our results, 2' - [2], 2'' - [3]; (Li$^+$- Ar), 3 - our results, 3' - [2].

A comparision of our data for $Li^+ - Ne$ collision with the cross sections for emission of a resonance line of lithium atom (transition $2p - 2s$, $\lambda = 670,8$ nm) reported in [7], shows that σ_c includes a considerable (~50%) contribution of the portion cross section of an electron capture by excited state $Li(2p)$ of lithium atom.

The contribution of the various channels into the total cross sections

117
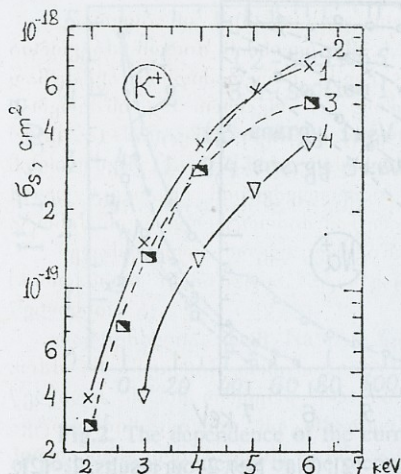
Fig. 5. Stripping: (K⁺-He), 1 - our results, 2 - [9], 3 - [6]; (K⁺-Ne), 4 - our results.

σ_i was estimated to define the mechanism of ionization process. For direct ionization channel such contribution was estimated by calculation of cross sections portion using a procedure described in [6]. To estimate the contributions of molecular and atomic autoionization channels [8] the experimental data about spectrum of the free electrons were used. It was obtained that in the $Na^+ - Ar$ collisions the direct ionization channel is predominated, whereas for the $Na^+ - He$ pair the process of atomic autoionization of neon is about 30% and direct ionization - about 10%. In the case of $Na^+ - He$ pair the atomic autoionization channel of helium is the main one.

In Fig.5 our experimental (curves 1 and 4) and calculated (cur.3) data of stripping cross sections σ_s at the $K^+ - He$, Ne collisions are compared with experiments data of the excitation cross section of ten autoionization states of K^+ ions at the collision $K^+ - He$ reported in [9] (cur.2) in arbitrary units.

The comparision shows that the main way of realization of stripping process at least for $K^+ - He$ pair in investigated energy region is connected with direct ionization mechanism.

Tbilisi I. Javakhishvili State University

REFERENCES:

1. N.V.Fedorenko et al. Sov. Zh. Tekh. Fiz., 26, 1929,1956.

2. I.P.Flaks, B.I.Kikiani, G.N.Ogurtsou. Sov.Zh.Tekh.Fiz., 35 1965,2076.

3. Z.Z.Latipov, A.A.Shaporenko. Sov Zh.Eksp.Teor.Fiz., 69, 1944, 1975; Sov.Zh.

Eksp. Teor.Fiz. 18, 4303, 1973., Sov. Zh. Tekh. Fiz., 43, 1300,1973.

   4. M.Barat, L.Lichten. Phys.Rev. A., 6, 211, 1973.

   5. B.M.Smirnov. "Asymptotic methods in the Theory of Atomic Collisions", Moscow, 1973. (Russian)

   6. E.A.Solov'ev. Sov. I.Eksp. Teor. Fiz., 81, 1681, 1981.

   7. S.Tsurubuchi, T.Iwai. J.Phys. B., 14,243,1981.

   8. W.Weizel, V.O.Beeck. J.Phys, 76, 250, 1932.

   9.H.Aizawa, K.Wakiya et al. J. Phys. B., 18,289,1985.

10 J.O.Olsen, T.Andersen, M.Barat et al. Phys. Rev.A., 19, 1457, 1979.

11. J.Van Eck, F.J. De Heer, F.J.Heer J.Kistemaker. Physika, 26, 1960, 629.

ბ.კიკიანი, რ.ლომსაძე, ნ.მოსულიშვილი

ნელი არადრეკადი დაჯახებები ტუტემეტალთა იონებსა და ინერტული გაზების ატომებს შორის

დასკვნა

   ნაკვეთილი ელექტრონული გარსის მქონე სისტემებისათვის (Li$^+$, Na$^+$ K$^+$ - He, Ne ,Ar) გაზომილია არადრეკადი პროცესების კვეთების აბსოლუტურ მნიშვნელობათა სიდიდეები. იონიზაციის σ_i, გადამუხტვის σ_c და დამჯახებელი იონის მიერ ელექტრონის დაკარგვის ("�′აგლეჯის") სრული კვეთების აბსოლუტურ მნიშვნელობათა ენერგიისაგან დამოკიდებულება შესწავლილია დამჯახებელ ნაწილაკთა 1-7 კვვ ენერგიის ინტერვალში. σ_i და σ_c სრული კვეთების შესასწავლად გამოყენებულია გაუმჯობესებული განივი ელექტრული ველის ("კონდენსატორის") მეთოდი, ხოლო σ_s პროცესთა შესასწავლად — დახახების შედეგად მიღებული სხრავი, პირველადი ორმუხტიანი იონების რეგისტრაციის მეთოდი. ნაშრომში ყურადღება გამახვილებულია ამ �′კვლევებისათვის დამახასიათებელ ისეთ ფაქტორ-ზე (ერთიერთთქმედების შედეგად მიღებული პირველადი ნაწილაკების დიდ კუთხეზე გაბნევა, მეორადი ნაწილაკების — იონებისა და თავისუფალი ელექტრონების დიდი კინეტიკური ენერგია), რომლებსაც ′შეუძლიათ გავლენა იქონიონ ექსპერიმენტული მონაცემების საიმედობაზე.

   აღნიშნული პროცესების მექანიზმის დადგენის მიზნით, ნაშრომში მოყვანილი ′შედეგები ′შედარებულია მსგავსი გაზომვების ავტორთა მონაცემებთან, რიგ ′შემთხვევებში კვეთები გათვლილია თეორიულად, მიდელურ ′წარმოდგენებში. ნანვრებია, რომ Li$^+$-Ar ′წყვილის ′შემთხვევაში ელექტრონის ′შაჭარა (გადამუხტვა) ′წარმოებს ლითიუმის ატომის ძირითად

ქ..., ხარკიებაში Li(1s²2s) და ელექტრონულ გადასვლას ადგილი ექვს ბირთვექს შორის მანძილის R~ 1,5 აქ Li⁺-Ne წყვილის შემოხვევაში... და... დამესტვა მიმდინარეობს ასევე ელექტრონის ჩაჭერით ჯირითად... მდგო... მარკიებაში და პროცესი რეალიზდება შეადედური მდგომარეობის Li⁺ - Ne(2p⁵3s) სისტემის ტერმზე გავლით. შედარებით დიდ ბირთვექს შორის მანძილზე R₀, Li⁺-He სისტემის შესწავდამ ანვესა, რომ აღნიშნული წყვილის სრულ კვეთაში მნიშვნელოვანი წვლილი (~ 50%) შეაქვს ლითიუმის ატომის მიერ ელექტრონის ჩაჭერას აღგხნებულ მდგომარეობაში Li(1s²2p).

შეფახებულია სრულ კვეთებში სხვადასხვა იონიზაციური პროცესების (პირდაპირი იონიზაცია, ატომური და მოლეკულური ავტოიონიზაცის) წვლიდი.

დადგენილია, რომ Na⁺-Ar წყვილისათვის - პირდაპირი იონიზაციის არხს ამ წყვილის იონიზაციის სრულ კვეთაში შეაქვს განსახადვერელი წვლიდი. მაშინ როდესაც Na⁺-Ne წყვილის შემოხვევაში, ნეონის ატომის ავტოიონიზაციური მდგომარეობის წვლიდი შეადგენს 30%, ხოლო პირდაპირი იონიზაციის – 10%.

Na⁺-He წყვილის შემოხვევაში – იონიზაციის სრულ კვეთაში მე-ფახსებული ჰელიუმის ატომის ავტოიონიზაციური მდგომარეობის წვლიდი ინდენტურია Na⁺-He წყვილისა.

დადგენილია აგრეთვე დამჯახებული ნაწილაკების მიერ ელექტრონის დაკარგვის პროცესის σ mექანიზმში K⁺-He, Ne დაჯახების დროს. K⁺-He – ის წყვილის მაგალითზე ნაჩვენებია, რომ ამ პროცესის რეალიზაციაში გან-მსაზღვრელი როლი პირდაპირი იონიზაციის არხს მიუძღვის.

INVESTIGATION OF TRANSITIONAL METALS IMPLANTED BY CARBON IONS

B. Eristavi, E. Diasamidze, E. Kutelia, N. Maisuradze,
R. Dekanosidze, N. Jalabadze

Abstract. Polycrystalline samples of *Mo*, *Ni* and *Ti* implanted by carbon ions (dose $1.10^{17} - 1.10^{18}$ cm^{-2} and energy 40-100keV) are investigated. Characterizations by electron Auger-spectroscopy (ASE) and electron diffractometry in dependence on the temperature of after-implantation annealing in temperature range 200-1000°C have been carried out. In implanted system of *Mo-C*, at dose $1 \cdot 10^{17}$ cm^{-2} hcp structure Mo_2C was formed. At increased dose the additional lines of $\gamma-MoC$ and $\gamma'-MoC$ (hexagonal structures) appeared. In the implanted system *Ni-C* (dose $4 \cdot 10^{17}$ cm^{-2}) carbon is located in the layers of the near-surface region forming an amorphous dissipative structure. In the dissipative structure carbon is not chemically bound with *Ni* and it is in a graphite like state. At dose of $6 \cdot 10^{17}$ cm^{-2} and higher carbon concentration in the implanted layer corresponds to required value and the carbide Ni_3C (hexagonal structure) is formed.This phase is stable up to the annealing temperature 400°C.In the implanted systems *Ti-C* (dose $5 \cdot 10^{17}$cm^{-2}) the phase *TiC* is not formed without after-implantation annealing and the formation of amorphous dissipative structure at the near-surface region is observed. Annealing at 200°C returns carbon from the dissipative region to the implanted layer,where the phase TiC (fcc structure) is formed. This phase is stable to 800°C of annealing temperature. In all cases heating of implanted samples over the temperatures leads 600°C to the carbide phase dissociation and reduction of the initial crystal structure of the samples.The additional bombardment without after-implantation annealing of the samples by Ar^+ ions leads to the formation of the carbide phase *TiC*.

1. Introduction

High-dose implantation of transitional metals by carbon ions may be

interesting in several aspects:1) fundamental research of interaction of high-energy ions with solid states, formation of dopped atoms dissipative stucture (exit of dopped atoms through implanted layer to near-suerface region) and dissipative structure of target atoms (a long-distance effect of ion bombardment); 2) formation of thin diamond-like films on solid surface; 3) formation of carbides of a given thickness on a given target in implantation metallurgy.

For modification of properties of target by ion implantation the transitional metals require high-dose of ions. It is considered that structural change is determined by two nonequilibrium processes: generation of radiation defects, which are larger than the number of their recombination and by the introduction of impurity which is much larger than equilibrium solubility. Therefore not only a chemical composition determines a structure, but it is determined by a complex of interrelations, when quick-particles come into collision with solid state.

When implanting the ions of higher dose, change of material properties most probably happens through the structural transition.Nonequilibrium distribution of impurity atoms and radiation defects may lead to unexpected metastable states. The search of relationship between the structure and properties is necessary for formation of new materials by ion bombardment.

The ion alloying of transitional metals by the ions of sp-elements: boron, oxygen and fluorine, always produce non-crystalline (amorophous) phases in implanted layer [1-3]. On the other hand bombardment of transitional metals by carbon and nitrogen ions always produce carbids and nitrids [4], correspodingly.

The purpose of this work is to investigatie dopped carbon and structural transition in thin films of Mo and in the near-surface layers of bulk polycrystalline samples of Ni and Ti.

2. Experimental

Polycrystalline films of molibdenium with thikness of 800-1000A^0 were thermally deposited on the vacuum cleaved rock salt (NaCl) at 250°C. Implantation were made at the energy of 40keV and 1-3.10^{17}cm^{-2} doses by the method described in [4].

In addition, investigation of the 10x10x1 mm polycrystaline samples of

Ni and Ti with 99.99% purity have also been carried out.The surface was prepared by the standard technology including mechanical polish by diamond powders and pastes on glass, calico and cambric,electrochemical polish and before-implantation homogenizing annealing at 1100°C.For each specimen annealing was carried out at 4-$5 \cdot 10^{-5}$ Pa for 30min.

Ion alloying of the samples prepared at room temperature in the system with cryogen jacket at liquid nitrogen temperature with single charge carbon (C^+) ions of energy 100keV and doses $1 \cdot 10^{17} cm^{-2}$ -$1 \cdot 10^{18} cm^{-2}$ was carried out. After-implantation annealing in vacuum 4-$5 \cdot 10^{-5}$ Pa was made at 200-1000°C (annealing time was 30min). For each case separate samples have been used.

Additionally two samples of titanium,implanted by C^+ ions with energy 100keV and dose $5 \cdot 10^{17}$ cm^{-2},were inestigated.One of these samples had been annealed before implantation while the other had not.After this,the samples were bombarded by Ar^+ ions with dose $2 \cdot 10^{16} cm^{-2}$ and energy 200keV.

The structural investigations of all the samples were made by electronograph EMR-102 at accelerating voltage 100keV. The samples of Ni and Ti were also invenstigated by Auger-electron spectroscopy (ASE) method on the LAS-2000 of "Riber" (France). Spectra have been obtained at the energy of primary electron beam of 3keV,time constant 1sec,modulation amplitude 1V,emission current of electrons 0.32A. Sputerring of samples were made by Ar^+ ion beam with the energy 5keV and ion current density $2 \cdot 10^{5}$ A/cm^2. The velocityof ion etching was $\approx 30 A^0/min$.

3. Experimental results and discussion

3.1.Molibdenium-carbon system

In implanted system Mo-C at dose $1 \cdot 10^{17} cm^{-2}$ the hep stucture Mo_2C is formed. By increasing the dose up to $3 \cdot 10^{17} cm^{-2}$ the additional lines of γ-MoC [5] and γ'-MoC [6] phases (with hexagonal stucture) appear on the diffraction patterns together with Mo_2C. Indiced scheme is shown in Fig.1.

In [7], transition to nitrides or carbides was a result of bombardment of vaporized or cathode sputtered films by different ions (for example,He^+ or Ar^+).These transitions took place on impurity contaminations and were explained as a radiation-stimulated polymorphy.

N	d.Å	(hkl)
1	2.8	(001)γ-MₒC
2	2.72	(100)γ'-MₒC
3	2.6	(100) Mo₂C
4	2.45	(101)γ'-MₒC
5	2.36	(002) Mo₂C
6	2.28	(101) Mo₂C
7	2.08	(103)γ'-MₒC
8	1.86	(101)γ-MₒC
9	1.75	(102) Mo₂C
10	1.67	(105)γ'-MₒC
11	1.56	(200)γ-MₒC
12	1.50	(110) Mo₂C
13	1.42	(002)γ-MₒC
14	1.35	(103) Mo₂C
15	1.31	(200) Mo₂C
16	1.19	(004) Mo₂C
17	0.97	(211) Mo₂C
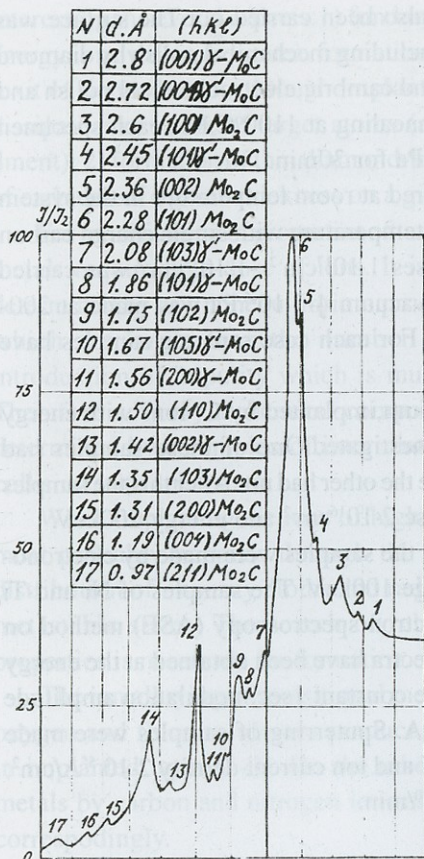
Fig.1. Intensities of elecron diffraction lines and interplanar distances in implanted system Mo-C, at energy 40keV and dose 3.10^{17}cm⁻².

It is considered that the preferable formation of one or another carbide at room temperature is determined by the thermodynamical probability. In the implanted system Mo-C, where Mo₂C was formed, thermodynamical potential of reaction at room temperature $\Delta Z^{\circ}_{298} = -0.53$ eV/at. A coherence of structures supports the formation of additional matastable phases γ-MoC and γ'-MoC with $\Delta Z^{\circ}_{298} \approx -0.10$ eV/at.

3.2. Nickel-carbon system

This implanted system has a thermodynamical prohibition on formation of NiC at room temperature ($\Delta Z^{\circ}_{298} \approx +0.33$ eV/at).

In Fig.2 distribution of carbon atoms in dependence on the depth of polycristalline specimens bombarded by C⁺ ions, 100keV energy and doses 1.10^{17}-1.10^{18} cm⁻² (the critical dose of transition is 8.10^{16} cm⁻²) is shown. At the doses $1.4.10^{17}$ cm⁻² (average calculated concentration of dopped carbon 2-7.10^{22} cm⁻³) considerable migration of carbon atoms from ion-alloyed layer to the surface is observed. The profile appears at dose 6.10^{17} cm⁻² (average concentration 8.10^{22} cm⁻³). KLL Auger-lines of carbon in dependence on time of surface sputtering for different doses and temperatures of after-implantation annealing is shown in Fig.3. Up to the dose 6.10^{17} cm⁻² in the whole depth carbon is not chemically bound with nickel and is in graphite
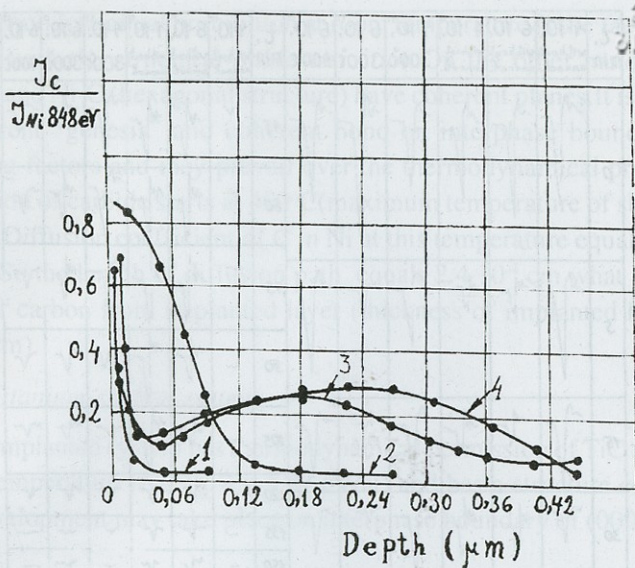
Fig.2. Profiles of carbon distribution in implanted system Ni-C at energy 100keV and doses: $1 - 1 \cdot 10^{17}$; $2 - 4 \cdot 10^{17}$; $3 - 6 \cdot 10^{17}$; $4 - 1 \cdot 10^{18} \text{cm}^{-2}$.

like state and forms amorphous dissipative structure. At the dose $6 \cdot 10^{17}$ cm^{-2} and higher, carbon in graphite like state is only on surface, in the depth it is in carbide state (Ni_3C type) that is indicated by the shape of KLL Auger-lines of carbon [8].

Considerable difference of calculated concentration of dopped carbon with the result shown in Fig.2 is probably connected with carbon migration to the surface and its evaporation.

Dose limit of phase transition obtained in approach [9] is $8 \cdot 10^{18}$ cm^{-2} (average concentration is $1.6 \cdot 10^{22}$ cm^{-3}), i.e. at dose $1 \cdot 10^{17}$ cm^{-2} the transition in carbide was supposed to happen. However, increased migration of carbon atoms from ion-alloyed layer to the surface decreases total energy of elastic interaction of carbon atoms with lattice, what,on the other hand decreases the total stress of ion-alloyed layer and prevents the phase transition. Another though less important reason of indicated disparity is that the cascade of interaction along the ion track creates impoverished zone. The average energy transfered to the first vipe-out atoms equals to 186eV; the average number

125

t, min	$4\cdot10^{17}$ without anneal.	$6\cdot10^{17}$ without anneal.	$1\cdot10^{18}$ without anneal.	$4\cdot10^{17}$ 300°C	$6\cdot10^{17}$ 300°C	$6\cdot10^{17}$ 400°C
0						
5						
15						
30						

t, min	$4\cdot10^{17}$ without anneal.	$6\cdot10^{17}$ without anneal.	$1\cdot10^{18}$ without anneal.	$4\cdot10^{17}$ 300°C	$6\cdot10^{17}$ 300°C	$6\cdot10^{17}$ 400°C
45						
60						
75						
90						
105						
120						
135						
150						
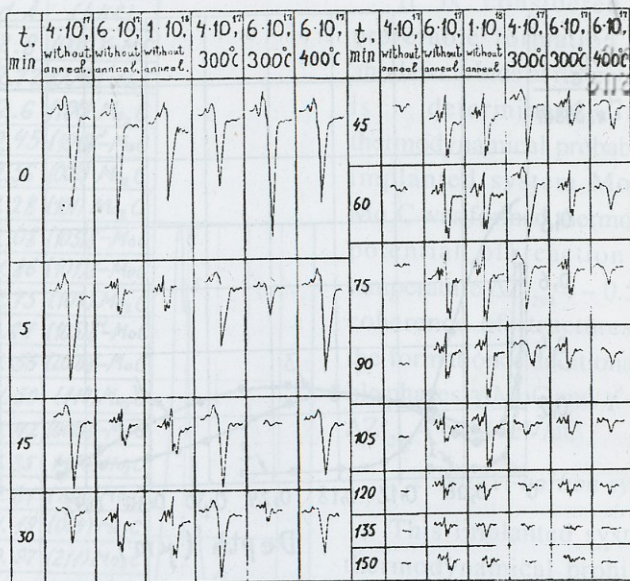
Fig.3. KLL Auger-electron spectra in implanted system Ni-C at different doses, sputtering time and annealing temperatures.

of atoms participating in the cascade per one vipe-out atom is 3.0; the average number of displacements per atom in the range of dose $1\cdot10^{17}$ cm^{-2}-$1\cdot10^{18}$ cm^{-2} equals 1.5-15. Around the impoverished zone there is the atmosphere of carbon atoms (a type of Kottrell atmosphere) what also decreases the total energy of interaction of carbon atoms with lattice. So the phase – transition takes place at the dose of $6\cdot10^{17}$ cm^{-2} (see Fig.3).

While annealing of implanted samples (dose 4.10^{17} cm^{-2}) carbon is in graphite-like state in the whole depth of implanted layer and after annealing at 800°C it is found only on the surface. In Fig. 3 the KLL Auger-line of carbon at annealing temperatures 300-400°C is shown, which corresponds to the temperature stability of Ni$_3$C.

Electron diffraction patten from samples alloyed by dose $1-4.10^{17}$ cm^{-2} show only the lines of fcc-structure of nickel. In the range of doses 6.10^{17}-1.10^{18} cm^{-2}, two lines of Ni$_3$C were found (with interplanar distances d=2.267A^0 and d=1.567A^0) together with nickel lines.

126
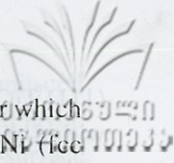
So thermodynamical prohibition at room temperature is the factor which interferes with the structural-phase transition.On the other hand, Ni (fcc structure) and Ni_3C (hexagonal structure) have coherent planes.It is possible, that coherent "genesis" and coherent bond on interphase boundaries are stimulating factors and they prevail over the thermodynamical prohibition. Dissociation of carbide starts at 400°C(maximum temperature of stable state is 370°C).Diffusion coefficient of C in Ni at this temperature equals $3.3.10^{11}$ cm^{-2}/sec. So the length of diffusion path equals $2.4 \cdot 10^{-4}$ cm what is enough for exit of carbon from implanted layer (thickness of implanted layer is $\approx$ $0.2 \cdot 10^{-4}$ cm).

3.3. Titanium-carbon system

This implanted system has thermodynamical permission of TiC formation at room temperature ($\Delta Z^0_{298} \approx -1.87$ eV/at) and has a structure coherence. Phase development may take place on interphase boundary of (0001) Ti and
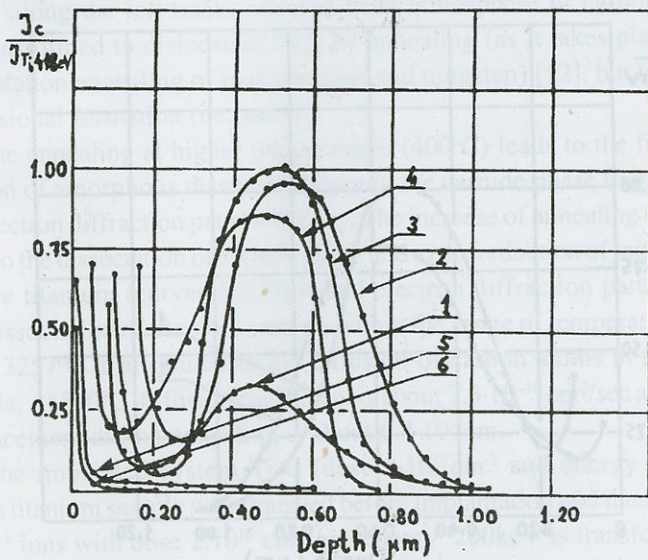
Fig.4. Profiles of carbon distribution in implanted system Ti-C, at energy 100keV, dose 5.10^{17} cm^{-2} and at different annealing temperatures. The annealing time after implantation is 30min for each specimen. 1 – without anneal; 2 – 200°C; 3 – 400°C; 4 – 600°C; 5 – 800°C; 6 – 1000°C.

(111) TiC. However, titanium as other transition metals of hexagonal lattice with d-states density of 1/10 to 2/10 has essential value of compressibility and comparatively small value of local elastic energy when titanium atoms are interacted with interstitial carbon atoms. These two factors are obctacles for structural-phase transition when carbon ions bombardment occurs.

The implantation were made at energy of ions 100keV and at the dose 5.10^{17} cm^{-2} (critical dose is 2.10^{17} cm^{-2}). As shown in Fig.4 (curve 1) TiC is not formed. This fact is confirmed by the relation of Auger-signal intensities between carbon and titanium [10]. Considerable amount of carbon atoms, which are not chemically bound with titanium, is observed on the surface. They have an amorphous dissipative structure in the near surface region. This fact is confirmed by the electron diffraction pattern (see Fig.5a).

After implantation annealing at the 200° C-30min carbon atoms return from dissipative region to the implanted layer, where formation of carbide TiC occurs (see curve 2 Fig.4 and electron diffraction pattern Fig.5b). In this case the volume of implanted layers considerably increases. Explanation
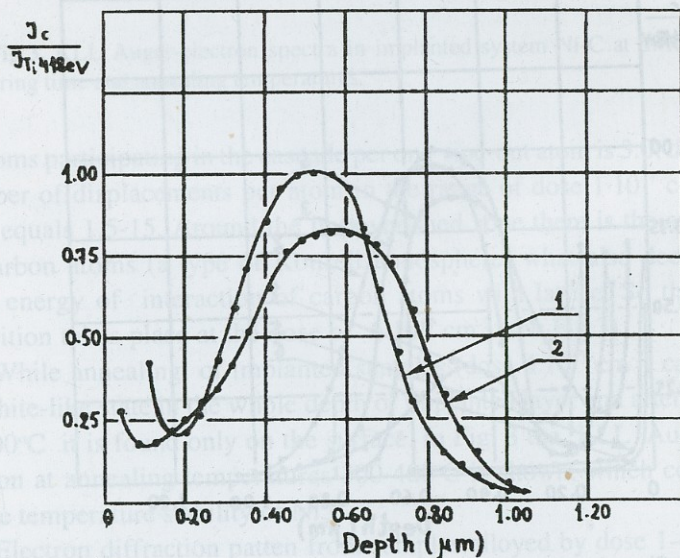
Fig.5. Electron diffraction patterns on reflection from implanted system Ti-C. The annealing time after implantation – 30min. a – without annealing. b – 200°C; c – 400°C; d – 800°C; zone axis [0001].

of this fact by carbide formation is not possible, because ratio of unit-cell volumes of TiC and Ti is $31.8/80.6 = 0.39$. Thickness of the implanted layer, according to the curve 2, Fig.4, is about $0.9.10^{-4}$cm. If we take near-surface layer of dissipative structure away ($0.25.10^{-4}$cm) and neglect the impurity swelling (atom of C in TiC has strictly covalent radius and linear increase of implanted layer to the surface is about 1.10^{-6}cm and take into consideration the thickness of the sputtered layer ($0.6.10^{-5}$cm), then growth of implanted layer volume in this case is $\ln V/V_0 = 0.87$. Where V is the volume of the implanted layer defined from the curve 2, Fig.4; V_0 is the volume of the implanted layer calculated by the parameters of the dopped atoms distribution function and by the projective path and path spread.

Growth of implanted layer volume up to 2.5 times at annealing temperature 200°C, as we consider is developed by vacancy mechanism. If we use empirical relation of vacancy formation with melting temperature [11], then this energy will be about 1.20-1.22eV. Energy of vacancy migration determined from activation energy of selfdiffusion equals 0.06-0.08eV. Threfore, vacancy cluster along the ion track, released from atmosphere of carbon atoms, is not transformed to dislocation loop by annealing (as it takes place at after-implantation annealing of molibdenium and tungsten) [12], but to the three-dimensional formation (i.e.pores).

The annealing at higher temperatures (400°C) leads to the full trasphormation of amorphous dissipative layer to the carbide phase (curve 3, Fig.4, and electron diffraction pattern Fig.5c). The increase of annealing temperature leads to the dissociation of carbide phase and to the reduction of initial structure of pure titanium (curves 5;6,Fig.4 and electron diffraction pattern Fig.5d). The dissociation of titanium carbide within the range of temperature stability up to 3257°C is attributed to the diffusion of carbon atoms in the titanium carbide. At 800°C diffusion coefficient is about $2.3 \cdot 10^{-10}$ cm^2/sec and diffusion displacement during annealing is about $6.4 \cdot 10^{-4}$cm.

The implanted system Ti-C (dose $5 \cdot 10^{17}$cm^{-2} and energy 100keV) in which titanium sample was annealed before implantation and then bombarded by Ar$^+$ ions with dose 2.10^{16} cm^{-2} and energy 200keV is transformed to the titanium carbide (curve 2 Fig.6). Calculated thickness of implanted Ti-C layer was equal to $3.1 \cdot 10^5$cm and thickness of the implanted Ti-Ar layer was equal to $2.6 \cdot 10^{-5}$ cm.

9.
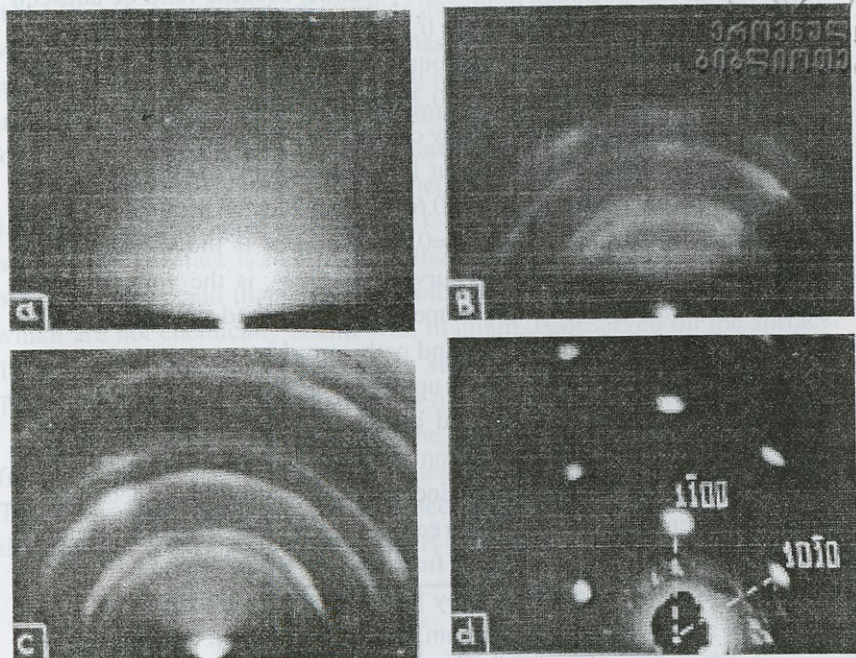
Fig.6. Profiles of carbon distributions in titanium.1-implanted by C^+,5.10^{17}cm^{-2} 100keV,Ar$^+$, 200keV, 2.10^{16}cm^{-2}, without annealing. 2 – annealed before implantation at 1100°C, 30min. Implantation by C^+, 5.10^{17}cm^{-2} and Ar$^+$,200keV, 2.10^{16}cm^{-2}.

The critical dose of amorphization during bombardment of Ti by Ar$^+$ ions according to the thermal model [13] is more than 10^{19}cm^{-2}. Taking into consideration impurity swelling of the implanted layer [14] and sputtering coefficient in Sigmunds theory we obtain a dose of implantation - 1.3·10^{18}cm^{-2}.

In our case radiation influence (2·10^{16}cm^{-2}) returns carbon atoms from amorphous dissipative film to the implanted layer and carbide TiC is formed.However,degree of swelling is increasing (lnV/V$_0$=1.34).

The implanted system Ti-C in which titanium sample was not annealed before implantation but then was bombarded by Ar$^+$ ions after implantation (dose 2.10^{16}cm^{-2} and energy 200keV), also leads to the transition to the titanium carbide (curve1,Fig.6), but it is less porous (lnV/V$_0$=0.77).

4.CONCLUSION

The results of the investigations could be briefly formulated as follows:

1.In the films of molibdenium implanted by carbon ions with energy 40keV and dose $1.10^{17}cm^{-2}$, Mo_2C is formed.At dose $3.10^{17}cm^{-2}$ metastable phases γ-MoC and γ'-MoC are appeared additionally.

2.In the implanted system Ni-C (energy-100keV;dose - $4.10^{17}cm^{-2}$) carbon is not chemically bound with Ni and is located in the layers of near-surface region forming an amorphous dissipative structure.At dose of $6.10^{17}cm^{-2}$ and higher,carbide Ni_3C is formed and this phase is stable to the annealing temperature 400^0C.

3.In the implanted system Ti-C (energy-100keV;dose - $5.10^{17}cm^{-2}$ the phase TiC without after-implantation annealing is not formed.After-implantation annealing in the temperature range $200-600^0C$ leads to the formation of fcc carbide of titanium. Annealing of the implanted samples over 600^0C leads to the carbide phase dissociation and reduction of initial crystal structure of the samples.

4.Formation of the titanium carbide in implanted Ti-C system is possible without after-implantation annealings by additional bombardment by argon (Ar^+) ions.

Georgian Technical University

REFERENCES

1. G.Linker. Sol.St.Commun. **57**, 9, 1986, 773.

2. G.V.Afanasiev, E.M.Diasamidze, A.N.Kalinin and N.M.Kutsia. Surface, 12,1986,72(USSR).

3. E.M.Diasamidze, C.A.Zaslavscki, N.M.Kutsia, A.N.Kalinin, R.N.Kutelia. Question of atomic science and engineering. Series Radiation damage physics and radiation material science, N3,(36),1985,36(USSR).

4. I.G.Gverdtsiteli, A.I.Guldamashvili, E.M.Diasamidze, A.N.Kalinin, R.N.Kutelia. Question of atomic science and engineering.Series Radiation physics

and radiation material science, N1 (20),1982,32(USSR).

5. G.V.Samsonov, G.Sh.Upadkhaia, V.C.Neshpor. Physical Material Science of Carbides.Kiev., 1974,455.

6. Powder Diffraction File. Alphabetical Index Inorganic phases, JSPO International Centre for difraction Data, 1985.

7. V.N.Bykov, V.A.Trogan, G.G.Zdorovtseva, V.S.Khaimovich. Phys. stat. sol. (a), 32,1975,53.

8. H.H.Madden. J.Vac.Sci.Technol., **18**, N3,1981,677.

9. T.Egami, J.Weseda. J.Non.Cryst.Sol.**64,** N1-2,1985,113.

10. K.Oishi and S.Usami. J.of the vacuum society of Japan.**25,**N4,1982,291.

11. M.Doyama,J.S.Koehler. Acta met. **24.**N9.1976,871.

12.R.N.Dekanosidze, E.M.Diasamidze, E.R.Kutelia, M.Sh.Kintsurashvili, N.E.Menabde, B.G.Eristavi. Surface, N6,1987,119(USSR).

13. E.M.Diasamidze. Surface, N8,1990,111(USSR).

14. E.M.Diasamidze, A.N.Kalinin. Physicsd Chemistry of material treatment. N3,1982,16 (Russian).

15. P.Sigmund. Phys.Rev., 184,N2,1969,383.

ბ. ერისთავი, ე. დიასამიძე, ე. ქუთელია, ნ. მაისურაძე,
რ. დეკანოსიძე, ნ. ჯალაბაძე

ნახშირბადით იმპლანტირებული გარდამავალი ლითონების კვლევა

დასკვნა

ნახშირბადით იმპლანტირებული Mo, Ni და Ti პოლიკრისტალური ნიმუშები გამოკვლეულია ოჟე-სპექტროსკოპიის და ელექტრონული დიფრაქციის მეთოდებით.

დადგენილია, რომ სისტემაში Mo-C მცირე დოზით იმპლანტირებისას ფორმირდება Mo$_2$C ფაზა. დოზის გაზრდით წარმოიქმნება მეტასტაბილური γ-MoC და γ'-MoC ფაზები.

სისტემაში Ni-C მცირე დოზით იმპლანტირებისას ნახშირბადი არ შედის ქიმიურ ბმაში ნიკელთან. დოზის გაზრდით ფორმირდება კარბიდული ფაზა Ni$_3$C.

სისტემაში Ti-C იმპლანტაციის შემდგომში გამოწვის გარეშე კარბიდი TiC არ წარმოიქმნება. იმპლანტაციის შემდგომ გამოწვა იწვევს TiC კარბიდის ფორმირებას. ნაჩვენებია, რომ TiC კარბიდული ფაზის წარმოქმნა სისტემაში Ti-C შესაძლებელია იმპლანტაციის შემდგომ გამოწვის გარეშე თუ ნიმუშებს დამატებით დავასხივებთ არგონის იონებით.

THE ATMOSPHERE OF ANNIHILATING VORTEX

L.Kiknadze, Yu.Mamaladze

ABSTRACT. The motion of a vortex in liquid helium II near the solid boundary is considered. Especially, the sequence of events in the course of which an annihilating vortex, a wall and parts of liquid contours, disposed between them, get confluent. In spite of some allegations no contradictions with Thomson's theorem accompany this process, and no new dynamical principle turns out to be necessary.

1. Introduction

1.1. The dynamics of vortex filaments (or "point vortices" in the case of plane flow) is so unusual that sometimes it seems to be opposed to Newton's one: the state of vortex array is fixed only by the configuration of vortex filaments (positions of vortex points), and there are no velocities in initial conditions (inertial terms are absent in equations of motion). But this is only specific form of Newton's second law: the sum of forces acting on massless object must be zero (if a vortex has a core, then the sum of acting forces is equal to the product of cores mass and acceleration).

The vortex dynamics was founded by Helmholtz [1], later developed in numerous works (Kelvin's ones [2,3] must be mentioned first of all among them), and was described in many manuals [4,5]. Nevertheless, misunderstandings turn out to be possible till now, and the purpose of this paper is to clarify some of the vexed questions.

They are connected both with classical hydrodynamics of ideal incompressible liquid and with the motion of quantized vortices in He II. Their dynamics is founded by Hall and Vinen [6] (see also reviews [7-12]). The main difference from classical liquid is that: (i) circulation is quantized in units $2\pi\hbar/m$, m being the mass of helium atom, (ii) the scattering of phonons and rotons on vortex filament causes the force of mutual friction which must be included in the sum of acting forces.

1.2. Helmholtz-Kelvin law of vortex motion in ideal incompressible liquid is

$$v_0 = v_{s0},$$ 1)

where v_0 is the velocity of vortex filament (linear vortex) and v_{s0} is the velocity of liquid in the position of vortex (excluding the rotation around it). If the filament is curved, then only the contribution of considered element must be excluded, but other parts of filament contribute to the motion of this element. But we restrict ourselves by plane flows with straight vortices perpendicular to the plane of motion.

Eq.(1) corresponds to equality

$$F_M = [\Gamma, v_{s0} - v_0] = 0$$ 2)

where F_M is the Magnus force, $\Gamma = \Gamma \tau$, Γ is circulation, and τ is the unit vector directed along filament.

1.3. In the same case of plane flow the law of vortex motion in He II is [6]:

$$v_0 = v_{s0} - \frac{\rho_n}{2\rho} B'(v_{s0} - v_{n0}) - \frac{\rho_n}{2\rho} B[\tau, v_{s0} - v_{n0}],$$ 3)

where v_{s0} and v_{n0} are the velocities of superfluid and normal components in the position of vortex point, B and B' are Hall-Vinen's coefficients of mutual friction [6-12], ρ_n is the density of normal component, ρ is the full density of He II. The corresponding force-equilibrium-equality is:

$$F_M + F_{sn} = 0,$$ 4)

where F_{sn} is the force of mutual friction [6,8].

2. Annihilation on the plane solid surface

2.1. Let us consider a vortex disposed on the distance d_0 from solid plane surface $y=0$ at the initial point $x_0(0)=0$, $y_0(0)=d_0$. If the vortex has the circulation $2\pi\hbar/m$, then its motion is caused by the image with circulation $(-2\pi\hbar/m)$ disposed at the point $x = x_0$, $y=-y_0$,

$$v_{s0x} = \frac{\hbar}{2my_0}, \qquad v_{s0x} = 0,$$ (5)

134

and the velocity of vortex according to Eq.(3) is

$$\frac{dx_0}{dt} = (1 - \frac{\rho_n}{2\rho}B')\frac{\hbar}{2my_0}, \quad \frac{dy_0}{dt} = -\frac{\rho_n}{2\rho}B\frac{\hbar}{2my_0}. \tag{6}$$

This equations are easily integrated and we have the following description of vortex annihilation:

$$y_0 = \left(d_0^2 - \frac{\hbar\rho_n}{2m\rho}Bt\right)^{1/2} = \left(\frac{\hbar\rho_n}{2m\rho}B(t_a - t)\right)^{1/2} \tag{7}$$

$$\frac{\rho_n}{2\rho}Bx_0 = (1 - \frac{\rho_n}{2\rho}B')(d_0 - y_0), \tag{8}$$

where $t_a = (\hbar\rho_n B/2\rho m)^{-1/2} d_0^2$ is the duration of annihilation process (the vortex disappears in the wall annihilating with its image at the point $x_0(t_a) = (1 - \rho_n B'/2\rho)(\rho_n B'/2\rho)^{-1} d_0, y_0(t_a) = 0$).

2.2.It is known [13] (see also [5]) that vortex moving according to Eq.(5) is followed by the atmosphere, the part of the liquid of which has the same transport velocity as the vortex.

In the following discussion the reference frame of the wall (in that Eqs.(5-8) are written) is changed by the reference frame of the vortex. The atmosphere is placed in so-called Kelvin's semioval (another half of oval surrounds the image), and the liquid in it moves on the closed streamlines. The liquid outside the atmosphere, overflowing it, flows along the wall on the unclosed streamlines. This picture of flow is stationary and streamlines coincide with trajectories of fluid particles.

2.3.In the case of arbitrary small B Eq.(6) principally differs from Eq.(5). Semioval breaks away from the wall (and from the semioval of the image). And what is more important, it is unremittingly
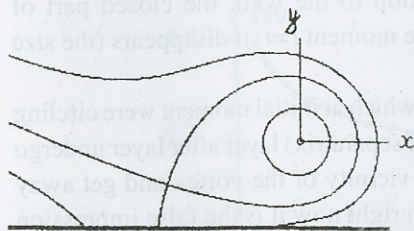
Fig.1 The streamlines corresponding to Eq.(10). They have the shape determined by the ratios x/y_0 and y/y_0, i.e. the loop of separatrix only decreases while $y_0 \to 0$, but the picture does not change.

135

decreasing in the process of approaching the wall. So the vortex has no atmosphere in the above- mentioned sense. But we can name so (in some restricted sense) the liquid disposed into the loop of separatrix shown in Fig.1.

2.4.In the reference frame of the vortex (x -axis is parallel to solid boundary, and y -axis is normal to it) the wall ($y=-y_0$) and the image ($x=0$, $y=-2y_0$) are moving, and the vortex is immovable at the point $x=0$, $y=0$. The velocity of liquid is determined by formula ($z=x+iy$):

$$v_x - iv_y = \frac{\hbar}{mi}\left(\frac{1}{z} - \frac{1}{z+2iy_0}\right) - \left(1 - \frac{\rho_n}{2\rho}(B'-iB)\right)\frac{\hbar}{2my_0}, \quad (9)$$

where the first term is the contribution of the vortex and its image in the velocity of liquid, the others are caused by the transformation to the reference frame of the vortex.

The family of streamlines is determined according to Eq.(9) by the equation $\Psi =const$, where

$$\Psi = \frac{\hbar}{mi}\ln\frac{x^2 + (y+2y_0)}{x^2+y^2} - \left(y(1 - \frac{\rho_n}{2\rho}B') + x\frac{\rho_n}{2\rho}B\right)\frac{\hbar}{2my_0} \quad (10)$$

is the current function.

Let us note by (x_c, y_c) the critical point, where $v_x=v_y=0$. The streamline $\Psi(x,y)=\Psi(x_c, y_c)$, which passes the critical point is a separatrix that separates the stream from the area of motion around the vortex on closed streamlines (in the case $B'=B=0$ the equation of separatrix transfers into the equation of Kelvin's oval). During the vortex motion to the wall, the closed part of separatrix (the loop) decreases and at the moment $t=t_a$ it disappears (the size of this loop is of the order of y_0).

2.5.It may seem that liquid particles, which at initial moment were circling around the vortex (were filling the loop of separatrix) layer after layer undergo qualitative change of motion: leave the vicinity of the vortex and get away from it along the wall. But as it is shown right now it is the false impression (the real picture is difficult to imagine because of difference between streamlines and trajectories in this nonstationary flow (the flow is nonstationary even in the vortex reference frame in that the wall is moving)).

Actually, because of continuity of motion, liquid particles, that once for-

med the closed line around the vortex, remain on one liquid contour surro-
unding the vortex forever. Location of liquid contours into and out of each
other also remains unchangeable. The part of liquid that once was the vortex
atmosphere remains with it forever and separates the vortex from liquid,
which has never been its atmosphere. Liquid contours that contain the vortex
do not cross each other during vortex motion to the wall. Thomson's theorem
also excludes the possibility of such crossing. The lower parts of those
contours remain between the vortex and the wall, and at the moment of
annihilation the vortex, these parts of liquid contours and the wall get confluent.

2.6. The Fig.2 illustrates these statements. The moment $t = 0.95\ t_a$ is
pictured on it, and the location of points which were forming closed streamline
at the initial moment $t = 0$ is shown (it is noted on each of them from which
angle they were seen from the vortex at initial moment). At the moment
$t = 0.95 t_a$ the vortex is already near the wall ($y_0(0.95 t_a)/d_0 = 7.10^{-2}$), the loop of
separatrix is very small, and former atmosphere is stretched along the wall,
but does not pass the vortex.

From Fig.2 we can see how the part of liquid contour disposed between
the vortex and the wall is stretching while the vortex is approaching the wall.
At the end of this process the liquid is almost motionless almost everywhere
except the vicinity of the vortex, especially between the vortex and the wall.
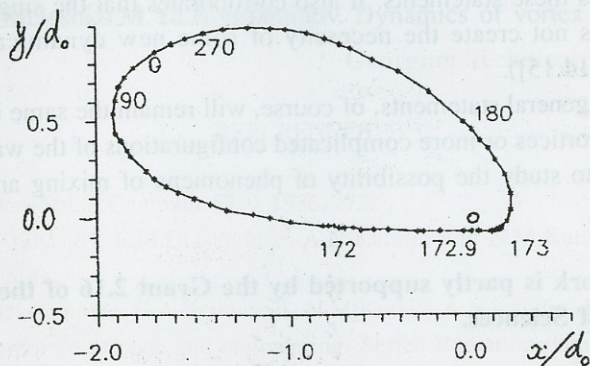
Fig.2 Here are shown at $t = 0.95 t_a$ the positions of points which at initial moment were
forming closed streamline inside the loop of separatrix. On each of them is noted from
which angle they were seen from the vortex at $t = 0$. The initial position of the wall is $y = d_0$.

137

2.7. The law of motion given by Eq.(1) is valid only for completely free vortex (only the Magnus force can act on it, but it is equal to zero). The motion considered in this paper is caused by Magnus force and mutual friction. The results of this consideration are valid for the motion of a vortex driven by any force. Actually, however one may move the vortex it never crosses the liquid contours surrounding it, and the circulation arround them is preserved independently of their disposition relative to separatrix. The liquid contour which was the separatrix and it may cease to be separatrix later, has the same feature. It is clear even from the fact that the surface surrounded by liquid contour cannot be changed while the loop of separatrix can undergo arbitrary transformations depending on circumstances: how and where the vortex is moving.

3. Summary

3.1. The difference between trajectories of liquid particles and streamlines, specific for nonstationary flows, makes the picture of such flow less clear, hard to imagine. E.g., it may cause the impression of the necessity for a vortex to cross some liquid contours. But this contradicts Thomson's theorem and is wrong because there exists no reason to infringe this theorem. The existence of liquid contour, which earlier did not surround a vortex but now surrounds it, is impossible. Our consideration of annihilation process corroborates these statements. It also corroborates that the singularity of a vortex does not create the necessity of some new dynamical principle (compare [14,15]).

3.2. All general statements, of course, will remain the same in the cases of several vortices or more complicated configurations of the wall. But it is interesting to study the possibility of phenomena of mixing and chaos in these cases.

E. Andronikashvili Institute of Physics of Georgian Academy of Sciences, Tbilisi I. Javakhishvili State university

REFERENCES

1. H.Helmholtz. J. Reine Angew. Math. 55,25,1858.

2. W.Thomson. Phil.Mag. ser.33, N226,511,1867.

3. W.Thomson. Trans.R.Soc. Edinbourgh, 25,217,1869.

4. H.Lamb. Hydrodynamics.Cambrige University Press,Cambrige,1932.

5. N.E.Kochin,I.A.Kibel,N.V.Roze. Theoretical Hydromechanics, v.1, M.-L.. 1948.

6. H.E.Hall,W.F.Vinen. Proc.Roy.Soc. A238,204,215,1956.

7. H.E.Hall.Phil Trans.Roy.Soc.A250,359,1957.

8. W.F.Vinen.In Progress in Low Temp.Phys..ed.Gorter. N.-H.Publ.Co.,Amsterdam,1961, v.III,ch.I,p.1-57.

9. E.L.Andronikashvili,Yu.G.Mamaladze.S.G.Matinyan,J.S.Tsakadze. Usp.Fiz.Nauk 73,3,1961(Soviet Phys.-Usp. 4,1,1961).

10. E.L.Andronikashvili,Yu.G.Mamaladze. Rev.Mod.Phys.38,567,1966.

11. E.L.Andronikashvili,Yu.G.Mamaladze. In Progress in Low Temp. Phys.,ed.Gorter, N.-H.Publ.Co.,Amsterdam,1967, v.V,ch.III,p.79-160.

12. E.L.Andronikashvili,Yu.G.Mamaladze,J.S.Tsakadze. Physics of Superfluid Helium, Tbilisi,1978,book 2.

13. W.Thomson.Phil.Mag. 34, N227,15,1867.

14. S.T.Beljaev,Yu.K.Krasnov. Dokl.Ak.Nauk SSSR, 305,808; 306, 566, 1989.

15. V.V.Meleshko,M.Yu.Konstantinov. Dynamics of vortex structures. Kiev, 1993.

Summary

141

შინაარსი